Large Blue Spectral Index From a Conformal Limit of a Rotating Complex Scalar

Daniel J. H. Chung* and Sai Chaitanya Tadepalli†

Department of Physics, University of Wisconsin-Madison, Madison, WI 53706, USA

One well known method of generating a large blue spectral index for axionic isocurvature perturbations is through a flat direction not having a quartic potential term for the radial partner of the axion field. In this work, we show how one can obtain a large blue spectral index even with a quartic potential term associated with the Peccei-Quinn symmetry breaking radial partner. We use the fact that a large radial direction with a quartic term can naturally induce a conformal limit which generates an isocurvature spectral index of 3. We point out that this conformal representation is intrinsically different from both the ordinary equilibrium axion scenario or massless fields in Minkowski spacetime. Another way to view this limit is as a scenario where the angular momentum of the initial conditions slows down the radial field or as a superfluid limit. Quantization of the non-static system in which derivative of the radial field and the derivative of the angular field do not commute is treated with great care to compute the vacuum state. The parametric region consistent with axion dark matter and isocurvature cosmology is discussed.

Contents

1.   INTRODUCTION

Having a large blue tilt in the axionic isocurvature spectrum allows cold dark matter (CDM) density perturbations to be enhanced on short length scales without being in conflict with the precision cosmology that exists for scales $k/a_0 \lesssim 1$ Mpc^{-1} [1–11]. The generation of isocurvature perturbations by spectator axions, its model-specific characteristics, and the related observational limitations have been extensively investigated in the past (see for example [12–48]). Although there are models of axion which naturally generate large blue tilted spectra when there are no quartic

---

*Electronic address: danielchung@wisc.edu

†Electronic address: stadepalli@wisc.edu

potential terms in the radial field [49, 50], there is no previous discussion in the literature regarding generating a large k range of very blue spectrum followed by a plateau from a well-motivated axion models that contain a quartic term in the radial potential [51, 52].[1] From a model building perspective, one can therefore ask whether the overdamped spectrum of [49] (i.e. a smooth spectrum composed of an exponentially large k-range with a very blue spectral index and followed by a zero spectral index plateau without any large bumplike features) can be a signature of flat direction models that are distinct from the quartic radial potential models. If the answer is affirmative, then not only is the time-dependent mass a property that one can infer [5] from measuring the spectral shape similar to that of [49], also the existence of flat direction would be inferrable from such a measurement.

Motivated by this question and also from the desire to find novel well-motivated beyond the Standard Model scenarios that generate a strongly blue tilted axionic isocurvature spectra, we consider a generic complex scalar sector with the radial direction field Γ, the angular field θ, and a quartic coupling λ. The quartic term usually controls the axion decay constant

$$\Gamma_{\text{vac}} = \sqrt{\frac{2M^2}{\lambda}} \tag{1}$$

(what people often denote as f_{PQ}) where the mass parameter M controls the tachyonic mass term responsible for spontaneous breaking of Peccei-Quinn (PQ) symmetry. For the blue isocurvature models, we require a large rolling period of the radial field Γ because it is the time-dependence of the background fields that map to the nontrivial positive power (i.e. blue tilt) of k in the dimensionless power spectrum. When $\Gamma \gg \Gamma_{\text{vac}}$ and the initial kinetic energy is negligible, we might naively expect Γ to roll to Γ_{vac} on a time scale of $(V''(\Gamma))^{-1/2}$. Such a fast roll for $V''(\Gamma) \gg H^2$ (making a large blue tilt) would generate the range of k over which the blue spectra is produced to be

$$\frac{k_{\text{break}} - k_{\text{longest}}}{k_{\text{longest}}} \sim \frac{H}{\sqrt{V''(\Gamma)}} \ll 1 \tag{2}$$

where k_{longest} is the length scale that leaves the horizon when Γ begins to roll and k_{break} is the scale that leaves the horizon when Γ reaches the minimum such that modes having $k > k_{\text{break}}$ will approximately be a flat spectrum.

However, if there is an axion background field motion in the conserved $U(1)_{\text{PQ}}$ angular direction, we know that the time scale to reach Γ_{vac} can be infinite in the limit that all $U(1)_{\text{PQ}}$ symmetry

---

[1] For models that generate a moderately large blue tilt, although not as large as the ones considered in this paper, see [53].

breaking terms are turned off and $\dot{a} \to 0$. Hence, in scenarios where the angular motion in the conserved angular momentum direction is large, we might expect to be able to have a similar radial rolling as the flat direction model of [49]. Unlike in the scenarios of [54, 55], we will use the initial conditions where the phenomenology generating rotations are occurring during inflation. In such angular momentum dependent scenarios, one naively expects the main limitations to obtaining a large $k_{\text{break}}/k_{\text{longest}}$ to be the dilution of the angular momentum due to the Hubble expansion. After substituting the kinetic derived $\dot{\theta}^2$ for the "angular momentum" L^2, there is the well known effective potential term

$$V_E(\Gamma, a) = \frac{\lambda}{4}\Gamma^4 + \frac{1}{2}\frac{L^2}{a^6\Gamma^2} \tag{3}$$

which naively indicates that the effect of L^2 will decay as a^{-6}, becoming irrelevant too fast to be of interest. However, the situation is a bit more interesting.

Because Γ is decreasing when $\Gamma > \Gamma_{\text{min}}$, the denominator $a^6\Gamma^2$ initially decreases only like a^{-4}: i.e. more mildly, giving intuitively a better chance for a blue spectrum to be generated for a larger number of efolds. Furthermore, this means that Γ^4 is also decreasing as a^{-4}, making the relative contribution of the angular momentum not diminish with the increasing scale factor. Indeed, this causes the potential to scale as the inverse mass dimension of the potential, hinting that this is a conformal limit. As will be explained in this paper, this is a time-independent conformal limit of a special type (different from a massless scalar field in Minkowski space or a massless equilibrium axion in dS space), and this will be utilized to generate a blue isocurvature spectrum for the axion field which is approximately $\delta\chi$: i.e. $\Delta_s^2 \propto k^2$ corresponding to a spectral index of $n_I = 3$.

In addition to constructing a novel model of generating a blue spectrum, we also systematically quantize the fields in this background-out-of-equilibrium situation which can be characterized by the novel nonvanishing of the commutator $[\partial_\eta \delta\chi, \partial_\eta \delta\Gamma]$ representing velocity correlation even in the absence of non-derivative correlations. Although the work of [56, 57] quantizes a similar theory[2] and agrees with our results, we present some distinct and unique details here regarding the axion spectrum (particularly regarding conformal symmetry representation) and apply it to isocurvature and dark matter phenomenology. One revelation is that the radial perturbations about the conformal background solution mix with the angular perturbations for any eigenstate of the Hamiltonian even at the quadratic fluctuation level, and the different energy eigenvectors (each eigenvector

---

[2] We do not use any methods of their quantization because their work appeared after we had finished that part of our paper.

representing the mixing) are not orthogonal. Indeed, it will be shown that a massive $\delta\Gamma$ that kinetically mixes with $\delta\chi$ has nearly identical conformal representation as $\delta\chi$. A more important revelation is that, despite the complicated quantum mode mixing arising from the time-dependent background, explicit quantization allows one to construct a time-independent Hamiltonian whose ground state well-represents the vacuum. Because of this and angular field translational symmetry, Goldstone theorem still applies during the conformal period, and the dispersion relationship is approximately linear in k as $k \to 0$ but with a different sound speed coefficient of $1/\sqrt{3}$, similar to a relativistic perfect fluid pressure wave. Indeed, it is well known that a quartic complex scalar with spontaneous $U(1)$ breaking is a simple model of a superfluid (see e.g. [58]).

As far as model parameters are concerned, there are the initial conditions of the background fields, the quartic coupling, and the usual axion parameters which control the dark matter abundances. The main theoretical limitation on extending this blue spectrum over a large k range is the requirement that the axion remains a spectator, which limits the coupling and the background field initial displacement value in the conformal regime. We also identify a range of initial condition deformations away from the conformal limit over which the isocurvature spectrum is approximate k^2, beyond which parametric resonance sets in and destroys the smooth blue spectrum. We identify the parameter regime in which this type of model can reproduce a spectrum of blue-tilt followed by a plateau.

The order of presentation will be as follows. In Sec. 2, we define the notation for the "vanilla" axion model and make general arguments of how a time-independent conformal limit and the spectral index $n_I = 3$ arises with the combination of large field displacements and angular momentum. In Sec. 3, we quantize the theory explicitly about the large phase angular momentum to make the vacuum choice precise and to compute the resulting normalization for the desired correlation function. We also give a simplified discussion of how the *intermediate-time* transition away from the time-independent conformal-era will not result in a large bump in the isocurvature spectrum. In Sec. 4, we discuss how deformations of the *initial conditions* away from the time-independent conformal limit will modify the spectrum. This will lead to oscillatory features in the spectrum. In Sec. 5, we present example isocurvature spectra plots and the parametric ranges over which the QCD axion phenomenology is compatible with observations. We then conclude with a summary. Many appendices follow that provide details of the results presented in the main body of the work. For example, the details of the conformal field representation will be given in Appendix A and the details of the quantization is presented in Appendix D.

2. SPECTATOR DEFINITION AND BASICS OF THE CONFORMAL LIMIT

In this section, we introduce the Lagrangian for our spectator field in terms of a complex scalar field Φ with an underlying global $U(1)$ PQ symmetry and lay out the basic physics central to the computation before delving into detailed computations in the subsequent sections.

2.1. Basic Action

Consider the following action for a spectator complex scalar field Φ containing the axion in a 4-dimensional FLRW spacetime

$$S = \int dt d^3x \sqrt{-g} \left(-\partial_\mu \Phi^* \partial^\mu \Phi - V \right) \tag{4}$$

where the potential is composed of the usual renormalizable terms symmetric under a global $U(1)$

$$V = -2M^2 \Phi^* \Phi + \lambda \left(\Phi^* \Phi \right)^2 \tag{5}$$

with a dimensionless self-coupling constant λ and a dimension-one mass parameter M. We will assume that the background metric $ds^2 = g^{(0)}_{\mu\nu} dx^\mu dx^\nu = -dt^2 + a^2(t)|d\vec{x}|^2$ is driven by an inflaton whose energy dominates over the energy of Φ. As is well known (see e.g. [4]), the non-adiabatic quantum fluctuations of Φ are diffeomorphism gauge invariant at the linear level and govern the spectator isocurvature perturbations that add to the usual curvature perturbations of the inflaton.

To make the $U(1)$ angular physics manifest, parameterize Φ as usual in terms of a radial field Γ and an axial field Σ:

$$\Phi = \frac{1}{\sqrt{2}} \Gamma e^{i\frac{\Sigma}{\Gamma}} \tag{6}$$

where Γ and Σ are real scalar fields. The potential V in terms of the real field Γ is

$$V = -M^2 \Gamma^2 + \frac{\lambda}{4} \Gamma^4 \tag{7}$$

with the stable vacuum at

$$\Gamma_{\text{vac}} = \sqrt{\frac{2M^2}{\lambda}}. \tag{8}$$

The kinetic terms of the Lagrangian in terms of fields Γ and Σ are similarly rewritten as

$$-\partial_\mu \Phi^* \partial^\mu \Phi = -\frac{1}{2} \left(\partial_\mu \Gamma \partial^\mu \Gamma - 2\frac{\Sigma}{\Gamma} \partial_\mu \Sigma \partial^\mu \Gamma + \left(\frac{\Sigma}{\Gamma} \right)^2 \partial_\mu \Gamma \partial^\mu \Gamma + \partial_\mu \Sigma \partial^\mu \Sigma \right) \tag{9}$$

where the $\Sigma \partial_\mu \Sigma \partial^\mu \Gamma$ coupling will later play a nontrivial role for the perturbations. We now define a dimensionless angular variable

$$\theta \equiv \frac{\Sigma}{\Gamma} \tag{10}$$

such that the action in terms of Γ and θ is

$$S = \int d^4x \sqrt{-g^{(0)}} \left(-\frac{1}{2} g^{(0)\mu\nu} \left(\partial_\mu \Gamma \partial_\nu \Gamma + \Gamma^2 \partial_\mu \theta \partial_\nu \theta \right) - \left(-M^2 \Gamma^2 + \frac{\lambda}{4} \Gamma^4 \right) \right). \tag{11}$$

where we note that the kinetic terms for the fields Γ and $\Gamma_{\text{vac}}\theta$ appear canonically normalized. This system has a conserved background angular momentum

$$L \equiv a^2 \Gamma_0^2 \partial_\eta \theta_0 \tag{12}$$

owing to the $U(1)_{\text{PQ}}$ symmetry where the subscript 0 indicates homogeneous background components of the fields and η is the conformal time variable defined as

$$\eta = \frac{-1}{aH}. \tag{13}$$

In principle, this large angular momentum may be generated by a CP violating non-renormalizable term as in the usual Affleck-Dine mechanism. We define any canonically normalized scalar field Υ during inflation to be a spectator if

$$\rho_\Upsilon \ll \rho_{\text{inflaton}} \tag{14}$$

where ρ_Υ represents the energy density of a field Υ. For an initial displacement of the radial field Γ away from its vacuum state Γ_{vac}, Eq. (14) translates to

$$\frac{1}{2} \left(\dot{\Gamma_0}^2 + \Gamma_0^2 \dot{\theta_0}^2 \right) + \frac{\lambda}{4} \Gamma_0^4 \ll 3M_P^2 H^2 \tag{15}$$

where $H = \dot{a}(t)/a(t)$ is the Hubble expansion rate. We will refer to this condition later when we define our spectator dynamics under different initial conditions. This will be one of the dominant constraints on the initial radial displacement of the system.

2.2. How conformal limit generates a blue spectrum

In this section, we will explain how a conformal limit spontaneously broken by a $U(1)$ time-translation locking can generate a blue spectral index of 3 for the axion. The details of this section

are given in Appendix A. One nontrivial aspect that will be explained below is how the angular time-dependence leads to a novel conformal phase that is distinct from the massless conformal phase of Minkowski spacetime.

Consider the Φ action Eq. (11) in the conformal coordinates defined by the background metric $ds^2 = a^2(\eta)\left(-d\eta^2 + |d\vec{x}|^2\right)$:

$$S = \int d\eta d^3x \left(\frac{-1}{2}\eta^{\mu\nu}\left(\partial_\mu Y \partial_\nu Y + Y^2 \partial_\mu \theta \partial_\nu \theta\right) - \left[-\frac{1}{2}\frac{a''}{a}Y^2 - M^2 a^2 Y^2 + \lambda \frac{Y^4}{4}\right]\right). \quad (16)$$

where $\eta_{\mu\nu}$ is the Minkowski metric, θ is given by Eq. (10), and $Y \equiv a\Gamma$. Note that only the $M^2 a^2 Y^2$ term breaks the scaling symmetry

$$a \to u^{-1}a \quad (17)$$

where u is a constant while the time-dependent term $(a''/a)Y^2$ term does not. On the other hand a'/a is time-dependent. The action of Eq. (16) therefore does not know about constant time hypersurface proper length scales or time-translation noninvariance when both $M^2 a^2 Y^2$ and $(a''/a)Y^2$ can be neglected. If we consider only the classical homogeneous background equation of $Y(x) \approx Y_0(\eta)$, as shown in the Appendix A, we can go to a classical background solution of

$$Y_0 = Y_c = \text{const} \quad (18)$$

$$\partial_\eta \theta_0 = \text{const} \quad (19)$$

in the limit

$$\sqrt{\lambda}Y_0 \gg Ma, \sqrt{a''/a}. \quad (20)$$

Hence, dynamically, we achieve the limit of Eq. (17) and the action written in terms of Y and θ (when considering quantum fluctuations about the classical solution) does not know about spatial proper length scales or time translation symmetry violations. This is intuitive since when $\sqrt{\lambda}Y_0 \gg Ma$, the conformal factor $a(\eta)$ scaling by a constant is a classical invariance. Furthermore, even though a''/a is time-dependent (despite it being conformally invariant) in quasi-dS spacetime, large $\sqrt{\lambda}Y_0$ limit allows one to neglect this term to give a static system. A key defining characteristic of this scenario is that $\dot{\theta}_0 \neq 0$ gives a tachyonic mass contribution $-\eta^{\mu\nu}Y^2 \partial_\mu \theta \partial_\nu \theta/2$ which is important for achieving $\sqrt{\lambda}Y_0 \gg Ma, \sqrt{a''/a}$ at the minimum of Y_0 effective potential. This in turn leads to a new perturbation mixing term

$$-\eta^{\mu\nu}Y^2 \partial_\mu \theta \partial_\nu \theta/2 \ni Y_0 \delta Y \partial_\eta \theta_0 \partial_0 \delta\theta \quad (21)$$

that changes the dispersion relationship. This is the reason why rotation is important for this scenario and leads to an interesting tree-level conformally invariant theory which is the subject of this paper. It is also important to note that once one expands about the background of Eqs. (18) and (19), there is a scale $\partial_\eta \theta_0$ in the theory, but because it arises from spontaneous symmetry breaking, it transforms under diffeomorphism that eventually will make the conformal representation similar to that of a massive scalar field theory with the mass parameter behaving as a spurion (see Appendix A for more details). Moreover, owing to the $U(1)$ symmetry, the spontaneous conformal symmetry breaking term $\partial_\eta \theta_0$ is a constant in the conformal time coordinates (as indicated by Eq. (19)).[3]

Now, let's consider the axion sector with a rescaling of Eq. (10) as

$$\theta = \frac{a\Sigma}{Y} \equiv \frac{\mathcal{A}}{Y}.$$ (22)

The action will be of the form

$$S \ni \int d\eta d^3x \left(\frac{-1}{2} \eta^{\mu\nu} \partial_\mu \delta\mathcal{A} \partial_\nu \delta\mathcal{A} + U(1) \textbf{ and } \text{time invariant mixing of } \delta Y \text{ and } \delta\mathcal{A} \right)$$ (23)

where $\delta\mathcal{A}$ are the scaled axion fluctuations about the constant $\partial_\eta \theta_0$ background solution that pairs with Eq. (18). The mixing of δY and $\delta\mathcal{A}$ coming from Eq. (21) is the main difference between the Minkowski spacetime's conformal massless field and the axion here. As will be shown in Appendix A, the scaling symmetry of Eq. (17), $SO(3)$ symmetry, spatial translation invariance, and time-translational symmetry together with PQ $U(1)$ symmetry tells us

$$\langle \delta\mathcal{A}(\eta, \vec{x}) \delta\mathcal{A}(\eta, 0) \rangle \underset{|\vec{x}| \to \infty}{\sim} \frac{c_A}{|\vec{x}|^2}$$ (24)

for a constant c_A or equivalently

$$\boxed{\langle \delta(\Gamma\theta)(\eta, \vec{x}) \delta(\Gamma\theta)(\eta, 0) \rangle \underset{|\vec{x}| \to \infty}{\sim} \frac{c_A}{a^2(\eta)|\vec{x}|^2}}$$ (25)

is the physical axion correlator.

Remarkably, despite the fact that $|\vec{x}|a \gg H^{-1}$, the fluctuations $\delta\mathcal{A}$ do not sense the spacetime curvature. In contrast, a generic minimally coupled massless real scalar field φ_s has a kinetic term for a rescaled $\Phi_s \equiv a\varphi_s$ of

$$S_\varphi = \int d\eta d^3x \left(\frac{1}{2} \left[(\partial_\eta \Phi_s)^2 - \left(\frac{a''(\eta)}{a(\eta)} \right) \Phi_s^2 - \sum_i (\partial_i \Phi_s)^2 \right] \right)$$ (26)

---

[3] Also, it is easy to check that there is no Q-ball formation in the current scenario.

which contains time-dependence through (a''/a): i.e. this theory is $a \to au$ invariant but it is not time-translation invariant. In such situations, one has

$$\langle \Phi_s(\eta, \vec{x}) \Phi_s(\eta, 0) \rangle \underset{|\vec{x}| \to \infty}{\sim} F\left(\frac{a''}{a}, |\vec{x}|\right) \tag{27}$$

where F is a functional of (a''/a) and a function of $|\vec{x}|$. Since the spatial derivatives become unimportant for Eq. (26) for long wavelength modes, the dependence of F on (a''/a) becomes important in this $|\vec{x}| \to \infty$ limit.[4] The absence of this analogous time-translation invariance breaking term for $\delta\mathcal{A}$ in Eq. (23) is partly due to the axionic nature of $\mathcal{A}$ in addition to being in the conformal radial sector discussed previously. This is a time-independent conformal phase of the axionic theory.

The Fourier-space isocurvature spectrum corresponding to Eq. (25) is

$$\Delta_s^2 \propto k^2 \tag{28}$$

which is conventionally described as having a spectral index of $n_I = 3$. In other words, the large Γ limit and a conformally compatible boundary conditions for the background field Γ_0 allowed the scaled axion field $\mathcal{A}$ to settle into a tree-level conformal theory that does not see the expanding universe. Explicit mode computations shown in the subsequent sections will support this general expectation based on conformality arguments. We should also note that Eq. (16) indicates that the field $\delta Y = a\delta\Gamma$ is expected to behave as a massive field in the long wavelength limit owing to the mass scale provided by $Y^2 (\partial_\eta \theta_0)^2$ with a large $\partial_\eta \theta_0$ supporting a large Eq. (18). This implies that δY two-point function in the long wavelength limit will behave as the massive correlator in flat space giving $\langle \delta Y \delta Y \rangle \propto k^3$ which implies

$$\langle \delta\Gamma \delta\Gamma \rangle = C_Y k^3 / a^2 / (\partial_\eta \theta_0) \tag{29}$$

(where C_Y is a constant) during the time-independent conformal era when $\partial_\eta \theta_0 = \sqrt{\lambda} \Gamma_0(\eta_i) a(\eta_i)$ (see Appendix A that explains the appearance of $\partial_\eta \theta_0$ from a conformal representation perspective). As explained in the Appendix A, we cannot read off k^2 behavior of Eq. (28) from conformal invariance alone because of the spontaneous breaking scale $\partial_\eta \theta_0$: it is a result of knowing *time-independent* conformal invariance and masslessness of the $\delta\mathcal{A}$ field (the latter coming from the Goldstone property of the spontaneously broken $U(1)_{PQ}$ symmetry).

The mixing of δY with $\delta\mathcal{A}$ through the $\eta^{\mu\nu} Y^2 \partial_\mu \theta \partial_\nu \theta$ term after the spontaneous symmetry breaking term $\partial_\eta \theta_0$ is turned on in Eq. (16) leads to an interesting dispersion relationship. Instead

---

[4] This infinity here literally means $|\vec{x}|a \gg H^{-1}$.

of the dispersion relationship of a free massless theory, it will be that of a relativistic perfect fluid acoustic wave: i.e.

$$\frac{d\omega}{dk} = \frac{1}{\sqrt{3}} \tag{30}$$

where ω is the frequency associated with the lighter eigenmode. This is an indication that the axion here is a perturbation about a nontrivially interacting background medium. One obvious consequence of this is that the perturbations freeze out a bit earlier when $k \approx a(t_k)\sqrt{3}H$ during inflation in contrast with the situation when $\sqrt{3} \to 1$. The fact that the dispersion relationship here is linear in k is just as for a Nambu-Goldstone boson: the shift symmetry is still intact even though there is a nontrivial mixing. In field theoretic situations where the system acts approximately as an isotropic, adiabatic fluid, one expects the trace of the energy momentum tensor to vanish if the system is conformal $P \approx \rho/3$ which implies that the sound speed is as given by Eq. (30).[5]

Before moving on to the details, we should also remark about what the usual axion conformal phase is after the initial time-independent conformal phase ends and the Γ has settled to its minimum leading to the ordinary axion quantum fluctuation physics. The theory in that case is that of a spacetime-curvature induced massive scalar field

$$S \approx \int d^4x \frac{1}{2} \left\{ -\eta^{\mu\nu}\partial_\mu (a\Sigma) \, \partial_\nu(a\Sigma) + \left(\frac{a''}{a}\right) (a\Sigma)^2 \right\} \tag{31}$$

which does have manifest conformal invariance of Eq. (17), but not time translation invariance nor masslessness since during inflation $(a''/a) = 2/\eta^2$ which leads to a well-known tachyonic mass for $\mathcal{A} = a\Sigma$. Hence, we see that the theory which we are analyzing in detail in this paper is a theory that goes from a time-independent spontaneously broken conformal phase to a time-dependent conformal phase, latter of which is the usual axionic isocurvature quantum fluctuation theory during inflation.

3.   EXPLICIT QUANTIZATION IN THE CONFORMAL LIMIT

Although we have given a conformal limit argument in Sec. 2.2 for the spectral index $n_I = 3$, we have not justified the selection of the vacuum state in the situation in which the background field $\partial_\eta \theta_0$ is large. Also, given the fast rotation which kinetically mixes the radial mode with the angular mode, we expect the dispersion relationship to change from the standard one leading to order unity

---

[5] This follows from the conservation of dilatation current $j_\mu = T_{\mu\nu}x^\nu$ if the dilatation is assumed to arise from a recoordinatization. More about the relationship between the diffeomorphism representation and the spurion representation is explained in Appendix. A.

changes in the power spectrum. To address these issues, we quantize the theory in the conformal limit explicitly.[6]

3.1. Conformal limit power quantization and power spectra

As shown in the Appendix D, we can quantize the two real scalar degrees of freedom

$$\delta\psi^n = (\delta Y, \delta X)^n \equiv (a\delta\Gamma, a\delta\chi)^n \equiv (a\delta\Gamma, a\Gamma_0\delta\theta)^n \tag{32}$$

governed by the quadratically expanded action

$$
\begin{aligned}
S_2 = \int d\eta d^3x \Big\{ &-\frac{1}{2}\eta_{\mu\nu}\partial^\mu\delta Y \partial^\nu\delta Y - \frac{1}{2}\eta_{\mu\nu}\partial^\mu\delta X \partial^\nu\delta X \\
&- 2\delta Y\eta_{\mu\nu}\partial^\mu\delta X\partial^\nu\theta_0 + \frac{2\delta X\delta Y}{Y_0}\eta_{\mu\nu}\partial^\mu Y_0\partial^\nu\theta_0 + \frac{\delta X}{Y_0}\eta_{\mu\nu}\partial^\mu\delta X\partial^\nu Y_0 + \frac{\delta Y\eta_{\mu\nu}\partial^\mu\delta Y\partial^\nu a}{a} \\
&+ \frac{1}{2}(\delta X)^2\eta_{\mu\nu}\left(\frac{\partial^\mu Y_0\partial^\nu Y_0}{Y_0^2} + 2\frac{\partial^\mu a\partial^\nu a}{a^2} - 2\frac{\partial^\mu a\partial^\nu Y_0}{aY_0}\right) \\
&- \frac{1}{2}(\delta Y)^2\eta_{\mu\nu}\left(\partial^\mu\theta_0\partial^\nu\theta_0 + \frac{\partial^\mu a\partial^\nu a}{a^2}\right) - \left(-\frac{2M^2 a^2}{2} + \frac{3\lambda}{2}Y_0^2\right)(\delta Y)^2 \Big\}.
\end{aligned}
\tag{33}
$$

in the coordinates $ds^2 = a^2(\eta)\left(-d\eta^2 + |d\vec{x}|^2\right)$ using

$$[\delta\psi^n(\eta,\vec{x}), \delta\psi^m(\eta,\vec{x})] = 0, \tag{34}$$

$$[\pi^n(\eta,\vec{x}), \pi^m(\eta,\vec{x})] = 0, \tag{35}$$

$$[\delta\psi^n(\eta,\vec{x}), \pi^m(\eta,\vec{x})] = i\delta^{nm}\delta^{(3)}(\vec{x}-\vec{y}) \tag{36}$$

as usual. What is special in the scenario considered in this paper is that the coefficients involving $\{X_0, Y_0, a\}$ are generally time-dependent, but in the conformal limit described by Eqs. (18), (19), and (20), the coefficients become time-independent: e.g.

$$Y_0 \equiv a\Gamma_0 \approx Y_c = \frac{L^{1/3}}{\lambda^{1/6}} = \text{constant} \tag{37}$$

which follows from the conditions given in Eqs. (12) and (A8). Here, Y_c represents a constant conformal background radial solution.

Since we are going to compute the quantum correlator to 0th order in λ while Eq. (37) does not allow us to set $\lambda = 0$, an explanation of the expansion is in order. Note that this conformal limit

---

[6] After the quantization part of this work was completed, the work [56, 57] appeared which quantizes a similar theory and agrees with the results here. One main difference is that we present more details here regarding the axion spectrum and apply it to isocurvature and dark matter phenomenology.

background is a solution to the classical equation of motion

$$\frac{\delta S}{\delta \Phi^*} = 0 \tag{38}$$

which corresponds to leading $\hbar \to 0$ field path. Keeping the nonlinear interactions for the classical equation means we are treating $\lambda |\Phi|^2 \Phi$ to be on equal footing as $M^2 \Phi$. On the other hand we are computing the quantum dynamics with $\lambda \to 0$ in considering the quadratic quantum fluctuations for the quantum correlator. Hence, we are taking the limit

$$O(\lambda |\Phi|^2 a^2) \sim O(\lambda Y_0^2) \gtrsim O(M^2 a^2) \tag{39}$$

in the quadratic computation. Eq. (37) then says we are in the parametric region in which

$$\lambda^{2/3} L^{2/3} \gtrsim O(M^2 a^2) \tag{40}$$

which will break down when a^{-2} has sufficiently diluted $L^{2/3}$.

In this regime when $Y_0 = Y_c$ and $\partial_\eta \theta_0$ are constants, the Hamiltonian density simplifies to

$$\mathcal{H} = \frac{1}{2} (\partial_\eta \delta Y)^2 + \frac{1}{2} (\partial_\eta \delta X)^2 + \frac{1}{2} (\partial_i \delta \Gamma)^2 + \frac{1}{2} (\partial_i \delta \chi)^2 - \frac{1}{2} (\delta Y)^2 (\partial_\eta \theta_0)^2 + \left(\frac{3\lambda}{2} Y_c^2 \right) (\delta Y)^2. \tag{41}$$

The Fock state diagonalizing the Hamiltonian can be constructed using the ladder operators as

$$\delta \psi^n = \int \frac{d^3 p}{(2\pi)^{3/2}} \left[a_{\vec{p}}^{++} c_{++} V_{++}^n e^{-i\omega_{++}\eta} + a_{\vec{p}}^{+-} c_{+-} V_{+-}^n e^{-i\omega_{+-}\eta} + h.c. \right] e^{i\vec{p}\cdot\vec{x}} \tag{42}$$

where

$$V_{++}^n = \begin{pmatrix} 1 \\ \mathcal{R}_{++} \end{pmatrix}, \quad V_{+-}^n = \begin{pmatrix} 1 \\ \mathcal{R}_{+-} \end{pmatrix}, \tag{43}$$

$$\mathcal{R}_{++} \equiv i \left(\frac{-2 \left(\frac{L}{Y_c^2} \right) \omega_{++}}{\frac{1}{2} \left(\omega_{++}^2 - \omega_{+-}^2 \right) + (\lambda Y_c^2) + 2 \left(\frac{L}{Y_c^2} \right)^2} \right), \tag{44}$$

$$\mathcal{R}_{+-} \equiv i \left(\frac{2 \left(\frac{L}{Y_c^2} \right) \omega_{+-}}{\frac{1}{2} \left(\omega_{++}^2 - \omega_{+-}^2 \right) - (\lambda Y_c^2) - 2 \left(\frac{L}{Y_c^2} \right)^2} \right), \tag{45}$$

$$\omega_{s_1 s_2} \equiv s_1 \sqrt{k^2 + 3\lambda Y_c^2 + s_2 Y_c \sqrt{\lambda (4k^2 + 9\lambda Y_c^2)}}, \tag{46}$$

$$c_{++} c_{++}^* = -\frac{\left(1 - \mathcal{R}_{+-}^2 \right) \omega_{+-} - 2i\partial_\eta \theta_0 \mathcal{R}_{+-}}{2 \left(\mathcal{R}_{+-} \omega_{+-} - \mathcal{R}_{++} \omega_{++} \right) \left(\mathcal{R}_{+-} \omega_{++} - \mathcal{R}_{++} \omega_{+-} \right)}, \tag{47}$$

$$c_{+-} c_{+-}^* = -\frac{\left(1 - \mathcal{R}_{++}^2 \right) \omega_{++} - 2i\partial_\eta \theta_0 \mathcal{R}_{++}}{2 \left(\mathcal{R}_{+-} \omega_{+-} - \mathcal{R}_{++} \omega_{++} \right) \left(\mathcal{R}_{+-} \omega_{++} - \mathcal{R}_{++} \omega_{+-} \right)}. \tag{48}$$

Note that V_{++} and V_{+-} are not orthogonal. In the IR limit $1 \ll k^2 \ll \lambda Y_c^2$, the two distinct frequency-squared values are

$$\omega_{\pm-}^2 \approx \frac{k^2}{3} + O\left(\frac{k^4}{\lambda Y_c^2}\right), \tag{49}$$

and

$$\omega_{\pm+}^2 \approx 6\lambda Y_c^2 + \frac{5k^2}{3} + O\left(\frac{k^4}{\lambda Y_c^2}\right) \tag{50}$$

corresponding to low and high frequency solutions and are separated by a large $O\left(\lambda Y_c^2/k^2\right)$ hierarchy. In the UV limit,

$$\lim_{k \gg \lambda Y_c^2} \omega_{\pm\pm}^2 \to k^2 \tag{51}$$

and the two frequency solutions become degenerate. When excited with the lighter normal frequency $\omega_{\pm-}$ the fluctuations $\delta\Gamma, \delta\chi$ have a group velocity

$$\lim_{k \ll \sqrt{\lambda}Y_c} \frac{d\omega_{\pm-}}{dk} \approx \frac{1}{\sqrt{3}} \tag{52}$$

corresponding to a radiation fluid with sound speed squared $c_s^2 \approx 1/3$. This is what we naively expect from the conformal limit discussed in Sec. 2.2 if the conformal limit of this interacting system is behaving like a relativistic perfect fluid which has an equation of state $P = \rho/3$ owing to the conformal symmetry current conservation. As is well known, such a fluid has a sound speed

$$c_s^2 = \frac{\partial P}{\partial \rho} = \frac{1}{3} \tag{53}$$

which implies that acoustic waves travel with speed $1/\sqrt{3}$ matching the group velocity Eq. (52). Another interesting analogy comes from the tightly coupled cosmic microwave background radiation to the electrons just before recombination. In that situation, in the limit that the baryon loading vanishes, the speed of sound is $1/\sqrt{3}$. Physically, the fast scattering of the electrons is inducing photon pressure on the nonrelativistic electrons, setting up an acoustic wave, similar to how a $\partial_\eta\theta_0$-induced mixing is generating an axion pressure-supported acoustic wave in the mixture of axions and heavy radial fields.

To choose the vacuum, we define it as usual as

$$a_{\vec{p}}^{+\pm}|0\rangle = 0 \tag{54}$$

since the ladder operators diagonalize the Hamiltonian. The nonadiabaticity at the end of the conformal period may lead to particle production since the WKB vacuum after the conformal

period will be different from this vacuum. Any particles produced during such time periods will be inflated away.[7]

An interesting consequence of this quantized system is that the π^n commutator equation of Eq. (35) which usually is not very constraining induces a special constraint of

$$[\partial_\eta \delta X, \partial_\eta \delta Y] = -2i\partial_\eta \theta_0 \delta^{(3)}(\vec{x} - \vec{y}) \tag{55}$$

which makes the kinetic contributions to the isocurvature **cross** correlators of radial and angular mode temporarily nonzero as long as $\partial_\eta \theta_0$ is not negligible. This leads to $\langle \partial_\eta \delta \Gamma \partial_\eta \delta \chi \rangle \neq 0$ even though $\langle \delta \Gamma \delta \chi \rangle = 0$ during this time-independent conformal era when $\partial_\eta \theta_0$ is constant. Eventually, the time-independent conformal era ends when the background radial modes reaches the minimum of the effective potential making $\partial_\eta \theta_0 \to 0$ and in turn causing this kinetic cross correlation to disappear as the system leaves the time-independent conformal phase to enter the usual time-dependent conformal phase of the stabilized axions.

The correlation functions of radial and angular directions in the time-independent conformal region (before the transition of the radial field at time t_{tr} to f_{PQ}) is

$$\Delta^2_{\frac{\delta\Gamma}{\Gamma_0}\frac{\delta\Gamma}{\Gamma_0}}(\eta < \eta_{\mathrm{tr}}) = \frac{1}{\Gamma_0^2(\eta)a^2(\eta)}\frac{k^3}{2\pi^2}\left(|c_{++}|^2 + |c_{+-}|^2\right) \tag{56}$$

$$\Delta^2_{\frac{\delta\chi}{\Gamma_0}\frac{\delta\chi}{\Gamma_0}}(\eta < \eta_{\mathrm{tr}}) = \frac{1}{\Gamma_0^2(\eta)a^2(\eta)}\frac{k^3}{2\pi^2}\left(|c_{++}\mathcal{R}_{++}|^2 + |c_{+-}\mathcal{R}_{+-}|^2\right) \tag{57}$$

where $c_{+\pm}$ and $\mathcal{R}_{+\pm}$ depend on k. In Fig. 1, we plot the correlation functions given in Eqs. (56) and (59) and compare them with the analytic approximations. We illustrate that for modes $k \ll \partial_\eta \theta_0$, the radial and angular isocurvature fluctuations during $t < t_{\mathrm{tr}}$ exhibit spectral dependencies of k^3 and k^2 respectively. The complicated k-dependence simplifies to

$$\lim_{k \ll \partial_\eta \theta_0} \Delta^2_{\frac{\delta\Gamma}{\Gamma_0}\frac{\delta\Gamma}{\Gamma_0}}(\eta < \eta_{\mathrm{tr}}) \approx \left(\frac{1}{3^{1/2}2^{3/2}}\right)\frac{1}{\Gamma_0^2(\eta)a^2(\eta)}\frac{k^3}{2\pi^2\partial_\eta\theta_0}, \tag{58}$$

$$\lim_{k \ll \partial_\eta \theta_0} \Delta^2_{\frac{\delta\chi}{\Gamma_0}\frac{\delta\chi}{\Gamma_0}}(\eta < \eta_{\mathrm{tr}}) \approx \frac{1}{3^{1/2}}\left(\frac{H/(2\pi)}{\Gamma_0(\eta_i)}\right)^2\left(\frac{k}{a(\eta_i)H}\right)^2 \tag{59}$$

on large length scales. Although the spectral indices here can be inferred from the symmetry representations and minimal dynamical considerations of Appendix A, the details of $1/\sqrt{3}$ and

---

[7] Any effects on nongaussianities from this will be left for a future work.
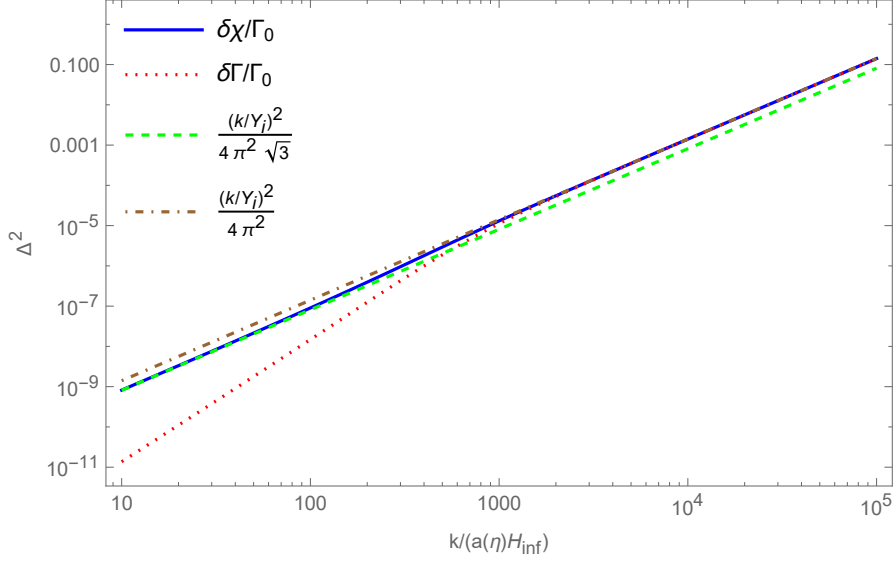
Figure 1: Plot illustrating the spectral dependence of the correlation functions given in Eqs. (57) and (56) corresponding respectively to the angular (solid blue) and radial (dotted red) directions in the time-independent conformal era. For modes $k \ll \partial_\eta \theta_0$, the radial and angular isocurvature fluctuations exhibit spectral dependencies of k^3 and k^2 respectively. The green dashed curve represents our analytic approximation taken from Eq. (59), where $Y_i = \Gamma_0(\eta_i)a(\eta_i)$. Note the presence of an additional normalizing factor of $1/\sqrt{3}$, resulting from the angular modes behaving like a radiation fluid with a sound speed $c_s^2 = 1/3$. Modes with $k \gg \partial_\eta \theta_0$ do not see the effective potential and thus resemble massless modes. These modes must be normalized with the usual Bunch-Davies (BD) vacuum state. The brown dotdashed curve provides an analytic approximation for pure massless modes normalized with the BD vacuum solution. The plot highlights smooth transition from the vacuum state for the strongly coupled axion, obtained from the minimization of the Hamiltonian density during the time-independent conformal era, to the usual BD solution. Notably, the spectral dependence of angular fluctuations $\propto k^2$ highlights that in the rotating axion model, angular fluctuations maintain conformality across all scales during $t < t_{\rm tr}$.

normalization factors appearing here are difficult to predict without explicit quantization. Although one may naively think $\partial_\eta \theta_0$ here acts as a scale similar to the horizon scale in ordinary curvature perturbations, making the spectral amplitude freeze out, the spectral amplitude is actually always approximately frozen during the time-independent conformal period. Since $\partial_\eta \theta_0 \gg a(\eta_i)H$ is typical for the parametric region of phenomenological interest, we can have a frozen subhorizon k^2 spectrum for a massless field. The $\delta\Gamma$ spectral index minus one is 3 while the $\delta\chi$ spectral index is characterized by $n_I - 1 = 2$ as anticipated. This says that the $\delta\chi$ correlator dominates over the $\delta\Gamma$ correlator by a factor of $\partial_\eta \theta_0/k$. The fact that $1/\sqrt{3}$ appears even for the massive $\delta\Gamma$ correlator is indicative of

the sound speed changing due to the presence of $\partial_\eta \theta$ induced mixing.

At approximately the time $t_{\rm tr}$, the time-independent conformal regime in this strongly mixed model comes to an end, and the radial field settles to the minimum of the potential at $f_{\rm PQ}$. From the EoM provided in Eq. (D3) for the axial perturbations $\delta\chi$, we infer that around this time, the axial perturbations transition to a massless axion state entering a time-dependent conformal era. Because $\Gamma_0(\eta)$ tends to follow $\delta\chi$ mode on superhorizon scales (see Appendix F) and because the radial kinetic energy is too small to generate nontrivial resonances, there is no evolution of Eq. (59) after the transition to the vacuum at time $t = t_{\rm tr}$. Therefore, the dimensionless power spectrum Eq. (59) can be used for $\eta > \eta_{\rm tr}$ as well. For modes that exit the horizon a long time after the radial field has settled to the minimum at $f_{\rm PQ}$, the spectrum is scale invariant. For these modes the initial amplitude of the axial field fluctuations is normalized with the usual BD vacuum state as $\sim 1/\sqrt{2k}$. Hence, we approximate the spectrum as

$$\lim_{k \gg \partial_\eta \theta_0} \Delta^2_{\frac{\delta\chi}{\Gamma_0} \frac{\delta\chi}{\Gamma_0}}(\eta \to 0) \approx \left(\frac{H/(2\pi)}{f_{PQ}} \right)^2 \tag{60}$$

which is the same as the usual equilibrium spectrum. In matching Eqs. (59) and (60), there is a sound-speed related factor shift in where the blue tilt region will match the plateau, and this is the hallmark of our current model flowing from one rotating phase conformal field theory to the usual Goldstone case which from the perspective Eq. (31) corresponds to a time-dependent scenario.

Note that Bunch-Davies boundary condition is in the limit $k/(aH) \to \infty$. If ∞ is interpreted modestly as $\partial_\eta \theta_0/k \gtrsim 1$, we see that the $\delta\Gamma$ correlation function dominates in the UV. This indicates that the kinetic term of $\delta\Gamma$ is important in the Bunch-Davies limit and $\delta\Gamma$ cannot be integrated out in this limit. Indeed, one can explicitly compute

$$\Delta^2_{\partial_\eta \delta\Gamma \partial_\eta \delta\chi}(k, \eta < \eta_{\rm tr}) = \frac{1}{a^2(\eta)} \frac{k^3}{2\pi^2} (i\partial_\eta \theta_0) \tag{61}$$

which says that there is a strong mixing between $\delta\chi$ and $\delta\Gamma$ in the modest kinematic range reasonable for standard Bunch-Davies boundary conditions.[8] Even more impressively, we know that **even** in the *small* k limit, there is essentially no distinction between the $\delta\Gamma$ kinetic correlator and the $\delta\chi$

---

[8] Because $\langle \partial_\eta \Gamma(\vec{x}) \partial_\eta \chi(\vec{y}) \rangle$ is not a Hermitian correlator, it does not have a direct measurability: the measurable correlation $\langle \partial_\eta \Gamma(\vec{x}) \partial_\eta \chi(\vec{y}) + \partial_\eta \chi(\vec{y}) \partial_\eta \Gamma(\vec{x}) \rangle$ vanishes at least at this order in perturbation theory. Nonetheless, the kinetic correlations will appear in quantum dynamics including interactions. We will leave this topic to a future investigation.

kinetic correlator

$$\lim_{k \ll \partial_\eta \theta_0} \Delta^2_{\partial_\eta \delta \Gamma \partial_\eta \delta \Gamma}(k, \eta < \eta_{\mathrm{tr}}) \approx \frac{1}{a^2(\eta)} \sqrt{\frac{3}{2}} \frac{k^3}{2\pi^2} \left(\partial_\eta \theta_0\right), \tag{62}$$

$$\lim_{k \ll \partial_\eta \theta_0} \Delta^2_{\partial_\eta \delta \chi \partial_\eta \delta \chi}(k, \eta < \eta_{\mathrm{tr}}) \approx \frac{1}{a^2(\eta)} \sqrt{\frac{2}{3}} \frac{k^3}{2\pi^2} \left(\partial_\eta \theta_0\right), \tag{63}$$

in the time-independent conformal phase. This says you cannot really integrate out $\delta \Gamma$ for any k if you care about the kinetic term.[9] This implies that the only way to justify completely integrating out the $\delta \Gamma$ mode in this cosmological context is not to use the standard Bunch-Davies conditions, but require a non-standard restriction of modes that satisfy

$$\frac{k}{\partial_\eta \theta_0} \ll 1 \tag{64}$$

and neglect kinetic aspects of inhomogeneity correlator physics.

3.2. Post-time-independent-conformal-era time evolution

After the time-independent conformal era ends, what happens to these spectra? In this section, we will consider the time evolution of our coupled system during inflation and determine the dimensionless power spectrum for the axial and radial fields as $\eta \to 0$. We consider the equation of motion for the background field Γ_0 derived from Eq. (11) and substitute $\partial_\eta \theta_0$ with the conserved angular momentum L defined by Eq. (12):

$$\partial_\eta^2 \Gamma_0 + 2 \frac{\partial_\eta a}{a} \partial_\eta \Gamma_0 + \left(-2M^2 a^2 + \lambda \Gamma_0^2 a^2 - \left(\frac{L}{a^2 \Gamma_0^2}\right)^2\right) \Gamma_0 = 0. \tag{65}$$

Note the in the limit $\eta \to 0$, the radial field settles to the minimum

$$\Gamma_{0,\mathrm{min}} = M \sqrt{\frac{2}{\lambda}} \equiv f_{\mathrm{PQ}} \tag{66}$$

and the angular velocity decays as H^3/a^2. Using the full solution for the background field Γ_0, we can obtain the evolution of the linear perturbations $\delta \phi_k^n = (\delta \Gamma_k, \delta \chi_k)^n$ for each mode k by solving the mode function $h_k^{jm}(\eta)$ using the Eq. (D15) derived in Appendix D:

$$\left[\delta^{nj} \partial_\eta^2 + \kappa^{nj} \partial_\eta + \left(\mathcal{W}^2\right)^{nj}\right] h_k^{jm}(\eta) = 0 \tag{67}$$

---

[9] Of course kinetic terms become more important for larger k values.

where n is the flavor index and m runs over distinct frequencies. We set the initial conditions at η_i for each of the two frequency solutions as follows:

$$
\begin{pmatrix} h_k^1(\eta) \\ h_k^2(\eta) \end{pmatrix}_{\eta=\eta_i}^{++} = c_{++} \begin{pmatrix} V_{++}^1(\eta_i) \\ V_{++}^2(\eta_i) \end{pmatrix} e^{-i\omega_{++}\eta_i}, \qquad \begin{pmatrix} \partial_\eta h_k^1(\eta) \\ \partial_\eta h_k^2(\eta) \end{pmatrix}_{\eta=\eta_i}^{++} = -i\omega_{++} \begin{pmatrix} h_k^1(\eta) \\ h_k^2(\eta) \end{pmatrix}_{\eta=\eta_i}^{++} \tag{68}
$$

and

$$
\begin{pmatrix} h_k^1(\eta) \\ h_k^2(\eta) \end{pmatrix}_{\eta=\eta_i}^{+-} = c_{+-} \begin{pmatrix} V_{+-}^1(\eta_i) \\ V_{+-}^2(\eta_i) \end{pmatrix} e^{-i\omega_{+-}\eta_i}, \qquad \begin{pmatrix} \partial_\eta h_k^1(\eta) \\ \partial_\eta h_k^2(\eta) \end{pmatrix}_{\eta=\eta_i}^{+-} = -i\omega_{+-} \begin{pmatrix} h_k^1(\eta) \\ h_k^2(\eta) \end{pmatrix}_{\eta=\eta_i}^{+-}. \tag{69}
$$

For modes $k \ll \partial_\eta\theta_0$, the above initial conditions correspond to the mode amplitudes

$$
\begin{pmatrix} h_k^1(\eta) \\ h_k^2(\eta) \end{pmatrix}_{\eta=\eta_i}^{++} \approx \frac{1}{6^{3/4}\sqrt{\partial_\eta\theta_0}} \begin{pmatrix} \sqrt{3} \\ -i\sqrt{2} \end{pmatrix} \tag{70}
$$

and

$$
\begin{pmatrix} h_k^1(\eta) \\ h_k^2(\eta) \end{pmatrix}_{\eta=\eta_i}^{+-} \approx \frac{1}{\sqrt{2}3^{3/4}} \begin{pmatrix} \sqrt{k}/\partial_\eta\theta_0 \\ i\sqrt{3}/\sqrt{k} \end{pmatrix} \tag{71}
$$

such that the canonical field amplitudes have the ratios

$$
\left| \frac{\delta\Gamma_k(\eta_i)}{\delta\chi_k(\eta_i)} \right|^{++} \approx \sqrt{\frac{3}{2}}, \tag{72}
$$

and

$$
\left| \frac{\delta\Gamma_k(\eta_i)}{\delta\chi_k(\eta_i)} \right|^{+-} \approx \frac{k}{\sqrt{3}\partial_\eta\theta_0} \tag{73}
$$

for the $++$ and $+-$ frequency solutions respectively. The fact that the radial mode amplitude vanishes in the $k \to 0$ limit indicates that the smaller frequency mode is primarily made of the angular mode at the initial time. Using these initial conditions for the mode functions h_k^{nr}, we evolve the coupled system from η_i to a late time η_f when the background radial field Γ_0 is settled at $f_{\rm PQ}$ and all modes of interest k are super-horizon. The above results also imply that the amplitude of the axial fluctuations for modes with $k \ll \partial_\eta\theta_0$ is dominated by the lighter frequency (ω_{+-}) solutions since

$$
\lim_{k \ll \partial_\eta\theta_0} \frac{|\delta\chi_k(\eta_i)|^{++}}{|\delta\chi_k(\eta_i)|^{+-}} \approx O\left(\sqrt{\frac{k}{\partial_\eta\theta_0}} \right). \tag{74}
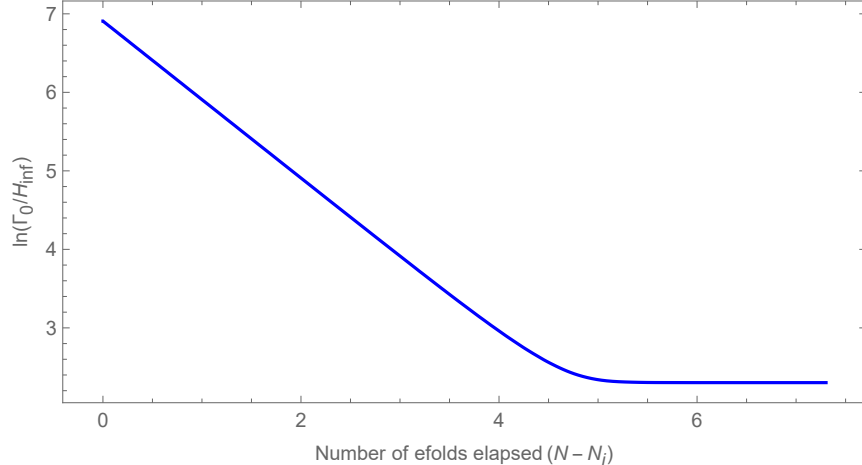$$

Figure 2: Plot showing the time evolution of the background radial field $\Gamma_0(t)$ during the quasi-dS phase of inflation. Starting from $\Gamma_0(\eta_i) = 1000H_{\text{inf}}$, the field takes approximately 5 efolds to settle to the minimum $M\sqrt{2/\lambda} = 10H_{\text{inf}}$. The initial evolution of the field $a(\eta)\Gamma(\eta) = $ constant.

3.2.1. Adiabatic time-evolution example

Let us consider an example where we initialize the background radial field Γ_0 at η_i with the time-independent conformal solution

$$a(\eta_i)\Gamma_0(\eta_i) = Y_c \equiv \frac{L^{1/3}}{\lambda^{1/6}}. \tag{75}$$

Furthermore, in this example, we set $H = H_{\text{inf}}$, $\lambda = 1$ and $f_{\text{PQ}} = 10H_{\text{inf}}$ such that $M = f_{\text{PQ}}/\sqrt{2}$. We choose the conserved angular momentum $L = \sqrt{\lambda}10^9 H_{\text{inf}}^3 a^3(\eta_i)$, hence $\Gamma_0(\eta_i) = 1000H_{\text{inf}}$. Note that even though the radial field has a large displacement away from the minimum along a quartic potential, the effective radial mass is only order H_{inf} due to the effects of the angular momentum. This cancellation is nothing more than the statement that stable orbits not passing through the origin exist with angular momentum conservation, and if the space does not expand, this orbit can persist indefinitely.

In Fig. 2, we show the time evolution of the background radial field. We observe that for our choice of fiducial values, the radial field takes approximately 5 efolds to settle to the minimum. This is close to the analytic estimate

$$\Delta N_{\text{settle}} \approx \ln\left(\frac{Y_c(\eta_i)/a(\eta_i)}{f_{\text{PQ}}\sqrt{1 + H^2/M^2}}\right). \tag{76}$$

In Fig. 3, we show the time evolution of the corresponding radial and axial mode functions for the two frequency solutions $\omega_{+\pm}$ for a fiducial wavenumber $k/a(\eta_i) = 10$. The mode amplitudes h_k^{2r}
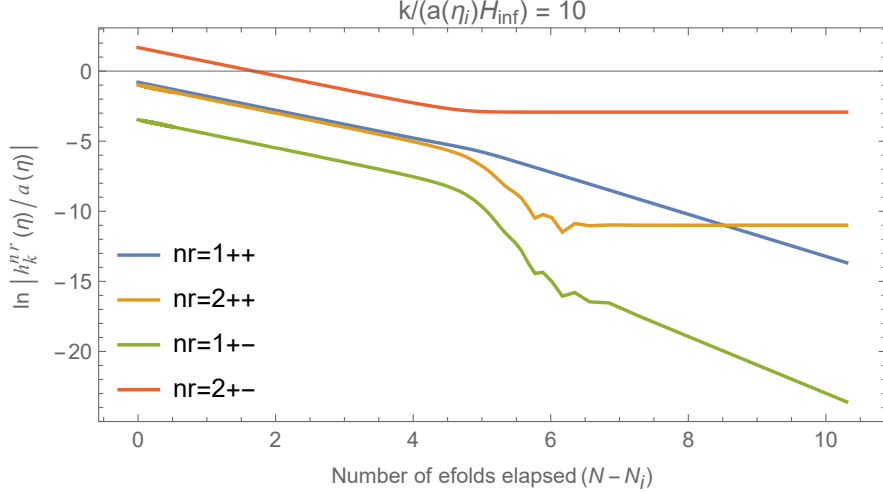
Figure 3: Plot showing the time evolution of the mode functions h_k^{nr}/a during the quasi de-Sitter phase of inflation for a fiducial mode $k/a(\eta_i) = 10H_{\rm inf}$ where the background radial field moves along a trajectory as expected in the time-independent conformal period as shown in Fig. 2. The mode amplitudes $h_k^{2+\pm}/a$ corresponding to the axial field freeze out when the background radial field settles to the minimum while the radial perturbations corresponding to $h_k^{1+\pm}$ persist in their massive state, undergoing continued decay.

corresponding to the axial field ($n = 2$) freeze out when the background radial field settles to the minimum at time t_{tr}. In contrast, the radial perturbations corresponding to h_k^{1r} persist in their massive state, undergoing continued decay. For the modes $k < \partial_\eta \theta_0 \equiv \sqrt{\lambda} Y_c$, the mode function h_k^{2r} corresponding to the lower frequency solution $\omega_r = \omega_{+-}$ has the larger amplitude. This is mainly due to the overall normalization factor of $1/\sqrt{\omega_r}$. Hence, a lower frequency yields a comparatively larger mode amplitude.

4. DEFORMATIONS AWAY FROM TIME-INDEPENDENT CONFORMAL LIMIT

The previous section described a special initial condition leading to a time-independent $\Gamma_0(\eta)a(\eta)$, leading to a time-independent conformal theory. Such cases are the analogs of circular orbits in mechanics. In this section, we describe deformations away from this time-independent conformal limit such that $\Gamma_0(\eta)a(\eta)$ will have oscillations. These will imprint oscillations into the power spectrum as we will show.

4.1. Equations of motion

Eq. (11) implies the background equations of motion (EoM) for the radial and angular degrees of freedom of

$$\partial_\eta^2 \Gamma_0 + 2\frac{\partial_\eta a}{a}\partial_\eta \Gamma_0 + \left(-2M^2 a^2 + \lambda\Gamma_0^2 a^2 - (\partial_\eta\theta_0)^2\right)\Gamma_0 = 0 \tag{77}$$

$$\partial_\eta^2\theta + 2\frac{\partial_\eta a}{a}\partial_\eta\theta_0 + 2\frac{\partial_\eta\Gamma_0}{\Gamma_0}\partial_\eta\theta_0 = 0 \tag{78}$$

where we have as usual assumed the background field to be spatially independent like the background metric. We distinguish the spatially inhomogeneous fluctuations of quantities Q with δQ. Eq. (78) leads to the conserved angular momentum L as defined in Eq. (12). This can be interpreted as there being a comoving homogeneous $U(1)$ charge density $\Gamma_0^2 \partial_t \theta_0$ that dilutes as a^{-3}. We also note from Eq. (77) that the background radial field has a force from $(\partial_\eta\theta_0)^2\,\Gamma_0$ that can cancel a part of $\left(\lambda\Gamma_0^3 - 2M^2\Gamma_0\right)a^2$ depending on the size of the angular momentum L. This is the key cancellation that allows the radial roll to be slow similar to the flat direction situation of [49] which is only lifted by $O\left(H^2\right)$ mass terms. The linear order perturbation variables $\delta\Gamma$ and $\delta\chi \equiv \Gamma_0\delta\theta$ in Fourier space satisfy the mode equations given in Eqs. (D2) and (D3). Here, we note that one can easily identify most of the axial fluctuation $\delta\Sigma$ with $\delta\chi$ since

$$\delta\Sigma = \Gamma\delta\theta + \theta\delta\Gamma \tag{79}$$

and in the limit $\delta\Gamma/\Gamma \ll \delta\theta/\theta$, the axial fluctuations are given as $\delta\Sigma \approx \delta\chi$. Eqs. (D2) and (D3) show that the fluctuations in the radial and angular directions are coupled at linear order via the dominant quadratic interaction term $\mathcal{L}_{\mathrm{int}} \supset -2\delta\Gamma a^2\eta_{\mu\nu}\partial^\mu\delta\chi\partial^\nu\theta_0$. This spontaneous conformal symmetry breaking induced coupling is a novel feature of field fluctuations about a rotating background.

In Sec. 3 we highlighted that the coupled $\delta\Gamma - \delta\chi$ system can be diagonalized with two sets of normal frequencies denoted as ω_{++} and ω_{+-}. In the IR limit corresponding to modes with $k^2 \ll \lambda Y_c^2$, the lowest frequency ω_{+-} has a dispersion relationship that is linear in k and the associated mode function resembles a Goldstone mode. In this limiting case corresponding to a Goldstone mode, it is possible to integrate out the radial mode $\delta\Gamma$ and obtain a decoupled EoM for the axial field fluctuations $\delta\chi$. To this end, we rewrite the EoM for the scaled radial fluctuation δY from Eq. (D7) and neglect the kinetic term $\partial_\eta^2\delta Y$:

$$-\partial_i^2\delta Y - 2\partial_\eta\theta_0\partial_\eta\delta X + \left(-2M^2 a^2 + 3\lambda Y_0^2 - (\partial_\eta\theta_0)^2 - \frac{\partial_\eta^2 a}{a}\right)\delta Y + 2\partial_\eta\theta_0\left(\frac{\partial_\eta Y_0}{Y_0}\right)\delta X = 0. \tag{80}$$

As noted in the discussion around Eq. (64), we can justify this step using the fact that we are not concerned with kinetic correlators. Going to the Fourier space and evaluating within the conformal regime, we obtain the expression

$$\left(k^2 - 2M^2 a^2 + 3\lambda Y_0^2 - (\partial_\eta \theta_0)^2 - \frac{\partial_\eta^2 a}{a}\right)\delta Y_k = 2\partial_\eta \theta_0 \partial_\eta \delta X_k. \tag{81}$$

The above expression allows us to replace δY_k in the EoM for the axial field. Thus, we arrive at the following decoupled EoM for the scaled axial field δX:

$$\partial_\eta^2 \delta X_k + 2\partial_\eta \theta_0 \, \partial_\eta \left(\frac{2\partial_\eta \theta_0 \partial_\eta \delta X_k}{\left(k^2 - 2M^2 a^2 + 3\lambda Y_0^2 - (\partial_\eta \theta_0)^2 - \frac{\partial_\eta^2 a}{a}\right)}\right)$$
$$+ \left(k^2 - 2M^2 a^2 + \lambda Y_0^2 - (\partial_\eta \theta_0)^2 - \frac{\partial_\eta^2 a}{a}\right)\delta X_k = 0 \tag{82}$$

which can be rewritten as

$$\partial_\eta^2 \delta X_k \left(1 + \frac{4(\partial_\eta \theta_0)^2}{\left(k^2 - 2M^2 a^2 + 3\lambda Y_0^2 - (\partial_\eta \theta_0)^2 - \frac{\partial_\eta^2 a}{a}\right)}\right)$$
$$+ \left(k^2 - 2M^2 a^2 + \lambda Y_0^2 - (\partial_\eta \theta_0)^2 - \frac{\partial_\eta^2 a}{a}\right)\delta X_k \approx 0 \tag{83}$$

where the factor associated with the kinetic term $\partial_\eta^2 \delta X_k$ evaluates to

$$\left(1 + \frac{4(\partial_\eta \theta_0)^2}{\left(k^2 - 2M^2 a^2 + 3\lambda Y_0^2 - (\partial_\eta \theta_0)^2 - \frac{\partial_\eta^2 a}{a}\right)}\right) \approx 3 \tag{84}$$

in the IR limit $\left(k \ll \sqrt{\lambda}Y_c\right)$ of the time-independent conformal solution $\left(\sqrt{\lambda}Y_c = \partial_\eta \theta_0\right)$. Therefore, in this limiting scenario, the strong coupling with the radial mode only changes the overall normalization for the kinetic term of $\delta \chi$.

In time coordinate t, the mass-squared term for the perturbations $\delta \chi$ can be identified from the decoupled EoM as

$$m_{\delta \chi}^2 = -\frac{\partial_t^2 \Gamma_0}{\Gamma_0} - 3\frac{\partial_t \Gamma_0}{\Gamma_0} = -2M^2 + \lambda \Gamma_0^2 - \frac{L^2}{a^6 \Gamma^4} \tag{85}$$

which goes to zero when the radial field settles to its vacuum state, say at time t_{tr}, and the angular momentum term is negligible. In this limit when $\delta \chi$ becomes massless, the quantum fluctuation mode $\delta \chi$ does not decay any further, whereas modes decay when $m_{\delta \chi}^2$ is non-negligible (even if the

modes are superhorizon). The isocurvature spectrum has a k dependence that is usually parameterized by the isocurvature spectral index n_I:

$$\Delta_s^2(k) \propto k^{n_I - 1}. \tag{86}$$

For a slowly varying mass of the linear spectator fluctuation $\delta\chi$, the decoupled EoM in Eq. (83) suggests that the spectral index n_I can be evaluated as

$$n_I(k) - 1 = 3 - 3\sqrt{1 - \frac{4}{9}m_{\delta\chi}^2(k)} \tag{87}$$

where $m_{\delta\chi}^2(k)$ is the effective mass-squared function from Eq. (85) evaluated at a time t_k when $k/a(t_k) \approx 1$. Hence, $m_{\delta\chi}^2(k)$ must be at least $O\left(H^2\right)$ for a blue isocurvature power spectrum, which can be achieved early in the evolution of $\Gamma(t)$ due to the cancellation between $\lambda\Gamma_0^2$ and $\dot{\theta}^2$. For the time-independent conformal solution where $Y_0 \equiv a\Gamma_0 = $ constant until $t < t_{tr}$, we have

$$-2M^2 + \lambda\Gamma_0^2 - \frac{L^2}{a^6\Gamma^4} = \frac{\partial_\eta^2 a}{a^3} = 2H^2 \quad \forall t < t_{tr} \tag{88}$$

which yields

$$m_{\delta\chi}^2(k < k_{tr}) = 2H^2 \tag{89}$$

and a spectral index

$$n_I(k < k_{tr}) - 1 = 2 \tag{90}$$

where the scale associated with the transition t_{tr} is given as

$$k_{tr} = \frac{a(\eta_{tr})}{a(\eta_i)}k_i. \tag{91}$$

For k-modes such that $t_k \gtrsim t_{tr}$ and $\dot{\theta}(t_k)$ is negligible, the $\delta\chi(t > t_k)$ spectator is massless, the $\delta\chi$ power spectrum flattens out and becomes scale invariant. This region is recognized as a massless plateau characterized by the familiar $[H^2/(2\pi f_{\rm PQ})]^2$ isocurvature amplitude. In contrast, the fluctuation $\delta\Gamma$ in the radial field has an effective mass-squared term $m_{\delta\Gamma}^2 = m_{\delta\chi}^2 + 2\lambda\Gamma_0^2$. In the limit $\Gamma \to f_{\rm PQ}$ and negligible angular velocity, the superhorizon fluctuations in $\delta\Gamma$ can continue to decay if $2\lambda f_{\rm PQ}^2 > 9/4H^2$ and will not contribute significantly to the power spectrum due to the decay. Preventing the decay will require $2\lambda f_{\rm PQ}^2 < O\left(H^2\right)$ such that radial fluctuations can also contribute to the overall power spectrum. However, these cases do not give rise to a time-independent conformal background solution as explained in Sec. 2 and thus do not result in an extremely blue spectral index (e.g. $n_I > 2.4$ [5]).

In Sec. 4.3, we will study how deviations away from the time-independent conformal solution impact the effective mass-squared parameter $m_{\delta\chi}^2$ in Eq. (85), and thus determine a particular parametric window of initial conditions within which one can obtain large blue isocurvature power spectrum for a rotating spectator field Φ.

4.2. Non-rotating scenario

Before we present the rotating case, we will briefly comment on the non-rotating complex scalar dynamics during inflation in the context of a quartic potential. In such cases, the angular velocity is taken to be zero and hence the net angular momentum is negligible. During inflation if the radial field Γ is frozen at some large displacement Γ_i, at some initial time t_i, away from the stable vacuum Γ_{vac}, the isocurvature fluctuations in the angular direction are scale-invariant and can be suppressed due to largeness of Γ_i. After Γ starts to roll towards Γ_{vac} due to the Hubble expansion rate dropping below the large mass of order $\sqrt{\lambda}\Gamma$, based on arguments similar to that presented around Eq. (16), one might naively conclude that there is a scale invariant isocurvature during the roll towards the minimum. However, this would be incorrect since Eq. (A8) shows that $Y_0 = 0$ with $\dot{\theta} = 0$ (i.e. rotations turned off), which contradicts the time-independent conformality requirement $Y_0 \gg \sqrt{a''/a}$.

Furthermore, after reaching the minimum, large amplitude oscillations of the background radial field can lead to parametric resonant enhancement of the angular fluctuations $\delta\chi$. Alternatively, if we consider large radial displacements such that $\lambda\Gamma^2/H^2 \gg 1$ during inflation, where the maximum radial displacement is bounded by the spectator condition given in Eq. (15), then the radial field is not frozen and oscillations of the radial field during inflation will give rise to similar parametric resonance (PR) effects for the isocurvature fluctuations.

More explicitly, the solution to the non-rotating background radial EoM in Eq. (77) for a quartic potential is given by elliptic functions. When the amplitude is large such that $\lambda\Gamma_0^2/H^2 \gg 1$, the elliptic solution can be approximated as ([59, 60])

$$\Gamma_0(t) \approx \Gamma_i e^{-H(t-t_i)} \cos\left(c\sqrt{\lambda}\Gamma_i/H\left(1 - e^{-H(t-t_i)}\right)\right) \tag{92}$$

where $c \approx 0.847$, Γ_i is the radial displacement at an initial time t_i, and we have considered a quasi de-Sitter scale factor $a(t)/a(t_i) = \exp(H(t - t_i))$ during inflation for an approximately constant inflationary Hubble parameter. As noted in the introduction, the field rolls down to the minimum

in a Hubble time. Due to the oscillating background radial field, the linearized EoM for the axial fluctuations $\delta\chi$ in Eq. (D3) now has a large amplitude oscillating mass-squared term

$$m_{\delta\chi}^2 \approx \lambda\Gamma_i^2 e^{-2H(t-t_i)} \cos^2\left(c\sqrt{\lambda}\Gamma_i/H\left(1 - e^{-H(t-t_i)}\right)\right). \tag{93}$$

In the absence of angular rotations, the EoM in Eq. (D7) for the scaled linear fluctuations $X = a\delta\chi$ takes the form

$$\partial_\eta^2 X + \left(k^2 + \left(-2M^2a^2 + \lambda Y_i^2 \cos^2\left(c\sqrt{\lambda}Y_i\left(\eta - \eta_i\right)\right) - \frac{\partial_\eta^2 a}{a}\right)\right)X(\eta) = 0 \tag{94}$$

where we have substituted $Y_0 = a\Gamma_0$ from the expression in Eq. (92). The above expression can be reframed in the form of a general Mathieu differential equation:

$$\partial_z^2 X + \left(A_\chi + 2q_\chi \cos\left(2z\right)\right)X = 0 \tag{95}$$

for

$$z = c\sqrt{\lambda}Y_i\left(\eta - \eta_i\right), \tag{96}$$

$$A_\chi = \frac{k^2 - 2M^2a^2 - \frac{\partial_\eta^2 a}{a}}{c^2\lambda Y_i^2} + 2q_\chi, \tag{97}$$

$$q_\chi = \frac{1}{4c^2}. \tag{98}$$

We note that the Mathieu parameter q_χ appears constant only as long as $\lambda\Gamma^2/H^2 \gg 1$. As $\lambda\Gamma^2/H^2 \to 1$, the background radial field cannot be approximated through elliptic functions and hence the angular fluctuations do not satisfy Mathieu equation anymore. Substituting for the value of c from above, we infer that $q_\chi \approx 0.35$ and $A_\chi \approx 2q_\chi$ for modes with $k^2 \ll \lambda Y_i^2$. For these modes, PR occurs in the first instability band. This results in a large exponential amplification of the fluctuations and may result in the formation of axion strings until back-reaction ceases PR. However, the inflation eventually dilutes these away and any disastrous cosmological effects from them are generically avoided.[10] Modes that lie barely outside the instability band do not undergo PR and extend over a short Δk-range of approximately $\Delta k/k_i \sim O(10)$. In Sec. 5, we will revisit the concept of PR resulting from minor deviations from the time-independent conformal solution and provide a thorough discussion on the underlying Mathieu system.

---

[10] In principle, these may produce gravity waves. We will defer the investigation of this issue to a future work.

4.3. Rotating scenario

As discussed around Eq.(87), to achieve a large blue isocurvature power spectrum we require that the background radial field Γ or the angular fluctuations $\delta\chi$ have an effective mass of $O(H)$ for a suitable N_{blue} number of e-folds during inflation. The blue-tilted part of the isocurvature spectrum has an approximate $\Delta k/k_i$-range equal to $\exp(N_{\text{blue}})$ and hence N_{blue} provides a parametric cutoff for the transition of the isocurvature power spectrum from a blue region to a massless plateau. The above requirements can be easily fulfilled for a tuned rotating complex scalar field Φ during inflation. We will now discuss this parametric range and dynamics in detail, computing an analytic estimate of the isocurvature spectrum as well as an expression for the parametric tuning. The perturbations away from the $n_I = 3$ limit can be viewed as perturbing the boundary conditions away from the time-independent conformal limit case presented in Appendix A.

We begin with the EoM for the background field $Y_0 = a\Gamma_0$:

$$\partial_\eta^2 Y_0 + \left(-2M^2 a^2 - \frac{\partial_\eta^2 a}{a} + \lambda Y_0^2 - \left(\frac{L}{Y_0^2}\right)^2\right) Y_0 = 0 \tag{99}$$

The above EoM implies that the time-independent conformal radial field Y_0 has an effective potential

$$V_{Y_0}(\eta) = \frac{1}{2}\left(-\frac{2M^2 + 2H^2}{H^2\eta^2} + \frac{1}{2}\lambda Y_0^2 + \frac{L^2}{Y_0^4}\right)Y_0^2 + \text{constant}. \tag{100}$$

For a constant background solution, the potential is driven by the quartic (self-interaction) term with an appropriately large angular velocity and a comparatively negligible Hubble friction and mass terms:

$$\lambda Y_0^2 \gg \frac{2M^2 + 2H^2}{H^2\eta^2} \implies \lambda \Gamma_0^2(\eta) \gg 2M^2 + 2H^2. \tag{101}$$

Thus, for a large angular velocity, the effective potential has a time-dependent local minimum at

$$Y_0(\eta) = (1 + \delta(\eta))\,Y_c \tag{102}$$

where $|\delta(\eta)| \ll 1$.

To study the quantum inhomogeneities about a background solution where $\delta(\eta)$ is nontrivial, we will below introduce two parameters $\{\kappa, \epsilon_L\}$ that control the deformations away from the time-independent conformal limit. Consider an initial displacement of the scaled radial field

$$Y_0(\eta_i) = Y_i \gg f_{\text{PQ}}a(\eta_i). \tag{103}$$

and parameterize initial radial velocity as

$$\partial_\eta Y_0|_{\eta_i} = \kappa\sqrt{6\lambda}Y_i^2 \tag{104}$$

at some initial time η_i and where κ is a dimensionless number. For a rotating ($L \neq 0$) complex scalar field, we parameterize the angular velocity as

$$\partial_\eta \theta_0|_{\eta_i} = (1 - \epsilon_L)\sqrt{\lambda}Y_i. \tag{105}$$

The corresponding value of the conserved angular momentum L is given as

$$L = (1 - \epsilon_L)\sqrt{\lambda}Y_i^3 \tag{106}$$

With this parameterization, a value of $\kappa = \epsilon_L = 0$ refers to the situation where the angular kinetic gradient approximately cancels with the radial potential gradient term at t_i with the residual $2M^2 \ll \lambda\Gamma_i^2$. This is the time-independent conformal limit boundary condition presented earlier. As we will show now, the approximate cancellation with $|\epsilon_L| \ll 1$ results in a pseudo-flat direction in radial dynamics that is only lifted by an $O(H^2)$ mass-squared term after integrating out residual UV degree of freedoms which arise as a result $\epsilon_L \neq 0$. Hence, there exists a parametric window for ϵ_L within which the leading approximation of a time-independent conformal background solution is stable against UV oscillations.[11]

With the above parameterization, the new time-independent conformal background solution is

$$Y_c = (1 - \epsilon_L)^{1/3}Y_i. \tag{107}$$

Next we write the complete solution of the background radial field as

$$Y_0(\eta) = Y_c + \Delta Y_0(\eta) \tag{108}$$

and substitute into Eq. (99) to obtain an EoM for ΔY_0:

$$\partial_\eta^2 (Y_c + \Delta Y_0) + \left(-2M^2 a^2 - \frac{\partial_\eta^2 a}{a} + \lambda \left(Y_c^2 + \Delta Y_0^2 + 2Y_c \Delta Y_0\right) - \frac{L^2}{(Y_c + \Delta Y_0)^4}\right)(Y_c + \Delta Y_0) = 0. \tag{109}$$

---

[11] A similar parameterization was given in [61] where the authors found numerically that the PR doesn't occur if $|\epsilon_L| \lesssim 0.2$. Therein, the authors show that post-inflation if $|\epsilon_L| \lesssim 0.2$, the rotating PQ field can lead to kinetic misalignment mechanism for axion production. However, in this paper, we are interested in rotations that occur during inflation and decay before the end of inflation.

Considering initial displacements and velocities not significantly deviating from a conformal solution Y_c, and thus parameterized by small values of ϵ_L and κ, we can examine small-amplitude oscillations $\Delta Y_0 \ll Y_c$. Hence, we linearize the EoM for ΔY_0 as

$$\partial_\eta^2 (\Delta Y_0) + \left(6\lambda Y_c^2\right) \Delta Y_0 \approx \left(2M^2 a^2 + \frac{\partial_\eta^2 a}{a}\right) Y_c \tag{110}$$

where the $O\left(H^2\right)$ terms on the RHS induce supplementary small amplitude deviations away from a constant background solution even when $\epsilon_L = \kappa = 0$. Using the initial condition $\Delta Y_0(\eta_i) = Y_i - Y_c$ and $\partial_\eta \Delta Y_0|_{\eta_i} = \kappa\sqrt{6\lambda} Y_i^2$ and by defining a new frequency parameter

$$f = \sqrt{6\lambda} Y_c \equiv \sqrt{6\lambda} Y_i \left(1 - \epsilon_L\right)^{1/3} \tag{111}$$

we obtain the approximate solution

$$\Delta Y_0(\eta) \approx (Y_i - Y_c) \cos\left(f\left(\eta - \eta_i\right)\right) + \frac{\sqrt{6} Y_c \left(2M^2/H^2 + 2\right) + 6\kappa\sqrt{\lambda} Y_i^2 \eta_i}{\sqrt{6} f \eta_i} \sin\left(f\left(\eta - \eta_i\right)\right)$$
$$+ Y_c \left(2M^2/H^2 + 2\right) \left(\cos\left(f\eta\right)\left(Ci\left(f\eta_i\right) - Ci\left(f\eta\right)\right) + \sin\left(f\eta\right)\left(Si\left(f\eta_i\right) - Si\left(f\eta\right)\right)\right) \tag{112}$$

where we have taken $\frac{\partial_\eta^2 a}{a} = 2H^2$ and Ci, Si are cosine- and sine-integral functions respectively defined as

$$Ci(z) \equiv -\int_z^\infty \frac{dt}{t} \cos t \tag{113}$$

$$Si(z) \equiv \int_0^z \frac{dt}{t} \cos t. \tag{114}$$

The oscillations have a constant frequency f in conformal time coordinate. During the conformal regime when $f\eta \gg 1$, we can reduce the Ci, Si functions in the above solution to obtain an approximate result:

$$\Delta Y_0(\eta) \approx (Y_i - Y_c) \cos\left(f\left(\eta - \eta_i\right)\right) + \frac{\kappa Y_i^2}{Y_c} \sin\left(f\left(\eta - \eta_i\right)\right)$$
$$+ Y_c \left(\frac{\left(2M^2 + 2H^2\right)}{f^2 \eta^2 H^2} - \frac{\left(2M^2 + 2H^2\right)}{f^2 \eta_i^2 H^2} \cos\left(f\left(\eta - \eta_i\right)\right)\right). \tag{115}$$

Therefore, an approximate analytic solution for the background radial solution is

$$Y_0(\eta) \approx Y_c \left(1 + \left(\frac{1 - (1 - \epsilon_L)^{1/3}}{(1 - \epsilon_L)^{1/3}}\right) \cos\left(f\left(\eta - \eta_i\right)\right) + \frac{\kappa}{(1 - \epsilon_L)^{2/3}} \sin\left(f\left(\eta - \eta_i\right)\right)\right)$$
$$+ Y_c \left(\frac{\left(2M^2/H^2 + 2\right)}{f^2 \eta^2} - \frac{\left(2M^2/H^2 + 2\right)}{f^2 \eta_i^2} \cos\left(f\left(\eta - \eta_i\right)\right)\right). \tag{116}$$

By comparing our analytic solution with the numerical results, we find that modifying f from Eq. (111) to

$$f = \sqrt{6\lambda} Y_c \left(1 + \delta\right) \equiv \sqrt{6\lambda} Y_i \left(1 - \epsilon_L\right)^{1/3} \left(1 + \delta\right) \tag{117}$$

with $\delta = 0.1137 \epsilon_L^{2.178}$ leads to a sub-percent level accuracy for $\eta < \eta_{\rm tr}$. For instance, $\delta \approx 0.006$ for $\epsilon_L = 0.25$. The additional empirical factor $(1 + \delta)$ accounts for minor correction to the frequency due to the residual nonlinear effects of our original nonlinear differential system in Eq. (109). We note that the kinetic energy induced oscillatory terms vanish in the limit $\{\kappa \to 0, \epsilon_L \to 0\}$ corresponding to the time-independent conformal boundary conditions. When the set $\{\kappa, \epsilon_L\}$ is nontrivial, then the effective action Eq. (A12) obtains a time-dependent conformal representation: i.e. even in the a''/a neglected approximation

$$
\begin{aligned}
S_2 \approx \int d\eta d^3 x \bigg\{ &-\frac{1}{2} \eta_{\mu\nu} \partial^\mu \delta Y \partial^\nu \delta Y - \frac{1}{2} \eta_{\mu\nu} \partial^\mu \delta X \partial^\nu \delta X - \frac{\delta X}{Y_0} \partial_0 \delta X Y_0'(\eta) \\
&+ \frac{2L}{Y_0^2(\eta)} \left[\partial_0 \delta X \delta Y - \frac{Y_0'(\eta)}{Y_0(\eta)} \delta X \delta Y \right] - \frac{1}{2} \frac{(Y_0'(\eta))^2}{Y_0^2(\eta)} (\delta X)^2 + \frac{1}{2} \left[\left(\frac{L}{Y_0^2(\eta)} \right)^2 - 3\lambda Y_0^2(\eta) \right] (\delta Y)^2 \bigg\}
\end{aligned}
\tag{118}
$$

the Y_0 dependent terms of this equation are violating time-translation invariance.[12] According to Eq. (116), for $|\kappa|, |\epsilon_L| \ll 1$, the radial field oscillates around the mean $\Gamma_i \left(a_i/a\right) \left(1 - \epsilon_L\right)^{1/3}$ with an amplitude

$$\Gamma_{\rm amp} = \Gamma_i \left(a_i/a\right) \sqrt{\left(1 - \left(1 - \epsilon_L\right)^{1/3}\right)^2 + \frac{\kappa^2}{\left(1 - \epsilon_L\right)^{2/3}}} \tag{119}$$

$$= \Gamma_i \left(a_i/a\right) \sqrt{\left(\epsilon_L/3\right)^2 + \kappa^2} + O\left(\{\epsilon_L^2, \kappa^2, \epsilon_L \kappa\}\right) \tag{120}$$

and a large frequency $O\left(f\right) \gg H$. These oscillations are small if

$$|\epsilon_L| \ll 1 \tag{121}$$

$$|\kappa| \ll 1. \tag{122}$$

Although there is an asymmetry of how fast ϵ_L rises for $\epsilon_L > 0$ versus $\epsilon_L < 0$ due to the fact that $\frac{d\Gamma_{\rm amp}}{d\epsilon_L}$ diverges at $\epsilon_L = 1$, the asymmetry magnitude is typically small. Since the parameters ϵ_L and κ induce similar deviations, we can remove this degeneracy by taking $\kappa \to 0$.

---

[12] Recall we had a simpler a''/a time-dependent conformal representation in Eq. (31).

The boundary of $\Delta Y_0 \lesssim 0.1 Y_c$ for small oscillations corresponds to $|\epsilon_L| \lesssim 0.3$ for $\kappa = 0$. As ΔY_0 increases due to an increasing $|\epsilon_L|$, the oscillating mass-squared term at the linear order can lead to PRs. The onset of PR for the radial and axial fluctuations of rotating complex spectator will be discussed in Sec. 5. There we will show that the mass-squared term for the radial modes δY_k leads to PR in the blue-tilted region of the spectrum if $\epsilon_L \gtrsim 0.25$ or $\epsilon_L \lesssim -0.37$. Including effects due to the strong coupling with the axial field, the PR can be avoided for $|\epsilon_L| \lesssim 0.1$.

Next we evaluate the mass-squared quantity $m_{\delta\chi}^2$. Using the analytic solution for the background radial field given in Eq. (116) and substituting Y_c from Eq. (37), we evaluate $m_{\delta\chi}^2$ in Eq. (85) up to linear order in ΔY_0 as

$$m_{\delta\chi}^2 = \left(-2M^2 a^2 + \lambda Y_0^2 - \frac{L^2}{Y_0^4}\right) a^{-2} \tag{123}$$

$$= -2M^2 + 6\lambda Y_c \Delta Y_0 a^{-2} + O\left(9\lambda \Delta Y_0^2 a^{-2}\right). \tag{124}$$

Substituting the solution for ΔY_0 from Eq. (115), we obtain the expression for the mass-squared $m_{\delta\chi}^2$ as

$$m_{\delta\chi}^2 \approx -2M^2 + a^{-2}\left(6\lambda Y_c Y_i \left(1 - Y_c/Y_i\right)\cos\left(f\left(\eta - \eta_i\right)\right) + \kappa 6\lambda Y_i^2 \sin\left(f\left(\eta - \eta_i\right)\right)\right)$$
$$+ \left(\frac{(2M^2/H^2 + 2)}{\eta^2}a^{-2} - a^{-2}\frac{(2M^2/H^2 + 2)}{\eta_i^2}\cos\left(f\left(\eta - \eta_i\right)\right)\right),$$

$$m_{\delta\chi}^2 \approx 2H^2 + a^{-2}\left(f^2\left((1-\epsilon_L)^{-1/3} - 1\right) - \frac{(2M^2/H^2 + 2)}{\eta_i^2}\right)\cos\left(f\left(\eta - \eta_i\right)\right)$$
$$+ f^2 a^{-2}\kappa\left(1 - \epsilon_L\right)^{-2/3}\sin\left(f\left(\eta - \eta_i\right)\right). \tag{125}$$

The last two terms in the above expression are fast oscillating large amplitude (since $6\lambda Y_i^2 \gg H^2$) contributions to the effective mass-squared function $m_{\delta\chi}^2$. As shown in Appendix B and also discussed in [62], if the ratio of the amplitude to frequency-squared of the oscillatory terms are much less than 1, then the effective mass-squared quantity is dominated by the slow-varying terms. Hence, from Eq. (125), we have the ratios of amplitude to frequency-squared for the two oscillating terms as approximately $O\left(\kappa\right)$ and $O\left(\max\left[\epsilon_L/3, (f_{\mathrm{PQ}}/\Gamma_i)^2\right]\right)$ respectively. Since small radial oscillations require bounds given in Eqs. (121-122), averaging over (which we will refer to as integrating out) the UV fluctuations to obtain an effectively slowly varying equation as discussed in Appendix B is justified.

Finally after integrating out the UV oscillations, the effective $O(H^2)$ mass-squared term up to

zeroth order in ϵ_L, κ is

$$m_{\delta\chi}^2 \approx 2H^2, \tag{126}$$

and using the definition given in Eq. (87) the isocurvature power spectrum for the rotating complex scalar has a blue spectral index of

$$n_I \approx 3. \tag{127}$$

In view of the conformal limit discussion of Sec. 2.2, this is simply a stability statement indicating that the UV oscillations do not change the leading approximation of conformal behavior when Eqs. (121) and (122) are satisfied.

In addition to the conformal arguments given in Sec. 2.2 and Eq. (127), here is yet another way to view the power spectrum from a horizon exit perspective. If we approximate the quantum fluctuations $\delta\theta$ in the angular modes as $H/(2\pi\Gamma_k)$ where Γ_k is the radial amplitude when the relevant mode exits the horizon at some time t_k, the isocurvature power spectrum is approximately

$$\Delta_s^2(k) \sim \left(\frac{H}{2\pi\Gamma_k\theta_i}\right)^2 \tag{128}$$

where θ_i is the final misalignment angle when the radial field settles to its stable vacuum[13]. Using the leading Eq. (125) (or equivalently the conformal solution Eq. (18)), we find

$$
\begin{aligned}
\Delta_s^2(k) &\sim \left(\frac{H}{2\pi\theta_i\Gamma_i\left(1-\epsilon_L\right)^{1/3}}\right)^2 \left(\frac{a(t_k)}{a_i}\right)^2 \\
&\sim \left(\frac{H}{2\pi\theta_i\Gamma_i\left(1-\epsilon_L\right)^{1/3}}\right)^2 \left(\frac{k}{k_i}\right)^2
\end{aligned}
\tag{129}
$$

where k_i corresponds to the mode exiting the horizon at t_i or conformal time η_i.

To determine θ_i, we integrate Eq. (78) to obtain

$$\theta(t) = \theta(t_i) + \int_{t_i}^t dt \frac{L}{a^3\Gamma^2}. \tag{130}$$

Since L is a constant and the radial field decays exponentially as $\Gamma \approx \Gamma_i\left(1-\epsilon_L\right)^{1/3}\left(a_i/a\right)$ until $\sqrt{\lambda}\Gamma(t) \rightarrow O\left(M, H\right)$, the integral in the above expression is dominated at early times $\left(t < t_{\mathrm{tr}}\right)$

---

[13] Consistent with its use in the literature, we denote the final misalignment angle as θ_i. It is important not to confuse this with the initial value of θ at time t_i.

and saturates as $\Gamma \to f_{\mathrm{PQ}}$. Substituting Eq. (116) as the analytic solution to the radial field and neglecting any $O(\epsilon_L)$ oscillations, we can approximate

$$\theta(t) \approx \theta(t_i) + \frac{L}{\Gamma_i^2 \left(1 - \epsilon_L\right)^{2/3} a_i^2} \int_{t_i}^{t} \frac{dt}{a} \tag{131}$$

$$\approx \theta(t_i) + \frac{\sqrt{\lambda}\Gamma_i}{\left(1 - \epsilon_L\right)^{1/3}} \left(\frac{1 - e^{-H(t-t_i)}}{H}\right) \tag{132}$$

where we took the scale factor as $a(t) \approx \exp\left(Ht\right)$. Hence for $t \gg t_i$,

$$\theta_i = \lim_{t \gg t_i} \theta(t) \approx \theta(t_i) + \frac{\sqrt{\lambda}\Gamma_i/H}{\left(1 - \epsilon_L\right)^{1/3}}. \tag{133}$$

Choosing to express θ_i in the interval $[-\pi, \pi]$ as is sometimes customarily done, we write

$$\theta_i + \pi \approx \left(\theta(t_i) + \frac{\sqrt{\lambda}\Gamma_i/H}{\left(1 - \epsilon_L\right)^{1/3}}\right) \quad \mathrm{mod}\ 2\pi. \tag{134}$$

The $\sqrt{\lambda}\Gamma_i/H/\left(1 - \epsilon_L\right)^{1/3}$ merely adds to the usual uncertainty in the vacuum θ angle.

4.3.1. Quasi-adiabatic time-evolution example

Let us consider an example of a rotating complex scalar with deviations away from the conformal solution. Similar to the example presented in Sec. 3.2.1, we set $\lambda = 1$ and $f_{\mathrm{PQ}} = 10H_{\mathrm{inf}}$. Further, we initialize the background radial field Γ_0 at η_i with the same value as in Sec. 3.2.1:

$$\Gamma_0(\eta_i) = 1000H_{\mathrm{inf}}. \tag{135}$$

To parameterize the deviations away from an adiabatic time-evolution for a perfect conformal solution, we set $\epsilon_L = 0.1$ and $\kappa = 0$ such that the conserved angular momentum from Eq. (106) is given as

$$L = 0.9\sqrt{\lambda}10^9 H_{\mathrm{inf}}^3 a^3(\eta_i). \tag{136}$$

Note that with the above parameterization, Eq. (107) implies that the new conformal background value is $Y_c \approx 965.49H_{\mathrm{inf}}a(\eta_i)$. In Fig. 2 we plot the time evolution of $\Gamma_0(t)$ from an initial amplitude $\Gamma_0(\eta_i)$ to f_{PQ}. In the same plot (see inset) we show a comparison of our analytic solution with the numerical result.

To study the evolution of the linear perturbations, we note that the time-scale of oscillations of the background radial field is much smaller than the evolution of the mean conformal solution, i.e

$$T_{\mathrm{osc}} \sim O\left(\frac{1}{\sqrt{6\lambda}\Gamma_0(\eta_i)}\right) \ll O\left(\frac{1}{H}\right). \tag{137}$$
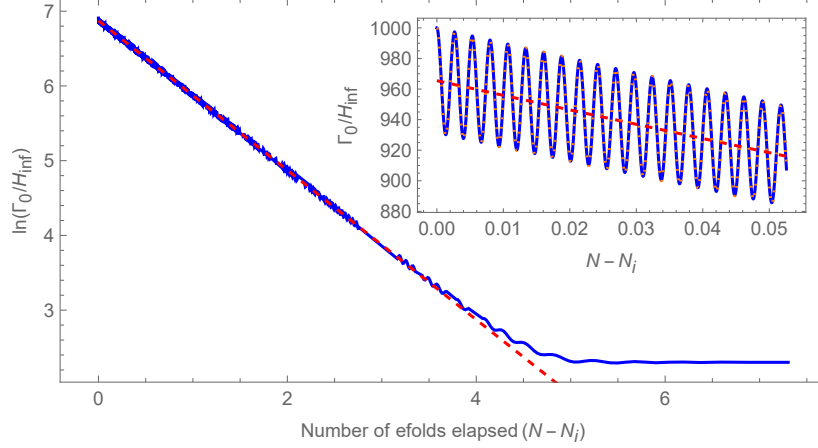
Figure 4: Plot showing the time evolution of the background radial field $\Gamma_0(t)$ (solid blue curve) during the quasi de-Sitter phase of inflation for deviations from conformal conditions, parameterized by $\epsilon_L = 0.1$ and $\kappa = 0$. Starting from $\Gamma_0(\eta_i) = 1000 H_{\text{inf}}$, the radial field quickly evolves along the conformal solution $\Gamma_c(\eta) = \frac{L^{1/3}}{\lambda^{1/6} a(\eta)}$ (red dashed line) while undergoing small amplitude $\sim O\left(\epsilon_L \Gamma_c(\eta_i)\right)$ oscillations along this trajectory. The oscillations have a frequency $\approx \sqrt{6\lambda} Y_c$. The orange dotted curve shown in the inset represents our analytic approximation for the small amplitude oscillations as given in Eq. (116).
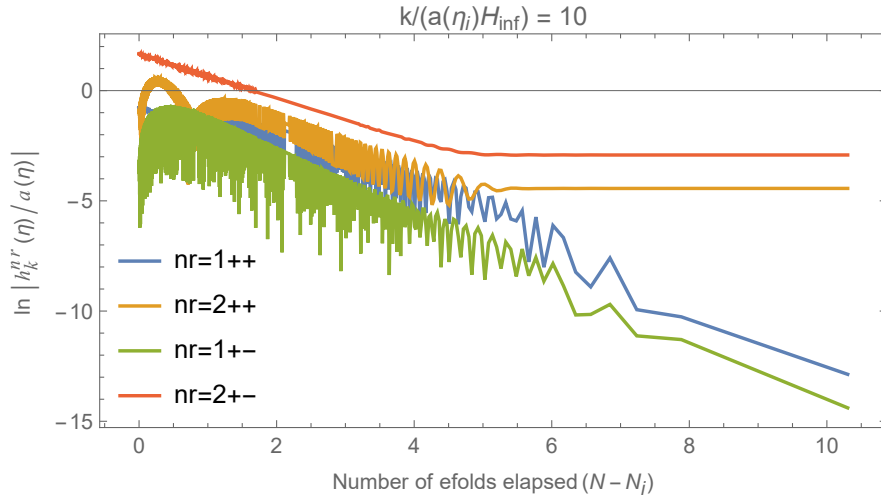

Figure 5: Plot showing the time evolution of the mode functions h_k^{nr} during the quasi de-Sitter phase of inflation for a fiducial mode $k/a(\eta_i) = 10 H_{\text{inf}}$ in the context of quasi-adiabatic example where $\epsilon_L = 0.1$ and $\kappa = 0$. Compared to Fig. 3, we observe that the mode amplitude show small amplitude oscillations similar to background radial field. Apart from these oscillations, the general evolution of the mode functions is similar to the case presented in Sec. 3.2.1.

Hence, we will time-average over these rapid oscillations, and assume an approximately conformal evolution of the background radial field. This assumption allows us to quantize this system similar to the analysis presented in Sec. 3. Therefore, we employ the same set of initial conditions for the two frequency solutions that we presented in Eqs. (68) and (69) to solve for the mode functions with a non-zero ϵ_L. In Fig. 5, we show the time evolution of the radial and axial mode functions for a fiducial wavenumber $k/a(\eta_i) = 10$ in the context of this quasi-adiabatic system with small deviations away from a conformal solution.

5. PLOTS AND DISCUSSION

In Sec. 3 we derived analytic expressions for the effective mass-squared term $m_{\delta\chi}^2$ for the axial fluctuations at the linear order. Subsequently we showed that for a particular conformal choice of background field boundary conditions, the isocurvature power spectrum Δ_s^2 has a blue index $n_I \approx 3$ and hence increases as k^2 before transitioning to a massless plateau in agreement with the general considerations of Sec. 2.2. Next, we considered deformations away from the conformal boundary condition, which generically induces radial background field oscillations which in turn nontrivially alter the perturbation dynamics. In this section, we give plots of the isocurvature power spectrum and briefly discuss the parameteric dependences. The dimensionless superhorizon isocurvature power spectrum of the axial field fluctuations is given as:

$$\Delta_s^2(k) = 4\omega_a^2 \frac{\Delta_{\delta\chi\delta\chi}^2(k, \eta_f)}{(f_{\mathrm{PQ}}\theta_i)^2} \tag{138}$$

where $\eta_f \to 0$ and $\Delta_{\delta\chi\delta\chi}^2$ is given in Eq. (E2) and $\omega_a \equiv \Omega_{\mathrm{axion}}/\Omega_{\mathrm{cdm}}$ assumes that the axions make up the CDM. Such axionic CDM would contribute to an approximately uncorrelated photon-dark matter isocurvature inhomogeneities in the post-inflationary cosmological evolution before the horizon reentry. Following the discussion under Eq. (59), we approximate the amplitude of the blue-tilted region of the spectrum as

$$\Delta_s^2(k < k_{\mathrm{tr}}) = \frac{\omega_a^2}{\pi^2\sqrt{3}} \left(\frac{H}{\Gamma_0(\eta_i)\theta_i}\right)^2 \left(\frac{k}{a(\eta_i)H}\right)^2. \tag{139}$$

From Eq. (60), we infer that the scale invariant part of the isocurvature spectrum is

$$\Delta_s^2(k \gg k_{\mathrm{tr}}) = \frac{\omega_a^2}{\pi^2} \left(\frac{H}{f_{\mathrm{PQ}}\theta_i}\right)^2. \tag{140}$$

In the plots presented in this section, we normalize the isocurvature power spectra $\Delta_s^2(k)$ with respect to the quantity $(f_{\mathrm{PQ}}\theta_i)^2 / (\omega_a H)^2$. Hence, we plot $4H^{-2}\Delta_{\delta\chi\delta\chi}^2(k, \eta_f)$ on the y-axis and the

analytic approximation for the normalized spectrum $\overline{\Delta_s^2}(k)$ can be expressed as

$$\overline{\Delta_s^2}(k < k_{\text{tr}}) = \frac{(f_{\text{PQ}}\theta_i)^2}{\omega_a^2 H^2}\Delta_s^2(k < k_{\text{tr}}) = \begin{cases} \frac{1}{\pi^2\sqrt{3}}\left(\frac{f_{\text{PQ}}}{\Gamma_0(\eta_i)}\right)^2\left(\frac{k}{a(\eta_i)H}\right)^2 & k < k_{\text{tr}} \\ \\ \frac{1}{\pi^2} & k \gg k_{\text{tr}} \end{cases}. \qquad (141)$$
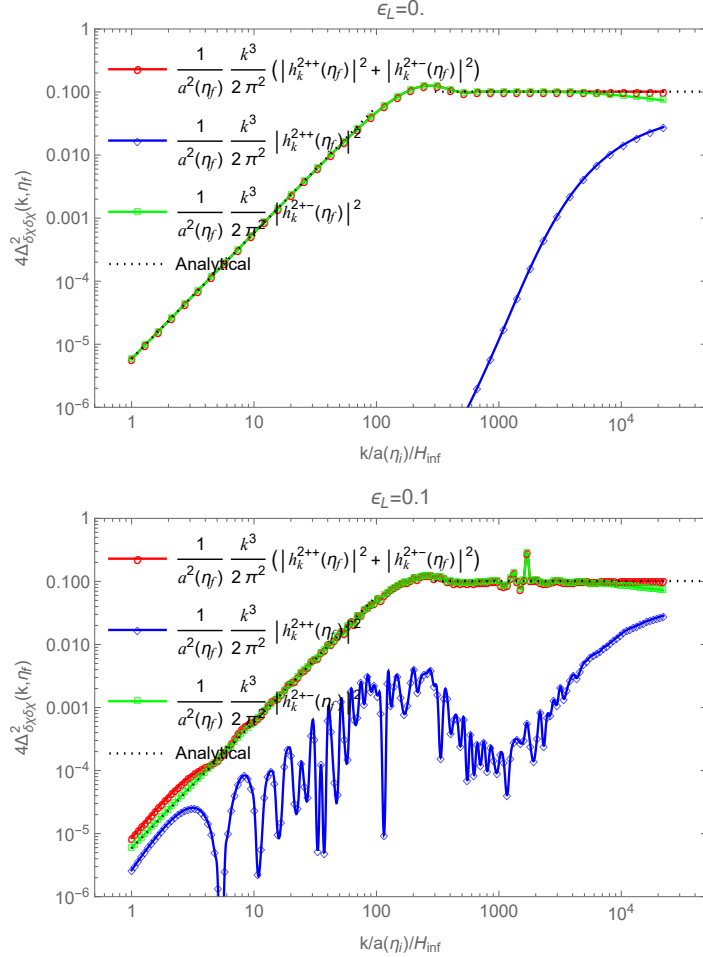

Figure 6: Plots showing the late-time conserved superhorizon isocurvature power spectra (normalized with $(f_{\text{PQ}}\theta_i)^2/\omega_a^2$ in Eq. (138)) of the axial field $\delta\chi$ for the two examples presented in Secs. 3.2.1 and 4.3.1. The plots are generated by numerically evolving the radial and axial mode fluctuations from η_i to $\eta_f \to 0$ and evaluating the final isocurvature spectrum using Eq. (138). The plots on the top (bottom) rows correspond to the parameter ϵ_L set to 0 (0.1) while keeping $\kappa = 0$. The power spectra have a spectral index $n_I \approx 3$ for modes $k < k_{\text{tr}}$ where $k_{\text{tr}}/a_i/H \approx \Gamma_i/f_{\text{PQ}}$. In each plot we show the final power spectrum (red curve, circular markers) and individual contributions from the ω_{++} (blue curve, diamond markers) and ω_{+-} (green curve, square markers) frequency modes. The spectrum is dominated by the Goldstone mode. Using Eqs. (139) and (140) we plot the analytic spectrum (black dotted curve) in the $k < k_{\text{tr}}$ and $k > 3k_{\text{tr}}$ regions of the spectra respectively. The small-amplitude oscillations seen in the $\epsilon_L = 0.1$ scenario are explained in the main text.

For the isocurvature spectrum normalized in this way, the amplitude of blue-tilted region only depends upon the ratio $\Gamma_0(\eta_i)/f_{\mathrm{PQ}}$.

In Fig. 6 we illustrate the isocurvature spectra for the two examples discussed in Secs. 3.2.1 and 4.3.1. These plots highlight that the isocurvature power spectrum has a blue index $n_I \approx 3$ for modes $k < k_{\mathrm{tr}}$ where $k_{\mathrm{tr}}/a_i/H_{\mathrm{inf}} \approx \Gamma_i/f_{\mathrm{PQ}}$. In each plot we show the contributions from the ω_{++} and ω_{+-} frequency modes, with the spectrum being predominantly influenced by the lighter (ω_{+-}) mode due to the mode normalization. For comparison we also include our analytic spectrum in the blue-tilted $k < k_{\mathrm{tr}}$ and massless-plateau $k > 3k_{\mathrm{tr}}$ regions of the spectrum. We lack an analytic prediction for the intermediate (bumpy) region. Due to the sub-dominant deviations from the conformal background solution in the $\epsilon_L = 0.1$ scenario, we observe tiny oscillations in the spectrum that can be attributed to the oscillation of the background radial field around the conformal background. Below we explore the impact of a non-zero ϵ_L on the isocurvature spectrum.

5.1. ϵ_L dependence

In Fig. 7, we plot several examples of isocurvature power spectra for the rotating complex scalar Φ for different values of ϵ_L highlighting the effect of a non-zero ϵ_L on the blue-tilted part of the spectrum. For all cases, the vacuum boundary conditions for the fluctuations are set according to Eqs. (68) and (69). As we will discuss below, the oscillations in the spectrum arise due to the deviation of the background radial field from a conformal background solution. There is also a contribution from the residual non-adiabaticity in the Bunch-Davies-like vacuum definition for the radial and axial fluctuations coming from our choice of initial conditions.

In Sec. 3, we showed that for a time-independent conformal background solution, the Hamiltonian for the coupled radial-axial field fluctuations can be diagonalized with frequency solutions $\omega_H = \omega_{\pm+}$ and $\omega_L = \omega_{\pm-}$ as given in Eq. (46). The isocurvature power spectrum for the IR modes is dominated by the lower frequency solution ω_L and is blue-tilted, $\Delta_s^2(k \lesssim k_{\mathrm{IR}}) \propto k^2$. In the $\epsilon_L \neq 0$ scenario, the conformal symmetry is broken in a time-dependent way through the choice of boundary condition leading to the background radial field Γ_0 having $O(\epsilon_L)$ amplitude high-frequency oscillations for $|\epsilon_L| \ll 1$. This is described by the approximate analytic solution given in Eq. (116). Compared to the constant solution Y_c, the amplitude of the oscillations can be defined by a new parameter x as

$$\left(\frac{Y_i - Y_c}{Y_c}\right) = x \sim O(\epsilon_L/3) \ll 1. \tag{142}$$

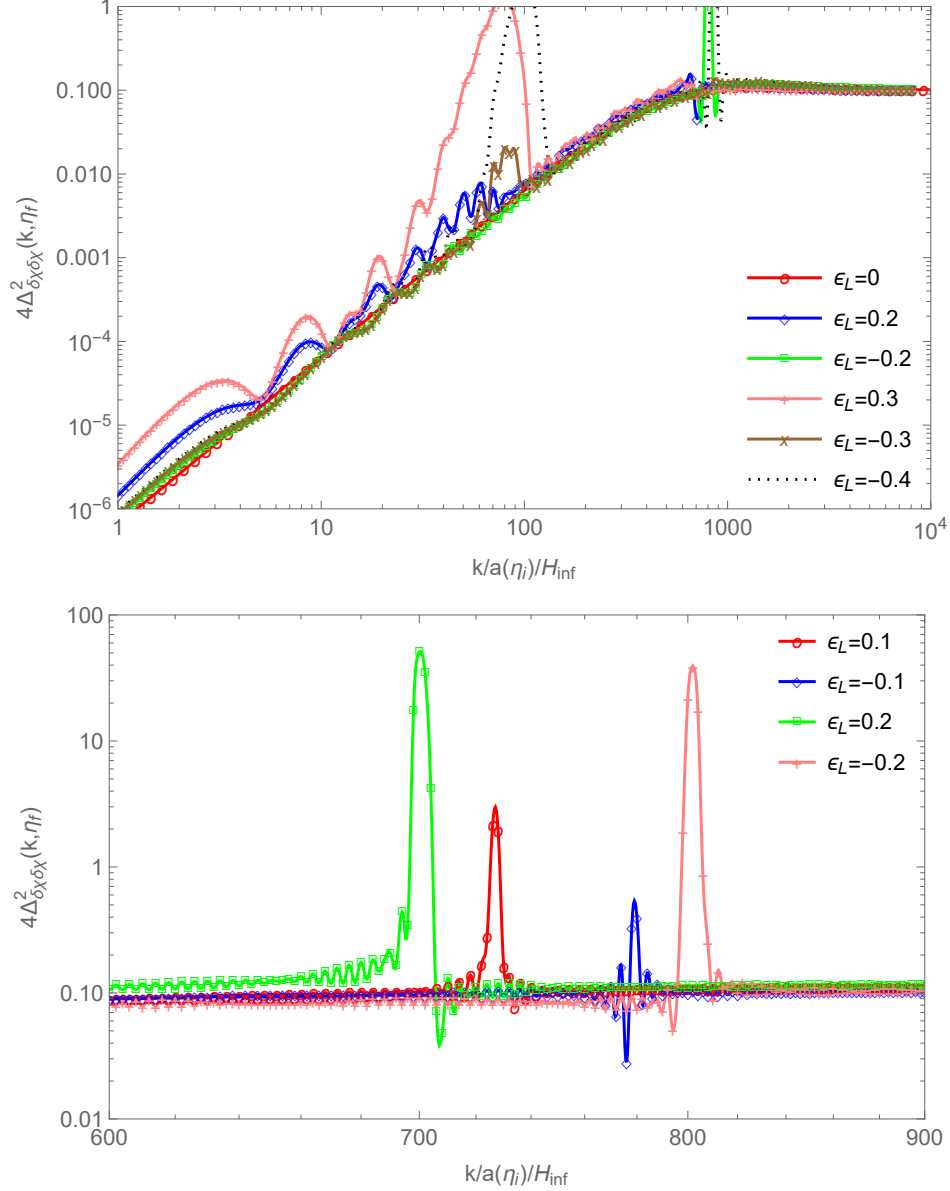Under these conditions, the oscillations of the background radial field induce coupling between

Figure 7: Plots showing isocurvature power spectrum for rotating complex scalar Φ for different values of ϵ_L. For generating these plots, we set $\lambda = 10^{-4}$, $M = H_{\mathrm{inf}}$ and $\kappa = 0$. The initial radial displacement at η_i is set at $300 f_{\mathrm{PQ}}$ such that the k-range of the blue part of the spectrum is approximately $k_{\mathrm{tr}}/k_i \sim 10^3$. The power spectrum has a blue index $n_I \approx 3$. We note that for $\epsilon_L \neq 0$, the spectrum exhibits oscillations that grow rapidly with ϵ_L. The plot in the top row shows parametric enhancement of the spectrum within the k^2 region for values of $\epsilon_L = +0.3$ and $\epsilon_L = -0.4$. In the bottom row, we plot the isocurvature spectra on a much finer k-bin to highlight sharp parameterically enhanced peaks at $k/H_{\mathrm{inf}}/a_i \approx 0.9 \left(2\sqrt{\lambda} Y_c\right)$ within the flat region.

the axial and radial field fluctuations which is $O(x)$ magnitude and time-dependent. This leads to a mixing between the normal mode-states e_L and e_H corresponding to ω_L and ω_H respectively. Qualitatively, it suggests that an initial excitation of the lighter frequency state at η_i will generate $O(x)$ excitations of the remaining frequency solutions through the time-dependent mixing term. Quantitatively, if the axial fluctuation is excited with the positive-frequency lighter eigenstate, $e^{-i\omega_L \eta}$, then the time-dependent mixing will generate a mixed state expressed approximately as

$$\delta\chi_k(\eta) \sim C_k \left[(1+O(x)) e^{-i\omega_L \eta} + O(x) e^{-i\omega_H \eta} + O(x) e^{+i\omega_H \eta} + O(x) e^{+i\omega_L \eta} \right] \tag{143}$$

where the C_k is an overall normalization of mode function χ_k. The isocurvature power spectrum during this phase ($\eta \ll \eta_{tr}$) can be approximately given as

$$\Delta^2_{\delta\chi\delta\chi}(k, \eta) \sim k^3 \delta\chi_k^* \delta\chi_k \tag{144}$$

$$\sim k^3 |C_k|^2 \left[1 + 2O(x) + 2O(x) \cos\left(2\omega_L \left(\eta - \eta_i\right)\right) + \right.$$

$$\left. 2O(x) \cos\left(\left(\omega_H + \omega_L\right)\left(\eta - \eta_i\right)\right) + 2O(x) \cos\left(\left(\omega_H - \omega_L\right)\left(\eta - \eta_i\right)\right) \right] + O(x^2). \tag{145}$$

Hence, we note that $|\epsilon_L| \ll 1$ deviations from a perfect conformal boundary condition "weakly" break time-independent conformal phase and generate $O(x)$-amplitude oscillatory signals on the blue-tilted part of the spectrum. These oscillations are approximately linear in k. In terms of normalized momentum $-k\eta_i$, the k-space frequencies for these oscillations in the blue-tilted region can be read from the above expression as

$$\omega_j \approx \left\{ \frac{2}{\sqrt{3}}, \frac{1}{\sqrt{3}} \pm \frac{5k}{6\sqrt{6\lambda Y_c^2}} \right\} (1 - \eta/\eta_i) \tag{146}$$

and the isocurvature spectrum can be conveniently expressed as

$$\Delta^2_{\delta\chi\delta\chi}(k \ll \sqrt{\lambda}Y_c, \eta \ll \eta_{tr}) \sim k^3 |C_k|^2 \left[1 + 2O(x) + \sum_{j=1}^{3} 2O(x) \cos\left(\omega_j \left(-k\eta_i\right)\right) \right]. \tag{147}$$

For $\eta \to 0$ and $k \ll \sqrt{\lambda}Y_c$, these frequencies are simply multiples of $1/\sqrt{3}$. Thus, the time-dependent conformal symmetry breaking boundary conditions imprint an oscillatory signal that is a signature of the Goldstone mode's dispersion relation. Since the k-space wavelength of these oscillations is $\lambda_k \approx 2\pi\sqrt{3}/\eta_i \sim O(10/\eta_i)$, these may be measurable.

To facilitate matching/fitting with the numerical/observational data, we transform the expression in Eq. (145) into a semi-analytic empirical form by introducing $\sim O(1)$ unknown coefficients $c_{0,1,2,3}$:

$$\Delta^2_{\delta\chi\delta\chi}(k, \eta) \propto 1 + 2x \left[c_0 + c_3 \cos\left(2\omega_L \left(\eta - \eta_i\right)\right) + \right.$$

$$\left. c_1 \cos\left(\left(\omega_H + \omega_L\right)\left(\eta - \eta_i\right)\right) + c_2 \cos\left(\left(\omega_H - \omega_L\right)\left(\eta - \eta_i\right)\right) \right]. \tag{148}$$

If $c_1 \approx c_2$, the above expression takes the form

$$\Delta^2_{\delta\chi\delta\chi}(k,\eta) \propto 1 + 2x \left[c_0 + c_3 \cos\left(2\omega_L\left(\eta - \eta_i\right)\right) + 2c_1 \cos\left(\omega_H\left(\eta - \eta_i\right)\right) \cos\left(\omega_L\left(\eta - \eta_i\right)\right) \right]. \quad (149)$$

To isolate the oscillations present in the data, we can normalize it with the smoother (no-wiggle (nw)) spectrum. The resulting normalized spectrum can then be fitted using the following empirical expression

$$\frac{\Delta^2_{\delta\chi\delta\chi}(k)}{\Delta^2_{\delta\chi\delta\chi,\mathrm{nw}}(k)} = 1 + 2x \left[c_0 + c_3 \cos\left(2\omega_L\left(-\eta_i\right)\right) + c_1 \cos\left(\left(\omega_H + \omega_L\right)\left(-\eta_i\right)\right) \right.$$

$$\left. + c_2 \cos\left(\left(\omega_H - \omega_L\right)\left(-\eta_i\right)\right) \right]. \quad (150)$$
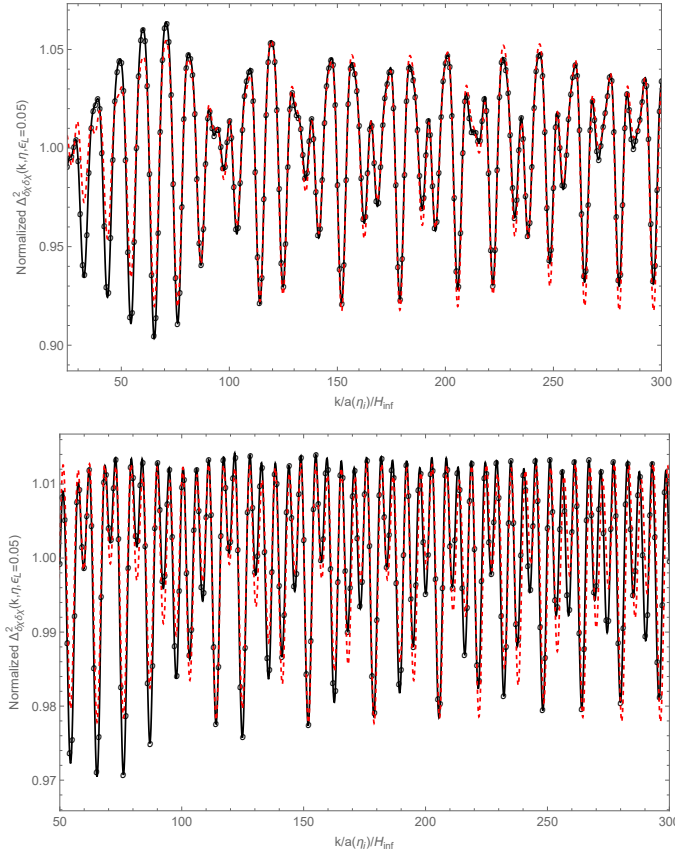

Figure 8: Plots showing the normalized isocurvature power spectra for $\epsilon_L = 0.05$. These plots are generated for a fiducial set of model parameters with $\lambda = 1$ and $\sqrt{2}M/H_{\mathrm{inf}} = 10$ such that $f_{\mathrm{PQ}} = 10H_{\mathrm{inf}}$. To highlight the oscillatory signal in the power spectra for a nonzero ϵ_L parameter, we have normalized the spectrum with the smooth, non-wiggly part of the spectrum. The numerical data is plotted in black color with circular markers and our semi-analytic empirical expression from Eq. (148) is depicted by the red-dashed curve. The top (bottom) plot shows the isocurvature spectrum before (after) the radial field reaches the f_{PQ}.

In Fig. 8, we illustrate the normalized isocurvature spectra for $\epsilon_L = 0.05$. Through the figure, we highlight the comparison between the numerical data and our semi-analytic empirical expression in Eq. (150). For the axial fluctuations initially excited with the positive-frequency lighter eigenstate $e^{-i\omega_L \eta}$, the time-dependent $O(\epsilon_L)$ oscillations will generate a mixed state with other frequencies, where the mixing is controlled by the $O(\epsilon_L/3)$ parameter as shown in Eq. (150). By fitting the numerical data, we obtain the best fit values of the coefficients as $\{c_0 = -0.0585, c_1 = 0.9544, c_2 = 1.0354, c_3 = -0.3518\}$. The normalized amplitude of the oscillation during this phase is $O(2x) \sim \epsilon_L \equiv 0.05$. After transition, the axial fluctuations corresponding to the heavier frequency state, $\pm\omega_H$, decay by a factor $\propto \min[1, O(H/M)]$. This is represented by the best fit values of the coefficients $\{c_0 = -0.0029, c_1 = 0.1444, c_2 = 0.1684, c_3 = -0.3311\}$ for the oscillations of the late-time spectrum as illustrated in the bottom plot.

Let's now go back to Fig. 7 and discuss its features for larger values of ϵ_L. The spectrum shows parameteric resonance enhancement of the mode amplitude for values of $\epsilon_L = +0.3$ and $\epsilon_L = -0.4$ in the blue-tilted region. To understand the onset of the PR and its dependence on ϵ_L, let us consider the uncoupled mode equation for the scaled radial fluctuations

$$\partial_\eta^2 \delta Y_k + \left(k^2 - \left(2M^2 + 2H^2 \right) a^2 + 3\lambda \left(Y_c + \Delta Y_0 \right)^2 - \frac{L^2}{(Y_c + \Delta Y_0)^4} \right) \delta Y_k = 0. \tag{151}$$

In this simplified discussion, we focus solely on the effect of deformation from the conformal background on the mass-squared term of the radial mode, neglecting any coupling with the axial mode. By neglecting the sub-dominant order Hubble mass terms and taking $\kappa = 0$, we expand up to linear order in ΔY_0. This yields the reduced EoM:

$$\partial_\eta^2 \delta Y_k + \left(k^2 + 2\lambda Y_c^2 + 10\lambda Y_c^2 \left(\frac{1 - (1 - \epsilon_L)^{1/3}}{(1 - \epsilon_L)^{1/3}} \right) \cos \left(f \left(\eta - \eta_i \right) \right) \right) \delta Y_k = 0 \tag{152}$$

where we recognize the mass-squared term for the radial fluctuations as

$$m_{\delta Y}^2 \approx k^2 + 2\lambda Y_c^2 + 10\lambda Y_c^2 \left(\frac{1 - (1 - \epsilon_L)^{1/3}}{(1 - \epsilon_L)^{1/3}} \right) \cos \left(f \left(\eta - \eta_i \right) \right). \tag{153}$$

In the above differential equation, we can identify the term $f_N = \sqrt{k^2 + 2\lambda Y_c^2}$ as the natural frequency of the oscillator and $f_D \approx f$ as the frequency driving the parametric excitation. Through a variable change $z = f \left(\eta - \eta_i \right) / 2$, we reframe the above equation in terms of a general Matheiu system:

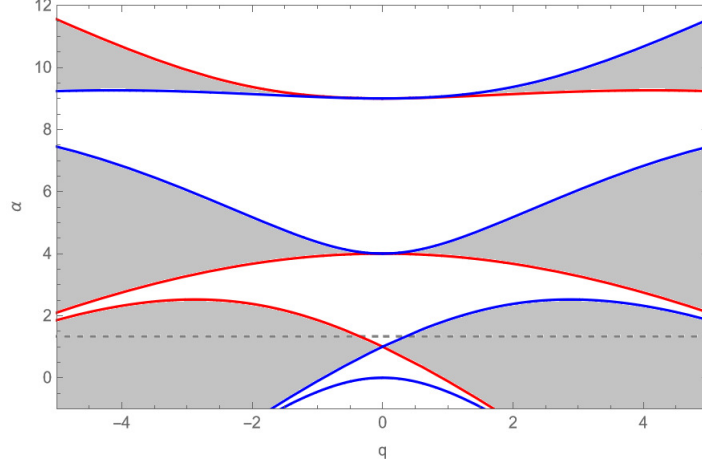$$\frac{d^2 u}{dz^2} + (\alpha - 2q \cos \left(2z \right)) u = 0 \tag{154}$$

Figure 9: Plot showing Mathieu stability chart in the $\alpha - q$ parameteric space for the first few stability bands. The instability occurs within the shaded (unbounded) regions. For a fixed value of $\alpha \approx 4/3$ (gray dashed line), we find that the system enters the first resonance band when the parameter $|q| \gtrsim 0.35$. The above figure is obtained by plotting even (blue) and odd (red) Mathieu functions.

and find the corresponding Mathieu parameters as

$$\alpha = \frac{4\left(k^2 + 2\lambda Y_c^2\right)}{6\lambda Y_c^2}, \tag{155}$$

$$q = -\frac{10\left(\frac{1-(1-\epsilon_L)^{1/3}}{(1-\epsilon_L)^{1/3}}\right)}{3}. \tag{156}$$

In terms of the original model parameters, we find that α depends only on one combination

$$\alpha = \alpha\left(\frac{k}{(1-\epsilon_L)^{1/3}\sqrt{\lambda}\Gamma_i}\right) \tag{157}$$

while q depends only on ϵ_L. If $f^2 \gg k^2$, then

$$\alpha \approx \frac{4}{3} + O\left(k^2/f^2\right) \tag{158}$$

causing α to be approximately independent of the parameters. Thus, we find that the parameter α is approximately a constant for modes that exit the horizon before axial field becomes massless, while $|q|$ increases linearly with ϵ_L.

An interesting behavior of a Mathieu oscillator is the excitation via parameteric resonance for a range of parameters α and q. In Fig. 9 we plot a stability chart of the Mathieu system highlighting regions/bands of stable and unstable solutions in the $\alpha - q$ parametric space. In the plot we fix
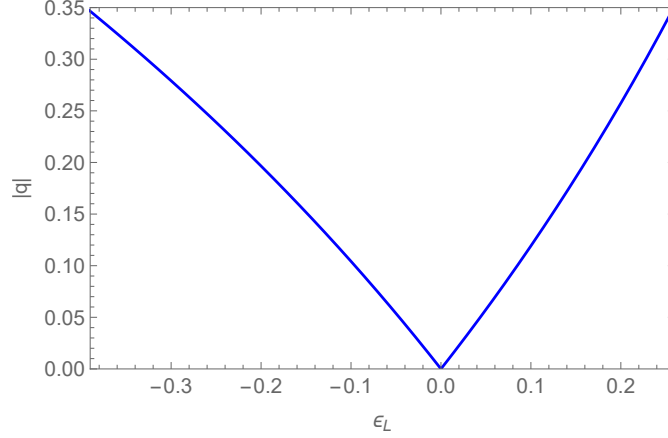
Figure 10: Plot of Mathieu parameter $|q|$ as a function of the rotational parameter ϵ_L using Eq. (156). In terms of rotational parameter ϵ_L, the oscillator becomes unstable for $\epsilon_L \lesssim -0.37$ and $\epsilon_L \gtrsim +0.25$. Also see Eq. (156).

$\alpha \approx 4/3$ as derived in Eq. (158). When the oscillator system falls within an unstable resonance band it leads to an almost exponential excitation of the amplitude. For the radial mode fluctuations of our rotating complex field, Eq. (158) suggests that the value of α is approximately a constant for small values of ϵ_L and Eq. (156) indicates that q increases almost linearly with ϵ_L as shown in Fig. 10. For a fixed value of $\alpha \approx 4/3$ (red dashed line), we find that the system enters the first resonance band and becomes unstable when the parameter $|q| \gtrsim 0.35$. From Fig. 10, we infer that the uncoupled radial mode fluctuations δY_k become unstable for $\epsilon_L \lesssim -0.37$ and $\epsilon_L \gtrsim +0.25$ for modes $k^2 \ll f^2$. The oscillator amplitude is resonantly enhanced and results in a nearly exponential amplification. This observation aligns with our findings in Fig. 7. A similar analysis for the uncoupled axial field yields a much smaller value of $\alpha \approx 2k^2 / \left(3\lambda Y_c^2\right)$ such that the instability in the blue region occurs only for values of $|q|$ close to unity.

Eq. (155) also suggests that modes close to $k^2 \approx 4\lambda Y_c^2$ yield a value of $\alpha \approx 4$, pushing the system towards the next resonance band. From Fig. 9, we infer that unlike the first, the second resonance band is significantly narrow for small values of $|q| \sim |\epsilon_L| \ll 1$. Consequently, only finely tuned values of k undergo PR, as depicted by the plot in the bottom row of Fig. 7, where we observe narrow parameterically enhanced peaks for modes $k \approx O\left(2\sqrt{\lambda}Y_c\right)$. Similarly, PR linked to the nth resonance band for $|q| \ll 1$ would manifest for correspondingly higher k modes, with the width and amplitude of the peaks decreasing with n.

The above discussion has a simple interpretation. In terms of the natural and driving frequencies

of a parameteric oscillator (defined below Eq. (151)), large exponential PR occurs when

$$f_N = n\frac{f_D}{2} \qquad n \in \{1, 2, 3, ...\} \tag{159}$$

where n refers to the nth resonance/instability band. For $q \ll 1$, the bands have the usual width $\sim q^n$ and hence the most important and broadest instability band is $n = 1$ when $q \ll 1$. In the first band, resonance occurs close to $f_N = f_D/2$. Hence resonance occurs when the mass of the oscillating radial field is exactly twice the effective mass for the quantum modes δY_k.

Due to the coupling between the radial and angular fluctuations, the parametrically enhanced radial fluctuations can drive angular fluctuations $\delta\chi$ to large amplitudes. This enhancement lasts as long as the radial mode stays within the first resonance band, a duration of about $O(1)$ Hubble time, after which the oscillatory mass behavior ceases in Eq. (151). It's essential to note that the above discussion on PR relies on the simplified "uncoupled" EoM for the radial mode δY_k. However, the presence of a strong derivative coupling with the axial mode can notably alter the PR dynamics. Our numerical investigations across various Lagrangian parameters and initial conditions indicate that PR generally does not manifest within the blue region of the spectra for $|\epsilon_L| \lesssim 0.1$. A more comprehensive examination of PR's dynamics is reserved for future studies.

5.2.   Maximum k-range

As the background radial field approaches its stable vacuum, the effective mass-squared term $m_{\delta\chi}^2$ for the axial fluctuations becomes approximately massless. If $M^2 a^2 / \left(6\lambda Y_c^2\right) < 1$ for N_{blue} number of e-folds, the mass term behaves as in Eq. (126), during which time, we have a blue spectrum. Hence, the range of scales across which the spectrum remains strongly blue-tilted is approximately $\exp\left(N_{\text{blue}}\right)$. Starting from the condition $\lambda Y^2 \gg \max\left(2M^2, a''/a\right)$ for a blue spectral index, one can show that

$$\exp\left(N_{\text{blue}}\right) \approx \frac{\Gamma_i}{f_{\text{PQ}}\sqrt{1 + H^2/M^2}}. \tag{160}$$

Using the spectator energy condition in Eq. (15), we can give an approximate upper bound on the maximum radial displacement Γ_i at t_i for a rotating complex scalar Φ with $|\epsilon_L| \ll 1$:

$$\frac{3\lambda}{4}\Gamma_{\text{max}}^4 \approx r_a 3 M_P^2 H^2 \tag{161}$$

or equivalently

$$\frac{\Gamma_{\text{max}}}{H} \approx 10^3\sqrt{0.2}\left(\frac{r_a}{0.01}\right)^{1/4}\left(\frac{1}{\lambda}\right)^{1/4}\sqrt{\frac{M_P/H}{10^6}} \tag{162}$$
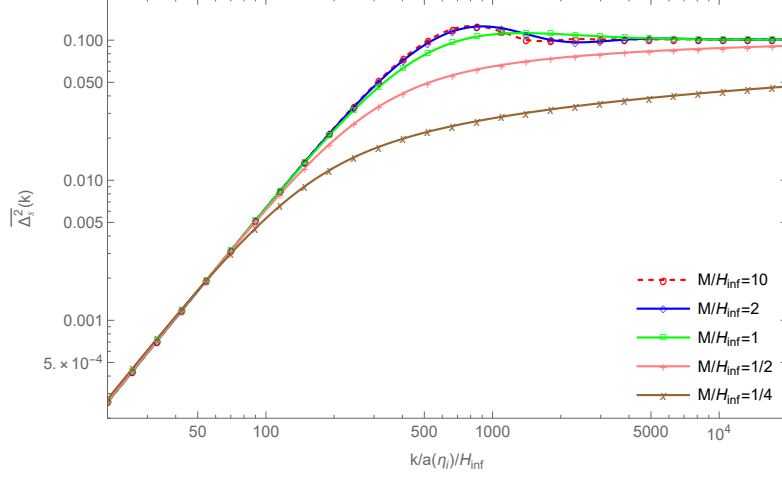
Figure 11: Plot showing comparison of the normalized isocurvature power spectra for different values of M with $\lambda = 10^{-4}$ and $\Gamma_i = 300 f_{\text{PQ}}$. For these choice of λ and M, the PQ scale $f_{\text{PQ}} \approx 100\, O(M)$. The transition from a spectral index $n_I = 3$ occurs at the transition scale $k_{\text{tr}}/k_i \approx \Gamma_i / f_{\text{PQ}} / \sqrt{1 + H^2/M^2}$. The plot also highlights the deviation of the isocurvature shapes at the transition to the massless plateau for different values of M. We observe the appearance of the spectral bump for $M \gtrsim 3H/4$ as given in Eq. (C6).

where we have assumed a negligible radial velocity at t_i. The parameter r_a gives the ratio of spectator energy density to that of inflaton's and must be much less than 1. Also, Eq. (162) states that the spectator energy bound is setting $\Gamma_{\max} \ll M_P$. This is a significant departure from [7, 49, 62, 63] in which the flat direction allowed the analog of the $\Gamma_{\max}$ field to reach $O(M_P)$ while the axionic sector still remained a spectator. Hence, even though the conformal limit liberated the quartic model from the constraints associated with the fast roll, the spectator condition has become more severe with the introduction of the quartic coupling, limiting $\max(\Gamma_i)$. Using Eq. (162), the maximum range for the blue part of the isocurvature spectrum for $M \sim O(H)$ is given by the expression

$$\max\left(k_{\text{tr}}/k_i\right) \approx \exp\left(\max N_{\text{blue}}\right) \approx 10^3 \sqrt{0.2} \left(\frac{r_a}{0.01}\right)^{1/4} \left(\frac{1}{\lambda}\right)^{1/4} \sqrt{\frac{M_P/H}{10^6}} \frac{1}{f_{\text{PQ}}/H}. \tag{163}$$

5.3. Spectral bump and M dependence

In Fig. 11, we show comparison between the isocurvature power spectra for different values of M while keeping $\lambda = 10^{-4}$, $\Gamma_i = 300 f_{\text{PQ}}$ fixed and $\epsilon_L, \kappa = 0$. From Eqs. (139) and (140), we note that the normalized isocurvature power spectra $\overline{\Delta_s^2}(k)$ is independent of λ and hence we do not study variation of λ parameter. The plot highlights the deviation in the shape of the power spectra for different values of M as the spectrum transitions from a blue region to a massless

plateau. We observe the appearance of a spectral bump (irrespective of λ) for values of $M \gtrsim M_c$ where $M_c = 3H/4$ is an approximate cutoff derived in Appendix C. This cutoff is essentially the usual dS oscillator equation having a critical mass$/H = 3/2$ but the mass at the asymptotic future minimum of the radial field effective potential is $2M$. As the value of M rises above the cutoff M_c, the asymptotic (late-time) behavior of the background radial field transitions from an exponential to oscillatory similar to the critical transition observed in damped oscillators. Thus, as the radial field Γ rolls down the potential and approaches its stable vacuum f_{PQ}, for values of $M \gtrsim M_c$ the radial field oscillates momentarily around the stable vacuum f_{PQ} before settling down. The oscillation of the radial field around f_{PQ} translates into oscillations of the mass-squared term $m_\Gamma^2 \equiv m_{\delta\chi}^2$ around zero. These "non-adiabatic" oscillations give rise to a bump in the power spectrum. However, due to the presence of the tachyonic drag force from the non-zero angular velocity term, the amplitude of the oscillations and the corresponding height of the spectral bump become saturated for larger values of M. Numerically, we find that for $M \gg H$, the amplitude of the bump is approximately a factor of 1.3 larger than the flat spectrum. On the other hand, when $M \lesssim M_c$, the radial field settles to the vacuum exponentially slow $\left(\Gamma \to f_{\mathrm{PQ}}\left(1 + \exp\left(-\frac{3}{4}\left(M/M_c\right)^2 t\right)\right)\right)$ and hence the power spectrum gradually converges, without any bump, to the massless plateau over a large range of modes k as seen from the plots in Fig. 11.

Blue-tilted isocurvature power spectra with spectral bumps have been discussed previously in [7, 62] for a SUSY embedding of the axion model as presented in [49] which we will refer to as the KK model. In the KK model, a blue power spectrum with $n_I = 3$ occurs when the Lagrangian parameter is fixed at $c_+ = 2$ (corresponding to the dynamical axion mass squared of $c_+ H^2$). Notably, a bump in the power spectrum at the transition "always" exists for the KK model, unlike the model discussed in this paper, where the bump vanishes for $M \lesssim M_c$ despite the blue spectral index remaining $n_I = 3$. This is an important distinguishing feature between the model discussed in this work and the flat-direction models like the KK model. This distinction arises from the proximity of the mass $\sqrt{c_+}H = \sqrt{2}H$ in the KK model to the critical mass $3H/2$. Moreover, the KK model lacks an additional drag force from a non-zero angular velocity term, unlike the model discussed in this work. This drag force slows down the motion of the radial field in our model towards the minimum of the potential, resulting in a gradual transition of the spectrum to the massless plateau. Consequently, the presence of a bump at the transition from a k^2-spectrum is a generic feature in the KK model due to its near-critical mass and absence of an additional drag force. Unlike the model discussed in this work, the height of the spectral bump in the overdamped KK model for
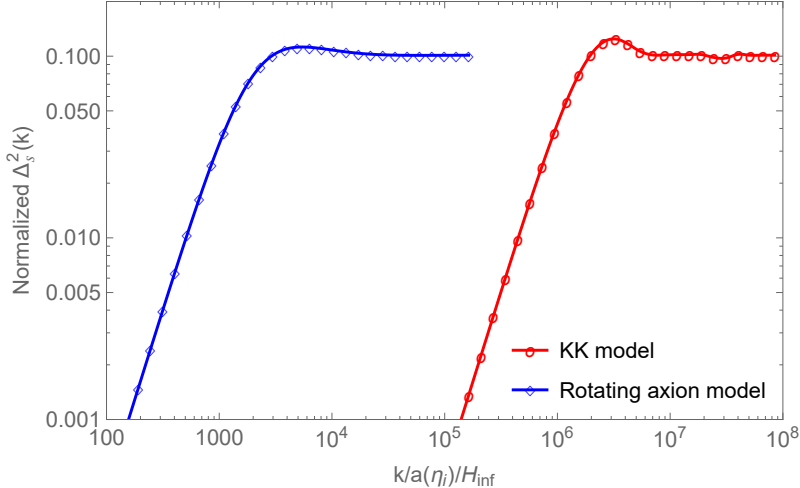
Figure 12: We present examples of normalized isocurvature power spectra for both the KK model and the rotating axion model. As discussed in the main text, the KK model can exhibit a significantly larger $\max\left(k_{\mathrm{tr}}/k_i\right)$ for the same values of f_{PQ} and H. This is due to the comparatively larger radial displacement allowed by the spectator condition in the KK model. For these plots, we set $f_{\mathrm{PQ}}/H = 100$ and $H/M_p = 10^{-9}$. The remaining Lagrangian parameters are set at $\{c_+ = 2, c_- = 2\}$ for the KK model and $\{\lambda = 2 \times 10^{-4}, M/H = 1\}$ for the current model. In both models, the initial radial velocity is set to zero. Without any adverse tuning of λ, a large $\max\left(k_{\mathrm{tr}}/k_i\right)$ in the KK model can serve as a distinguishing feature between the two models.

$c_+ = 2$ can be larger than the flat spectrum by at most a factor of 3 where the height is governed by the parameter c_- ([62]).

Additionally, the maximum k-range for the blue part of the spectrum in the KK model can be much larger than that achievable from the rotating axion model. This difference arises because the potential of the KK model is quadratically dominated, compared to the quartic potential of the rotating axion model. In Fig. 12, we plot examples of normalized isocurvature power spectra for both the KK model and the rotating axion model. We emphasize that the KK model can exhibit a significantly larger $\max\left(k_{\mathrm{tr}}/k_i\right)$. In the absence of any adverse tuning of λ, such a large $\max\left(k_{\mathrm{tr}}/k_i\right)$ can serve as another distinguishing feature between the two models.

5.4. Bounds on the conformal axion model

Since the bounds for the blue isocurvature spectrum is weak for $k_{\mathrm{tr}}/a_{\mathrm{today}} \gtrsim 1\ \mathrm{Mpc}^{-1}$ [1–11], the plateau part of isocurvature spectrum Δ_s^2 can be much larger than $O(10^{-2})\Delta_\zeta^2$ (where Δ_ζ^2 is the adiabatic spectrum) if $k_{\mathrm{tr}}/k_i \gtrsim 10^4$. Nonetheless, there is a constraint on the isocurvature for

this shape of the spectrum as explored by [7, 8]. To this end, we will discuss how all of following conditions being satisfied simultaneously within this conformal scenario *applied to QCD axions* is difficult, although relaxing any one constraint gives a sizeable parameter region:

1. The axion is a QCD axion

2. $\max\left(k_{\mathrm{tr}}/k_i\right) \gg O(10^3)$

3. $\lambda = O(1)$

4. All of DM being composed of axions.

5. Isocurvature not violating the current bounds.

The second condition is something that is desired for the interest of future observations and allows much larger signals than the current bound of $\Delta_s^2/\Delta_\zeta^2 \lesssim 0.02$ associated with the scale invariant CDM-photon isocurvature spectrum. The third condition comes from naturalness/simplicity of axion models. On the other hand, if the fourth condition is relaxed to CDM fraction being $\omega_a = 0.1$ (which is still quite sizeable and may even be detectable depending on the size of the electromagnetic coupling [64]), then an appreciable parameter region opens up where the isocurvature primordial amplitude can be larger than the adiabatic amplitude. Of course, for non-QCD axions, depending on the dark matter scenario, the rest of the conditions can be satisfied.

Shown in Fig. 13 is an illustration of the predictions from the present scenario assuming that the axions are QCD axions. The break in the blue spectrum given by Eq. (163) contains the following parametric dependences:

$$\max\left(\frac{k_{\mathrm{tr}}}{k_i}\right) \sim \frac{\sqrt{M_P H}}{\lambda^{1/4} f_{\mathrm{PQ}}}. \tag{164}$$

The prediction for the break spectral value depends on the initial value $\Gamma(t_i)$ and k_{tr}/k_i can be maximally as large as what is shown in the solid and dashed diagonal lines. Hence, the conformal scenario of $\Gamma(t) \propto 1/a$ lives to the left of these diagonal lines.

To derive the diagonal curves in Fig. 13, note that fixing ω_a and θ_i essentially fix f_{PQ} since

$$\omega_a = \frac{\Omega_a h^2}{0.12} \tag{165}$$

$$\approx 2\left(\theta_i^2 + \left(\frac{H}{2\pi f_{\mathrm{PQ}}}\right)^2\right)\left[\ln\left(\frac{e}{1-\theta_i^2/\pi^2}\right)\right]^{7/6}\left(\frac{f_{\mathrm{PQ}}}{10^{12}\mathrm{GeV}}\right)^{7/6} \tag{166}$$
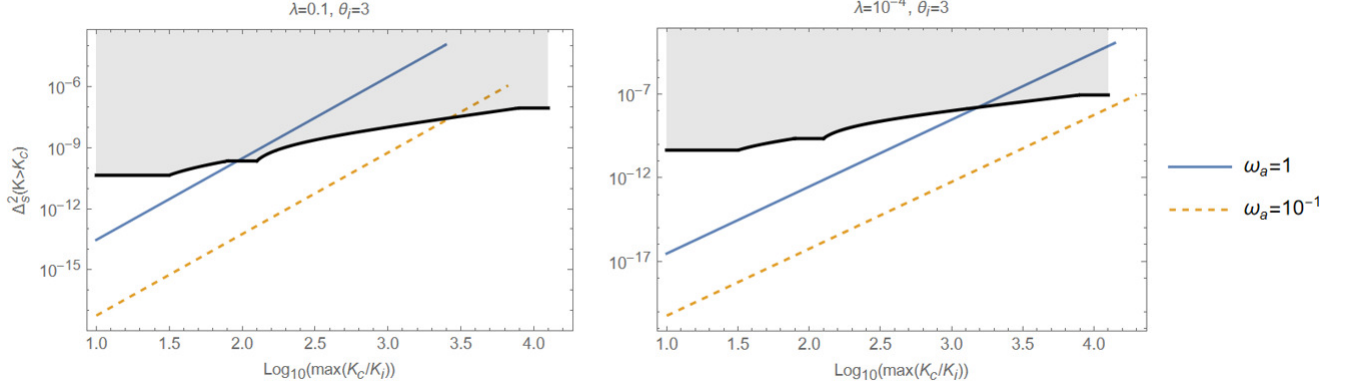
Figure 13: Left figure illustrates a natural coupling $\lambda = 0.1$ scenario with spectator energy fraction taken as $r_a = 10^{-2}$. As $\max\left(k_{\mathrm{tr}}/k_i\right) \sim \sqrt{M_P H/\sqrt{\lambda}}/f_{\mathrm{PQ}}$ increases, the inflationary expansion rate H has to become larger with a fixed λ and f_{PQ} (where the latter is fixed by the axion fraction of CDM denoted as ω_a), making the isocurvature amplitude rise. The isocurvature bound in the shaded region is an approximate extrapolation based on [7] assuming that the data induced bounds for that work applies to the current scenario because of the similarity in the spectral shape. Only the small segment near $k_{\mathrm{tr}}/k_i \approx 10^2$ and 10^4 can be read off easily from [7], and the rest of the black curve above $k_{\mathrm{tr}}/k_i = 10^{1.5}$ represents a smooth interpolation. The horizontal solid black curve below $k_{\mathrm{tr}}/k_i = 10^{1.5}$ represent the phenomenological [7, 8] $\Delta_s^2/\Delta_\zeta^2 \approx 2 \times 10^{-2}$ CDM-photon isocurvature bound applicable to *scale invariant spectrum*. The allowed region in the $\left(\Delta_s^2(k > k_{\mathrm{tr}}), \max\left(k_{\mathrm{tr}}/k_i\right)\right)$ plane is the left of the solid and the dashed diagonal lines (and below the shaded region), and the exact location for the model prediction depends on the Γ initial conditions. The reason why the solid and dashed diagonal lines cut off before reaching the top of the plot is because we impose $H/f_{\mathrm{PQ}} < 0.1$ bound such that there is no symmetry restoration during inflation. The right figure is similar to the left figure, except λ has been decreased to a more tuned value of 10^{-4}. The main lesson from these plots is that $\lambda \sim O(1)$ coupling is incompatible with large break k_{tr}/k_i (such as $k_{\mathrm{tr}}/k_i \sim 10^4$ which phenomenologically allows larger isocurvature signal) if all of the dark matter is made of axion dark matter.

according to [65].[14][15] Combining this fact with our knowledge that the plateau part of the spectrum ($k \gg k_{\mathrm{tr}}$ part) is given by

$$\Delta_{\delta a}^2\left(k \gg k_{\mathrm{tr}}\right) \approx 4\left(\frac{H}{2\pi f_{\mathrm{PQ}}\theta_i}\right)^2, \tag{167}$$

we see that the isocurvature amplitude in the plateau depends just on H with f_{PQ} fixed. Since we now want the axion sector to be a spectator to inflation and H controls the energy density during

---

[14] Here the ln factor approximately taking into account the anharmonic effects of axion oscillations has been included to obtain the $O(10)$ enhancement that exists for $\theta_i = 3$.

[15] Some models in the literature explore scenarios where f_{PQ} during inflation differs from the late-time f_a for the axions, potentially relaxing isocurvature constraints. For further details, see [66] and the references therein.

inflation, a larger H is needed if the initial $\Gamma(t_i)$ displacement that we desire for a larger

$$\max\left(\frac{k_{\mathrm{tr}}}{k_i}\right) \approx \exp\left(H\Delta t\right) \approx \frac{\max\left[\Gamma(t_i)\right]}{f_{\mathrm{PQ}}} \tag{168}$$

carries a larger energy, where the $\exp(H\Delta t)$ comes from the conformal scaling behavior of $\Gamma(t)$.

The spectator condition with the initial energy in $\Gamma(t_i)$ being r_a fraction of the total sets the maximum $\Gamma(t_i)$ value to

$$\Gamma_i^{\max}(k_{\mathrm{tr}}/k_i) \approx \left(\frac{4M_P^2 H^2 r_a}{\lambda}\right)^{1/4} \tag{169}$$

where we are assuming that the kinetic energy is negligible initially. In practice, we take $r_a \lesssim 10^{-2}$ since the slow roll parameters are of $O(10^{-2})$. Hence, we find that H is a function of k_{tr}/k_i in Eq. (167). More explicitly, Eqs. (168) and (169) give

$$\frac{H^2}{f_{\mathrm{PQ}}^2} = \frac{\lambda f_{\mathrm{PQ}}^2}{4M_P^2 r_a}\left[\max\left(\frac{k_{\mathrm{tr}}}{k_i}\right)\right]^4 \tag{170}$$

or when inserted into Eq. (167)

$$\Delta_s^2\left(k > k_{\mathrm{tr}}\right) \approx 10^{-5}\left(\frac{3\lambda/r_a}{10^{-2}}\right)\left(\frac{\theta_i}{3}\right)^{-2}\left(\frac{z(\theta_i)}{38}\right)^{-12/7}\left(\frac{\max\left(k_{\mathrm{tr}}/k_i\right)}{10^4}\right)^4 \omega_a^{26/7} \tag{171}$$

where

$$z(\theta_i) \equiv \theta_i^2\left[\ln\left(\frac{e}{1 - \theta_i^2/\pi^2}\right)\right]^{7/6} \tag{172}$$

and we have neglected the H dependence in Eq. (166): i.e. the formula applies to $\{\theta_i \gg 0.02, H/f_{\mathrm{PQ}} \lesssim 0.1\}$. Note that $\lambda \sim O(1)$ is in tension with $\max\left(k_{\mathrm{tr}}/k_i\right) \sim 10^4$ with the axions being all of the CDM since the isocurvature at the break would then be already five orders of magnitude larger than the adiabatic perturbations. Making θ_i smaller does not help to alleviate the isocurvature constraints while maintaining a large k_{tr}/k_i and ω_a.

Note that the bound of

$$f_{\mathrm{PQ}} \gtrsim 10^9\mathrm{GeV} \tag{173}$$

coming from white dwarf cooling time merely sets a lower bound on ω_a for a given θ_i according to Eq. (166):

$$\omega_a \gtrsim 6 \times 10^{-4}\left(\theta_i^2 + \left(\frac{H}{2\pi f_{\mathrm{PQ}}}\right)^2\right)\left[\ln\left(\frac{e}{1 - \theta_i^2/\pi^2}\right)\right]^{7/6}\left(\frac{f_{\mathrm{PQ}}^{\min}}{10^9\mathrm{GeV}}\right)^{7/6}. \tag{174}$$

Hence, with $\theta_i = 3$ and neglecting the $H/(2\pi f_{\mathrm{PQ}})$ term, we find $\omega_a \approx 0.02$ which rules out 10^{-3} as a possibility to plot in Fig. 13. With smaller θ_i, a smaller ω_a is certainly consistent with Eq. (173), but that leads to a more stringent constraint associated with the existing isocurvature bounds because of Eq. (171).

6. CONCLUSION

In this paper, we have shown that modifying the initial conditions of a generic $U(1)$ symmetric quartic potential complex scalar model can lead to a novel axion isocurvature scenario in which a transition takes place from a time-independent conformal phase to the time-dependent conformal phase, the latter being the usual equilibrium axion scenario. Such time-independent spontaneously broken conformal phase initial condition is controlled by a large classical background phase angular momentum $\partial_\eta \theta_0(\eta_i) \gg Ma(\eta_i) \gtrsim Ha(\eta_i)$ and a large radial field displacement $\Gamma_0(\eta_i) \sim \partial_\eta \theta_0(\eta_i)/\sqrt{\lambda}$. With such initial conditions for the background, the quantum perturbations remarkably enter a nontrivial time-independent spontaneously symmetry-broken conformal phase characterized by a long wavelength spectral index of $n_I - 1 = 2$ and a Goldstone dispersion with a sound speed of $1/\sqrt{3}$. Interestingly, the cross-correlation function $\langle \partial_\eta \delta\Gamma \partial_\eta \delta\Sigma \rangle$ during this time-independent conformal phase between the radial and the axion fields does not vanish even though $\langle \delta\Gamma \delta\Sigma \rangle = 0$ to leading order in perturbation theory.

After the Γ_0 reaches the usual spontaneous PQ symmetry breaking minimum, the theory enters the usual time-dependent conformal phase characterized by the time-dependent effective mass term $a''/a = 2/\eta^2$. For k values corresponding to this time region, denoted as $k > k_{\rm tr}$, the isocurvature spectrum is the well-known $n_I - 1 = 0$ flat plateau, and the Goldstone dispersion has a sound speed of 1. One nontrivial phenomenological result established in this paper is that the spectral transition from $n_I = 3$ to $n_I = 1$ for realistic parameter ranges can be sudden such that there is no large bump connecting these two regions. This means that this quartic potential model can behave qualitatively differently from the overdamped supersymmetric (SUSY) scenarios of [49] where there is a bump [63]. Furthermore, if the k range over which the blue spectral index sets in is sufficiently large, then the present model becomes more fine tuned compared to the flat direction models. In the sense of making parameters less tuned, the SUSY models in this context can be considered analogous to the low-energy SUSY models solving the Higgs mass hierarchy problem.

With two-parameter initial condition perturbations away from those generating the time-independent spontaneously broken conformal phase, we have shown that the smooth $n_I = 3$ to $n_I = 1$ spectra transition scenarios are stable with $O(0.1)$ deformations of $\sqrt{\lambda}a(\eta_i)\Gamma_0(\eta_i)/\partial_\eta\theta_0(\eta_i)$ and $\partial_\eta[a\Gamma_0]/\left(\sqrt{6\lambda}a^2(\eta_i)\Gamma_0^2(\eta_i)\right)$. On the other hand, small deviations of the spectral amplitudes linear in these deformation ratios eventually gain a nonlinear dependence as these deviations grow beyond magnitudes of around 0.3. Afterwards parametric resonances strongly set in and destroy the

original qualitative shape of the spectra. The small oscillatory features apparent in small deformation cases are well-fit by a simple formula characteristic of the $1/\sqrt{3}$ sound speed of the conformal phase.

We have also explored the parametric region for which this scenario is phenomenologically interesting. Requiring the *simultaneous* satisfaction of constraint of the axion being a QCD axion, maximum $n_I = 3$ blue spectral interval $[k_i, k_{\text{tr}}]$ satisfying $k_{\text{tr}}/k_i \gg O(10^3)$, quartic coupling of order unity, all of the DM being composed of axions, and isocurvature not violating the current bounds, no viable parameter region exists. On the other hand, with the relaxation of these constraints, there is a phenomenologically viable parametric region as shown in Fig. 13. Because the energy density rises steeply compared to the flat direction scenarios as the radial field is displaced, the spectator condition imposes a significant constraint that makes this scenario sensitive to the quartic coupling.

There are many natural future directions to explore. Given the natural similarities between this model and the SUSY flat direction model of [49], it would be interesting to see whether non-Gaussianities can break the degeneracy. Indeed, there is a peculiar feature of the time-independent conformal spectra which kinetically cross correlates the radial mode and the axial mode, and this kinetic mixing does not exist in the SUSY flat direction model. Hence, we would expect the non-Gaussianities to be different between the two models even if the isocurvature spectra are similar. Another interesting direction is in exploring the observability of the oscillatory features in the power spectra. As noted above, in the quasi-conformal model, there are oscillatory features in the isocurvature spectra for small deviations away from time-independent conformality and since those oscillations encode the $1/\sqrt{3}$ sound speed information, it would be interesting to see if observations can measure this sound speed. Of course, work even remains to be done in assessing the observability of the oscillatory features in the underdamped SUSY models [62] as noted in [67].

Appendix A: Conformal limit for the background

In this section, we describe how a large Γ/M and Γ/H limit together with a certain classical boundary condition corresponds to a spontaneously broken approximate conformal limit of the field theory of Γ and Σ during which $\Gamma a =$ nonzero constant $+ \delta(\Gamma a)$ where a is the scale factor corresponding to the metric

$$ds^2 = a^2(\eta) \left[-d\eta^2 + |d\vec{x}|^2 \right]. \tag{A1}$$

We begin by deriving the effective action from a general $U(1)$ symmetric renormalizable theory that spontaneously breaks an approximate conformal symmetry with a large phase angular momentum. We then use the conformal symmetry parameterization to generate an automorphism of the correlation functions. This allows one to derive a differential equation for the correlation functions whose general solution is given. We will then use the spontaneously broken $U(1)$ coset representation to derive $|\vec{x} - \vec{y}|^2$ for the δX correlators and use the absence of this symmetry for δY correlators to argue for the $|\vec{x} - \vec{y}|^{-3} (\partial_\eta \theta_0)^{-1}$ dependence.

Start with a general renormalizable $U(1)$ invariant action action given by Eq. (16):

$$S = \int d\eta d^3x \left\{ -\frac{1}{2} \eta^{\mu\nu} \partial_\mu Y \partial_\nu Y - \frac{1}{2} \eta^{\mu\nu} Y^2 \partial_\mu \theta \partial_\nu \theta - \left(-\frac{1}{2} \frac{a''}{a} Y^2 - M^2 a^2 Y^2 + \frac{\lambda}{4} Y^4 \right) \right\} \tag{A2}$$

where $Y \equiv a\Gamma$. Note that this theory is almost invariant under the following constant u scaling conformal (dilatation) transform:

$$a \to a u^{-1} \tag{A3}$$

were it not for the $M^2 a^2 Y^2$ term. Look for $Y =$ constant solutions to the equation of motion for $Y(x) = Y_0(\eta)$:

$$\frac{1}{\eta^{00}} Y_0^{-3} L^2 - \left(\frac{a''}{a} + 2M^2 a^2 \right) Y_0 + \lambda Y_0^3 = 0. \tag{A4}$$

where we used the $U(1)$ generated conservation law to set

$$-\eta^{00} Y_0^2 \partial_\eta \theta = L \tag{A5}$$

with L being a constant. Because metric scaling will be involved later, here we have chosen to keep η^{00} explicit coming from the conserved quantity being proportional to the $U(1)$ charge density j^0 and not its associated 1-form j_0. Eq. (A4) has an approximately time-independent solution

$$Y_0 = \frac{L^{1/3}}{(-\eta^{00} \lambda)^{1/6}} \tag{A6}$$

when

$$\lambda Y_0^2 \gg \frac{a''}{a} + 2M^2 a^2. \tag{A7}$$

Substituting Eq. (A5) into (A6), we find

$$Y_0 = Y_c \equiv \frac{\sqrt{-\eta^{00}} |\partial_\eta \theta_0|}{\sqrt{\lambda}} \tag{A8}$$

which is a constant by the virtue of Eq. (A6). Since Y_c is a constant, we know from this equation that $\theta'_0(\eta)$ is a constant. In terms of Γ and θ fields, these solutions represent

$$\Gamma \approx \Gamma_0(\eta) = \frac{\sqrt{-\eta^{00}}\,|\theta'_0(\eta)|}{a(\eta)\sqrt{\lambda}} \tag{A9}$$

$$\theta \approx \theta_0(\eta) = \theta_0(\eta_i) + \eta\partial_\eta\theta_0(\eta_i) \tag{A10}$$

indicating that this is a nontrivial approximate time-dependent background in terms of the canonical real radial field.

Now, define

$$X \equiv Y_c\theta. \tag{A11}$$

By neglecting a''/a and $M^2 a^2$ consistently with Eq. (A7), the action now turns out to be completely independent of the scale factor a:

$$S[X, Y, \eta_{\mu\nu}, Y_c] \approx \int d\eta d^3x \sqrt{\eta}\left(-\frac{1}{2}\eta^{\mu\nu}\left[\partial_\mu Y\right]\left[\partial_\nu Y\right] - \frac{1}{2}\eta^{\mu\nu}\left[\partial_\mu X\right]\left[\partial_\nu X\right]\left(\frac{Y}{Y_c}\right)^2 - \frac{\lambda Y^4}{4}\right) \tag{A12}$$

showing explicitly that we have a conformal theory enjoying the symmetry

$$S[Xu, Yu, \eta_{\mu\nu}u^{-2}, Y_cu] = S[X, Y, \eta_{\mu\nu}, Y_c]. \tag{A13}$$

where u is a constant.

Here, the arguments $\eta_{\mu\nu}$ and Y_c of S are viewed as externally input parameters, and we transform them as we would a spurion. Note that the conformal representation here is different from the dilatation subgroup representation of diffeomorphism (see e.g. [68]) especially because we are scaling Y_c which is a parameter, as in a spurion representation of the conformal group in a free massive scalar theory. On the other hand, rewriting Eq. (A9) as

$$Y_c = a(\eta)\Gamma_0(\eta) \tag{A14}$$

shows that the transform $\{\eta_{\mu\nu}, X, Y, Y_c\} \rightarrow \{\eta_{\mu\nu}u^{-2}, Xu, Yu, Y_cu\}$ comes from scaling the scale factor by a constant as $a \rightarrow au^{-1}$, such that the symmetry of Eq. (A13) being an element of the conformal group is evident.[16] We will see how these symmetries together with diffeomorphism will give rise to constraints on the correlation functions of interest below.

---

[16] If we had used $Y_c = \sqrt{-\eta^{00}}\,|\theta'_0(\eta)|/\sqrt{\lambda}$, we would have still ended up with the conformal transform $a^2(\eta_i)\eta_{00} = \eta_{00} \rightarrow a^2(\eta_i)u^{-2}\eta_{00} = \eta_{00}u^{-2}$ giving $Y_c \rightarrow uY_c$.

Expand the fields as

$$X(x) = \theta_0(\eta)Y_c + \delta X(x) \tag{A15}$$

$$Y(x) = Y_c + \delta Y(x) \tag{A16}$$

where $\theta_0(\eta)$ is given by Eq. (A10) and look for the effective action governing the perturbations only. The perturbation-only action is

$$S_2[\delta X, \delta Y, \eta_{\mu\nu}, Y_c, \partial_\eta \theta_0] = \int d\eta d^3x \sqrt{\eta} \left(\frac{-1}{2} \eta_{\mu\nu} \partial^\mu \delta Y \partial^\nu \delta Y - \frac{1}{2} \eta_{\mu\nu} \partial^\mu \delta X \partial^\nu \delta X \right. \tag{A17}$$

$$\left. -2\delta Y \eta_{\mu\nu} \partial^\mu \delta X \partial^\nu \theta_0 - \frac{1}{2} (\delta Y)^2 \eta^{\mu\nu} (\partial_\mu \theta_0 \partial_\nu \theta_0) - \left(\frac{3\lambda}{2} Y_c^2 \right) (\delta Y)^2 \right) \tag{A18}$$

which enjoys the conformal symmetry

$$S_2 \left[\delta X u, \delta Y u, \eta_{\mu\nu} u^{-2}, Y_c u, \partial_\eta \theta_0 \right] = S_2 \left[\delta X, \delta Y, \eta_{\mu\nu}, Y_c, \partial_\eta \theta_0 \right] \tag{A19}$$

where the constant $\partial_\eta \theta_0$ does not transform. However, as we will see below, $\partial_\eta \theta_0$ will transform under diffeomorphism because of the time derivative.

Carry out a coordinate change (diffeomorphism) $d\underline{x}^\mu = u dx^\mu$ leading to

$$\underline{\eta_{\mu\nu}} = u^{-2}\eta_{\mu\nu} \tag{A20}$$

and $\underline{\phi}(\underline{x}) = \phi(x) = \phi(\underline{x}u^{-1})$ leading to the diffeomorphism invariant action transforming as

$$S_2[\delta X, \delta Y, \eta_{\mu\nu}, Y_c, \partial_\eta \theta_0] = \int d^4 \underline{x} \sqrt{\underline{\eta}} \mathcal{L}(\underline{\delta X}(\underline{x}), \underline{\delta Y}(\underline{x}), \underline{\eta_{\mu\nu}}, \underline{Y_c}, \underline{\partial_\eta \theta_0}) \tag{A21}$$

$$= \int d^4 \underline{x} u^{-4} \sqrt{\eta} \mathcal{L} \left(\delta X(\underline{x}u^{-1}), \delta Y(\underline{x}u^{-1}), u^{-2}\eta_{\mu\nu}, Y_c, u^{-1}\partial_\eta \theta(\eta_i) \right) \tag{A22}$$

Scaling variables, we find

$$S_2[\delta X u^{-1}, \delta Y u^{-1}, \eta_{\mu\nu} u^2, Y_c u^{-1}, \partial_\eta \theta_0] = \int d^4 x \sqrt{\eta} \mathcal{L}(u^{-1}\delta X(xu^{-1}), u^{-1}\delta Y(xu^{-1}), \eta_{\mu\nu}, Y_c u^{-1}, \partial_\eta \theta_0 u^{-1}).$$
$$\tag{A23}$$

Because of Eq. (A19), this is equivalent to

$$S_2[\delta X u^{-1}, \delta Y u^{-1}, \eta_{\mu\nu} u^2, Y_c u^{-1}, \partial_\eta \theta_0] = S_2[\delta X, \delta Y, \eta_{\mu\nu}, Y_c, \partial_\eta \theta_0] \tag{A24}$$

and thus

$$S_2[\delta X, \delta Y, \eta_{\mu\nu}, uY_c, u\partial_\eta\theta_0] = \int d^4x \sqrt{\eta} \mathcal{L}(u^{-1}\delta X(xu^{-1}), u^{-1}\delta Y(xu^{-1}), \eta_{\mu\nu}, Y_c, \partial_\eta\theta_0) \quad \text{(A25)}$$

$$= S_2[u^{-1}\delta X(xu^{-1}), u^{-1}\delta Y(xu^{-1}), \eta_{\mu\nu}, Y_c, \partial_\eta\theta_0] \quad \text{(A26)}$$

Let's see the implication of this on the Feynman correlator which will be equivalent to the in-in equal time correlator that we seek at free field level:

$$\langle \delta X(\eta, \vec{x}) \delta X(\eta, \vec{y}) \rangle_{g, Y_c, \partial_\eta\theta_0} = \frac{\int D\delta X D\delta Y e^{iS_2[\delta X, \delta Y, g, Y_c, \partial_\eta\theta_0]} \delta X(\eta, \vec{x}) \delta X(\eta, \vec{y})}{\int D\delta X D\delta Y e^{iS_2[\delta X, \delta Y, g, Y_c, \partial_\eta\theta_0]}} \quad \text{(A27)}$$

Change variables

$$\int D\delta X D\delta Y = \int D\left[u^{-1}\delta\tilde{X}(zu^{-1})\right] D\left[u^{-1}\delta\tilde{Y}(zu^{-1})\right] \quad \text{(A28)}$$

to conclude

$$\langle \delta X(\eta, \vec{x}) \delta X(\eta, \vec{y}) \rangle_{\eta_{\mu\nu}, Y_c, \partial_\eta\theta_0} = \frac{\int D\delta X D\delta Y e^{iS_2[\delta X, \delta Y, \eta_{\mu\nu}, uY_c, u\partial_\eta\theta_0]} u^{-2}\delta X(\eta u^{-1}, \vec{x}u^{-1})\delta X(\eta u^{-1}, \vec{y}u^{-1})}{\int D\delta X D\delta Y e^{iS_2[\delta X, \delta Y, \eta_{\mu\nu}, uY_c, u\partial_\eta\theta_0]}}$$

$$\text{(A29)}$$

or more explicitly

$$\langle \delta X(\eta, \vec{x}) \delta X(\eta, \vec{y}) \rangle_{\eta_{\mu\nu}, Y_c, \partial_\eta\theta_0} = u^{-2} \left\langle \delta X(\eta u^{-1}, \vec{x}u^{-1})\delta X(\eta u^{-1}, \vec{y}u^{-1}) \right\rangle_{\eta_{\mu\nu}, uY_c, u\partial_\eta\theta_0}. \quad \text{(A30)}$$

To derive the differential equation governing the correlator by assuming $SO(3)$ and spatial translation invariance, start by writing

$$\langle \delta X(\eta, \vec{x}) \delta X(\eta, \vec{y}) \rangle_{\eta_{\mu\nu}, Y_c, \partial_\eta\theta_0} = f(\eta, |\vec{x} - \vec{y}|, Y_c, \partial_\eta\theta_0) \quad \text{(A31)}$$

where $f(\eta, w, s, P)$ is a function of variables $\{\eta, w, s, P\}$. This and Eq. (A30) says

$$u^{-2}f(\eta u^{-1}, u^{-1}|\vec{z}|, uY_c, u\partial_\eta\theta_0) = f(\eta, |\vec{x} - \vec{y}|, Y_c, \partial_\eta\theta_0) \quad \text{(A32)}$$

Taking a derivative with respect to u and setting $u = 1$, we find

$$-2f(\eta, z, Y_c, \partial_\eta\theta_0) - \eta\partial_\eta f(\eta, z, Y_c, \partial_\eta\theta_0)|_{w_1=\eta} - z\frac{\partial}{\partial z}f(\eta, z, Y_c, \partial_\eta\theta_0)$$

$$+ Y_c\partial_{Y_c}f(\eta, z, Y_c, \partial_\eta\theta_0) + \partial_\eta\theta_0\partial_{(\partial_\eta\theta_0)}f(\eta, z, Y_c, \partial_\eta\theta_0) = 0 \quad \text{(A33)}$$

governing the correlator. A general solution to this equation is

$$f(\eta, z, Y_c, \partial_\eta\theta_0) = \frac{\exp\left(C_f\left(\ln\frac{z}{-\eta}, \ln\left[(-\eta)Y_c\right], \ln\left[(\partial_\eta\theta_0(\eta_i))(-\eta)\right]\right)\right)}{\eta^2} \quad \text{(A34)}$$

where $C_f(w_1, w_2)$ is a general function of two variables. Now, S_2 time translation invariance implies f being time-translation-invariant. This results in the differential equation

$$-2 + \sum_{i=1}^{3} \partial_{w_i} C_f(w_1, w_2, w_3) = 0 \tag{A35}$$

whose general solution is

$$C_f(w_1, w_2, w_3) = -2w_1 + B_f(w_1 + w_2, w_1 + w_3) \tag{A36}$$

giving

$$f(\eta, z, Y_c, \partial_\eta \theta_0) = \frac{\exp\left(B_f(\ln[zY_c], \ln[z\partial_\eta \theta_0(\eta_i)])\right)}{z^2}. \tag{A37}$$

Furthermore, we know for circular orbits

$$Y_c \lambda^{1/2} = \sqrt{-\eta^{00}} \left(\partial_\eta \theta_0\right) \tag{A38}$$

and thus combine Y_c and $\partial_\eta \theta_0$ dependence to conclude

$$\langle \delta X(\eta, \vec{x}) \delta X(\eta, \vec{y}) \rangle_{\eta_{\mu\nu}, Y_c, \partial_\eta \theta_0} = \frac{E_f^X \left(\ln\left[|\vec{x} - \vec{y}| \left(\partial_\eta \theta_0(\eta_i)\right)\right]\right)}{|\vec{x} - \vec{y}|^2} \tag{A39}$$

$$\langle \delta Y(\eta, \vec{x}) \delta Y(\eta, \vec{y}) \rangle_{\eta_{\mu\nu}, Y_c, \partial_\eta \theta_0} = \frac{E_f^Y \left(\ln\left[|\vec{x} - \vec{y}| \left(\partial_\eta \theta_0(\eta_i)\right)\right]\right)}{|\vec{x} - \vec{y}|^2} \tag{A40}$$

which are manifestly time-independent but contain arbitrary $|\vec{x} - \vec{y}|$ dependences unlike in the case of massless scalar fields in Minkowski space.

Next, note the $U(1)$ induced shift symmetry $\delta X \to \delta X + C$ has an associated current

$$j^\mu = \eta^{\mu\nu} \left\{ \partial_\nu \delta X + 2\delta Y \partial_\nu \theta_0 \right\}. \tag{A41}$$

whose conservation is

$$-\partial_0^2 \delta X - 2\partial_0 \delta Y \partial_0 \theta_0 + \partial_i^2 \delta X = 0 \tag{A42}$$

which is notably linear. In normal mode-Fourier space, Eq. (A42) is

$$\omega^2 \delta X_{\omega,k} + 2i\omega \delta Y_{\omega,k} \partial_0 \theta_0 - k^2 \delta X_{\omega,k} = 0. \tag{A43}$$

In the large k limit, we have the usual Goldstone condition $\omega^2 = k^2$ for any nonvanishing $\delta X_{\omega,k}$. The fact that the two modes have $\omega = \pm k$ dispersion possibilities can be viewed as a consequence of

approximately in tact CPT symmetry in that limit. For small k, there is at least one massless mode that is independent of $\delta X_{\omega,k}$ and $\delta Y_{\omega,k}$ as long as $\omega \delta X_{\omega,k}$ and $\delta Y_{\omega,k}$ do not diverge. Let's label that massless mode frequency as ω_0. Indeed, because of the $\partial_\eta \theta_0$ dependent mixing in Eq. (A18), both $\delta X_{\omega_0,0}$ and $\lim_{k\to 0} \delta Y_{\omega_0,k}/\omega_0$ do not vanish.

According to Eq. (A18), we see that the Lagrangian has a mode contribution

$$-2\delta Y \eta^{\mu\nu} \partial_\mu \delta X \partial_\nu \theta_0 - \frac{1}{2}(\delta Y)^2 \eta^{\mu\nu}(\partial_\mu \theta_0 \partial_\nu \theta_0) - \left(\frac{3\lambda}{2}Y_c^2\right)(\delta Y)^2 \tag{A44}$$

$$\sim \begin{pmatrix} \delta X_{\omega_0,k}^* & \delta Y_{\omega_0,k}^* \end{pmatrix} \begin{pmatrix} 0 & -i\omega_{0,k} \\ i\omega_{0,k} & -2(\partial_\eta \theta_0(\eta_i))^2 \end{pmatrix} \begin{pmatrix} \delta X_{\omega_0,k} \\ \delta Y_{\omega_0,k} \end{pmatrix} \tag{A45}$$

which in the $\partial_\eta \theta_0(\eta_i)/\omega_{0,k} \to \infty$ limit has δX decoupling from δY and $(\partial_\eta \theta_0(\eta_i))|\vec{x}-\vec{y}| \to \infty$ not changing the approximate correlation function for $\langle \delta X \delta X \rangle$. In that approximation, the factor $E_f^X(\ln[|\vec{x}-\vec{y}|(\partial_\eta \theta_0(\eta_i))])$ in Eq. (A39) has an expansion for large $|\vec{x}-\vec{y}|$ as

$$E_f^X(\ln[|\vec{x}-\vec{y}|(\partial_\eta \theta_0(\eta_i))]) = c_1 + W_X\left(\frac{1}{|\vec{x}-\vec{y}|(\partial_\eta \theta_0(\eta_i))}\right) \tag{A46}$$

where c_1 is independent of $|\vec{x}-\vec{y}|$ and $W_X(w)$ is a function where $W_X(0) = 0$. This and Eq. (A39) implies the correlator in Fourier space behaving as k^2 corresponding to a spectral index of $n_I = 3$ matching Eq. (28). Hence, unlike the ordinary massless Minkowski field, one has to use $U(1)$ Goldstone dynamical information contained in Eq. (A45) to fix the $|\vec{x}-\vec{y}|^{-2}$ scaling for the $\langle \delta X \delta X \rangle$ correlator.

With this same $\partial_\eta \theta_0(\eta_i)/\omega_{0,k} \to \infty$ approximation, we see from Eq. (A45) that a decoupled δY becomes infinitely heavy as $(\partial_\eta \theta_0(\eta_i)) \to \infty$. Since this means that $\langle \delta Y(\eta, \vec{x}) \delta Y(\eta, \vec{y}) \rangle$ should vanish with the same limit, we expect

$$E_f^Y(\ln[|\vec{x}-\vec{y}|(\partial_\eta \theta_0(\eta_i))]) \propto \frac{1}{|\vec{x}-\vec{y}|(\partial_\eta \theta_0(\eta_i))} + O\left(\frac{1}{|\vec{x}-\vec{y}|^2(\partial_\eta \theta_0(\eta_i))^2}\right) \tag{A47}$$

if the expansion is analytic in inverse powers of $|\vec{x}-\vec{y}|(\partial_\eta \theta_0(\eta_i))$. Explicit computations justify the analyticity.

Now, the sound speed of δX cannot quite be read off from this expression since $X = Y_c(\theta(\eta_i) + \eta \partial_\eta \theta(\eta_i)) + \delta X$ generates a mixing between δY and $\partial_\eta \delta X$. This mixing generated change in the sound speed, which is the most theoretically interesting aspect of the system studied in this paper, and other aspects of this system are addressed in the main body of the text when we quantize the theory.

Appendix B: WKB approximation for oscillating potentials

In this section, we explain Eq. (B19) which is a generalization of the WKB ansatz applicable for dispersion relationships with a fast time-oscillation component.

Consider the following differential equation

$$\partial_\eta^2 y + m^2(\eta)y = 0. \tag{B1}$$

The WKB method allows us to approximate the solution to the above differential equation as

$$y(\eta) \approx \sum_\pm \frac{c_\pm}{\sqrt{m(\eta)}} \exp\left(\pm i \int^\eta d\eta\, m(\eta)\right) \tag{B2}$$

given

$$\partial_\eta m(\eta) \ll m^2(\eta) \tag{B3}$$

and hence the mass-squared function must be slowly varying.

Let us now consider the situation where the mass-squared term is

$$m^2(\eta) = K^2 + A\cos(f\eta) \tag{B4}$$

where K, A are constants and we are interested in cases with $K^2 < A$ and $f \gg 1$ such that the mass-squared function is characterized by high frequency large amplitude oscillations. It is easy to note that the WKB approximation as given above is inappropriate and diverges at the zeros of m^2. Although one may use matching solutions at the zero crossings, such an approach is unwieldy for a fast oscillating potential and doesn't capture the long-time characteristic behavior of the system.

Another well-known approach begins with noting that Eq. (B1) with the mass-squared function given in Eq. (B4) satisfies the Mathieu differential equation

$$\partial_x^2 y + (a - 2q\cos(2x))\, y = 0 \tag{B5}$$

where

$$2x = f\eta \tag{B6}$$

$$q = \frac{-A/2}{f^2/4} \tag{B7}$$

$$a = \frac{K^2}{f^2/4} \tag{B8}$$

with the generalized solution

$$y = \sum_{\pm} c_{\pm} \text{Me}^{\pm}(\text{r}, \text{q}, \text{x}) \tag{B9}$$

$$\text{Me}^{\pm} = \text{ce}(r, q, x) \pm i \, \text{se}(r, q, x) \tag{B10}$$

for *ce*, *se* as the generalized angular Mathieu functions. In the limiting case $|q| \ll 1$, the Mathieu function has the following series expansion in powers of q

$$\text{Me}^{\pm}(\text{r}, \text{q}, \text{x}) \approx \exp(\pm irx) + \frac{q}{4}\left(\frac{\exp(\pm i(r-2)x)}{r-1} + \frac{\exp(\pm i(r+2)x)}{r+1}\right) + O(q^2) \quad \text{for } r \neq 1 \tag{B11}$$

where

$$r \approx \sqrt{a + \frac{1}{2(1-a)}q^2}. \tag{B12}$$

Using this, we can identify

$$rx \approx \eta\sqrt{K^2 + \frac{A^2}{2(f^2 - 4K^2)}} \tag{B13}$$

in the limit

$$\frac{2A}{f^2} \ll 1, \text{ and } \frac{A}{f} < K, \tag{B14}$$

and the exact Mathieu solution given in Eq. (B9) can be approximated up to first order in q as

$$y \approx \sum_{\pm} c_{\pm}\left(\exp(\pm iK\eta) + \frac{A}{2f^2}\left(\frac{\exp(\pm i(K-f)\eta)}{\frac{2K}{f} - 1} + \frac{\exp(\pm i(K+f)\eta)}{\frac{2K}{f} + 1}\right)\right). \tag{B15}$$

Hence, in the limit $2A/f^2 \ll 1$, we observe that the solution to the oscillatory mass-squared function in Eq. (B4) is a superposition of states with the dominant state having a frequency $\sim K$. Therefore, up to an accuracy of r_a, the WKB approximate solution to the differential Eq. (B1) can be given as

$$y_{\text{WKB}} \approx \sum_{\pm} \frac{c_{\pm}}{\sqrt{K}} \exp\left(\pm i \int^{\eta} d\eta K\right) + O(r_a) \tag{B16}$$

where

$$r_a \approx \frac{A}{2f^2} \times \max\left(\frac{1}{\frac{2K}{f} - 1}, \frac{1}{\frac{2K}{f} + 1}\right). \tag{B17}$$

Note that as long as $r_a \ll 1$, the dominant frequency of the WKB approximation is given by the slow-varying mass parameter such that the WKB method no longer suffers from any oscillatory divergences. The above results motivate us to draw following important conclusions.

Given a differential equation of the form

$$\partial_\eta^2 y + \left(K^2(\eta) + A(\eta)\cos\left(f\eta\right)\right) y = 0 \tag{B18}$$

where $K(\eta)$ and $A(\eta)$ are slow-varying non-oscillatory functions, the solution to the above differential equation can be approximate through the following WKB ansatz

$$y_{\text{WKB}} \approx \sum_\pm \frac{c_\pm}{\sqrt{K(\eta)}} \exp\left(\pm i \int^\eta d\eta K(\eta)\right) + O\left(\frac{A(\eta)}{2f^2} \times \max\left[\frac{1}{\frac{2K(\eta)}{f} - 1}, \frac{1}{\frac{2K(\eta)}{f} + 1}\right]\right) \tag{B19}$$

if

$$2A(\eta)/f^2 \ll 1, \text{ and } A(\eta)/f < K \tag{B20}$$

where

$$\partial_\eta K(\eta) \ll K^2(\eta). \tag{B21}$$

For $f \gg K$, then the solution exhibits a large hierarchy in states such that the system can be described as a superposition of IR and UV states

$$y \approx y_{\text{IR}} + y_{\text{UV}} \tag{B22}$$

with the corresponding frequencies as

$$\text{freq}_{\text{IR}} \approx K \tag{B23}$$

$$\text{freq}_{\text{UV}} \approx f \tag{B24}$$

and the amplitudes

$$\left|\frac{y_{\text{UV}}}{y_{\text{IR}}}\right|_\eta \approx \frac{A(\eta)}{2f^2} \ll 1. \tag{B25}$$

Appendix C: Late time behavior and M cutoff

In this Appendix we discuss the asymptotic (late-time) behavior of the background radial field as it settles to its stable vacuum and explore the associated mass parameter M-dependence. We will see that as the radial field settles to its vacuum, the system can be characterized as an oscillator with various damping. The damping characteristic is determined by M/M_c where the critical value M_c is what we construct below

To study the late-time behavior of the radial field as it settles to f_{PQ}, we consider displacements of the radial field around f_{PQ} parameterized as

$$\Gamma_0(\eta) = f_{\text{PQ}} \left(1 + r(\eta)\right) \tag{C1}$$

and substitute into the EoM for the radial field Γ_0 given in Eq. (65) to obtain an EoM for the function $r(\eta)$:

$$\partial_\eta^2 r + 2\frac{\partial_\eta a}{a}\partial_\eta r + 2M^2 a^2 \left(-1 + (1+r)^2 - \frac{1}{2M^2 a^6}\left(\frac{L/f_{\text{PQ}}^2}{(1+r)^2}\right)^2\right)(1+r) = 0. \tag{C2}$$

In the limit where $\Gamma_0 \to f_{\text{PQ}}$, the angular velocity term can be neglected since it decays as La^{-2} and so we reduce the above expression to

$$\partial_\eta^2 r + 2\frac{\partial_\eta a}{a}\partial_\eta r + 2M^2 a^2 \left(-1 + (1+r)^2\right)(1+r) \approx 0. \tag{C3}$$

For small displacements $r \ll 1$,

$$\partial_\eta^2 r + 2\frac{\partial_\eta a}{a}\partial_\eta r + 4M^2 a^2 r \approx 0. \tag{C4}$$

The above differential equation has the solution

$$\lim_{\Gamma_0 \to f_{\text{PQ}}} r(\eta) \approx c_1 \eta^{\frac{3}{2}\left(1-(M/H)\sqrt{\frac{1}{(M/H)^2}-\frac{16}{9}}\right)} + c_2 \eta^{\frac{3}{2}\left(1+(M/H)\sqrt{\frac{1}{(M/H)^2}-\frac{16}{9}}\right)} \tag{C5}$$

From the above asymptotic solution, we infer that

$$M_c = \frac{3}{4}H \tag{C6}$$

is a critical value that characterizes the damped oscillations of the radial field around the vacuum. For $M > M_c$, the argument of the exponential in Eq. (C5) obtains an imaginary part and the radial field Γ_0 behaves as an underdamped oscillator. For values of $M \ll M_c$, the radial field is overdamped and settles to the vacuum as

$$r(\eta) \to c_1 \eta^{\frac{3}{4}\left(\frac{M}{M_c}\right)^2}. \tag{C7}$$

In the underdamped case which occurs when $M > M_c$, the radial field oscillates around the minimum at f_{PQ} until the oscillations decay away. These oscillations are characterized by the expression:

$$r(\eta) \approx \eta^{\frac{3}{2}}\left(c_1 \eta^{-i\nu} + c_2 \eta^{+i\nu}\right) \tag{C8}$$

$$\approx \eta^{\frac{3}{2}}\left(c_1 \cos\left(\nu \ln|\eta|\right) + c_2 \sin\left(\nu \ln|\eta|\right)\right) \tag{C9}$$

where

$$\nu = \frac{3/2}{M_c}\sqrt{M^2 - M_c^2} \tag{C10}$$

is real.

Appendix D: Details of quantization

Here we present the details of the quantization of the radial-axion system in the presence of large phase angular momentum background classical solution. The nontriviality will be coming from the nonvanishing of the cross-commutator $[\partial_\eta \delta X, \partial_\eta Y] \propto \partial_\eta \theta_0$ even though $[\delta X, \delta Y] = 0$. This quantization is what allows us to compute the sound speed and the vacuum structure rigorously.

In terms of the linear order field fluctuations $\delta\phi^n = (\delta\Gamma, \delta\chi)$ where $\delta\chi = \Gamma_0 \delta\theta$, we derive the EoM from the action in Eq. (11) using the Euler-Lagrange equation

$$\partial_\mu \frac{\partial \mathcal{L}_2}{\partial (\partial_\mu \phi^n)} = \frac{\partial \mathcal{L}_2}{\partial \phi^n} \tag{D1}$$

where $\mathcal{L}_2$ is the component of the Lagrangian which is quadratic order in linear perturbations. The EoM for $\delta\Gamma$ and $\delta\chi$ are obtained from the above expression as

$$\partial_\eta^2 \delta\Gamma - a^{-2}\partial_i^2 \delta\Gamma + 2\frac{\partial_\eta a}{a}\partial_\eta \delta\Gamma - 2\partial_\eta\theta_0\partial_\eta\delta\chi + \left(-2M^2 a^2 + 3\lambda\Gamma_0^2 a^2 - (\partial_\eta\theta_0)^2\right)\delta\Gamma + 2\partial_\eta\theta_0\frac{\partial_\eta\Gamma_0}{\Gamma_0}\delta\chi = 0, \tag{D2}$$

$$\partial_\eta^2 \delta\chi - a^{-2}\partial_i^2 \delta\chi + 2\frac{\partial_\eta a}{a}\partial_\eta \delta\chi + 2\partial_\eta\theta_0\partial_\eta\delta\Gamma + \left(-2M^2 a^2 + \lambda\Gamma_0^2 a^2 - (\partial_\eta\theta_0)^2\right)\delta\chi - 2\partial_\eta\theta_0\frac{\partial_\eta\Gamma_0}{\Gamma_0}\delta\Gamma = 0. \tag{D3}$$

Eqs. (D2) and (D3) form a system of coupled ODEs and can be expressed compactly as

$$\partial_\eta^2 \delta\phi^n - \partial_i^2 \delta\phi^n + 2\frac{\partial_\eta a}{a}\partial_\eta\delta\phi^n + \kappa^{nm}\partial_\eta\phi^m + \left(\mathcal{M}^2\right)^{nm}\delta\phi^m = 0 \tag{D4}$$

where

$$\kappa^{nm} = \begin{pmatrix} 0 & -2\partial_\eta\theta_0 \\ 2\partial_\eta\theta_0 & 0 \end{pmatrix}, \tag{D5}$$

and

$$\left(\mathcal{M}^2\right)^{nm} = \begin{pmatrix} a^2\left(-2M^2 + 3\lambda\Gamma_0^2\right) - (\partial_\eta\theta_0)^2 & 2\partial_\eta\theta_0\frac{\partial_\eta\Gamma_0}{\Gamma_0} \\ -2\partial_\eta\theta_0\frac{\partial_\eta\Gamma_0}{\Gamma_0} & a^2\left(-2M^2 + \lambda\Gamma_0^2\right) - (\partial_\eta\theta_0)^2 \end{pmatrix}. \tag{D6}$$

Note that the linear perturbations $\delta\phi^n$ are kinetically coupled through the coefficient $\partial_\eta\theta_0$. We will refer to all scenarios where $\partial_\eta\theta_0 \gg H^2$ as strongly coupled. By defining new field variables $\delta\psi = a\delta\phi^n = (a\delta\Gamma, a\delta\chi) \equiv (\delta Y, \delta X)$, we can rewrite the above system of equations as

$$\partial_\eta^2 \delta\psi^n - \partial_i^2 \delta\psi^n + \kappa^{nm}\partial_\eta\psi^m + \left(\mathcal{M}^2\right)^{nm}\delta\psi^m = 0 \tag{D7}$$

where we modify $\left(\mathcal{M}^2\right)^{nm}$ as

$$\left(\mathcal{M}^2\right)^{nm} = \begin{pmatrix} -2M^2a^2 + 3\lambda Y_0^2 - (\partial_\eta\theta_0)^2 - \frac{\partial_\eta^2 a}{a} & 2\partial_\eta\theta_0 \left(\frac{\partial_\eta Y_0}{Y_0}\right) \\ -2\partial_\eta\theta_0 \left(\frac{\partial_\eta Y_0}{Y_0}\right) & -2M^2a^2 + \lambda Y_0^2 - (\partial_\eta\theta_0)^2 - \frac{\partial_\eta^2 a}{a} \end{pmatrix} \tag{D8}$$

and $Y_0 = a\Gamma_0$.

We will quantize this system of coupled fields $\delta\psi^n \equiv (\delta Y, \delta X)^n$ using the commutator relations defined in Eq. (35). From the Lagrangian, we find the canonical momenta as

$$\pi^1 = \frac{\partial\mathcal{L}_2}{\partial\left(\partial_\eta\delta Y\right)} = -\partial^0\delta Y = \partial_\eta\delta Y, \tag{D9}$$

and

$$\pi^2 = \frac{\partial\mathcal{L}_2}{\partial\left(\partial_\eta\delta X\right)} = \partial_\eta\delta X + 2\delta Y\partial_\eta\theta_0. \tag{D10}$$

Hence, we arrive at the following commutator expressions for the fields $\delta\psi^n$ and their time-derivatives $\partial_\eta\delta\psi^n$:

$$[\delta\psi^n, \delta\psi^m] = 0,$$
$$[\delta\psi^n, \partial_\eta\delta\psi^m] = i\delta^{nm}\delta^{(3)}\left(\vec{x} - \vec{y}\right)$$
$$[\partial_\eta\delta\psi^n, \partial_\eta\delta\psi^m] = i\delta^{(3)}\left(\vec{x} - \vec{y}\right)\begin{bmatrix} 0 & 2\partial_\eta\theta_0 \\ -2\partial_\eta\theta_0 & 0 \end{bmatrix} \tag{D11}$$

which is remarkable since $[\delta X, \delta Y] = 0$ while $[\partial_\eta\delta X, \partial_\eta\delta Y] \neq 0$. As expected in the decoupling limit when $\partial_\eta\theta_0 \to 0$, the kinetic cross commutators vanish.

Next we write the most general solution for $\delta\psi^n$ in terms of time-independent non-Hermitian ladder operators a_k^{nr} and mode function h_k^{nr} as

$$\delta\psi^n(\eta, \vec{x}) = \int \frac{d^3k}{(2\pi)^{3/2}}\delta\psi^n(\eta, \vec{k})e^{i\vec{k}\cdot\vec{x}} = \sum_r \int \frac{d^3k}{(2\pi)^{3/2}}\left(a_k^r h_k^{nr}(\eta) + a_{-k}^{r\dagger}h_k^{nr*}(\eta)\right)e^{i\vec{k}\cdot\vec{x}} \tag{D12}$$

where n is the flavor index and r counts the number of distinct frequency solutions. The time-derivative of the field is

$$\partial_\eta\delta\psi^n = \sum_r \int \frac{d^3k}{(2\pi)^{3/2}}\left(a_k^r \partial_\eta h_k^{nr}(\eta) + a_{-k}^{r\dagger}\partial_\eta h_k^{nr*}(\eta)\right)e^{i\vec{k}\cdot\vec{x}}. \tag{D13}$$

The ladder operators $a_{\vec{k}}^r$ satisfy relation

$$[a_{\vec{k}}^r, a_{\vec{p}}^{s\dagger}] = F^{rs}\delta^{(3)}(\vec{k} - \vec{p}) \tag{D14}$$

where the coefficients F^{rs} must be determined by solving for mode function h_k^{nr} and using canonical commutator relation given in Eq. (D11). Substituting our general solution from Eq. (D12) into Eq. (D7) we obtain

$$\left[\delta^{nj}\partial_\eta^2 + \kappa^{nj}\partial_\eta + (\mathcal{W}^2)^{nj}\right] h_k^{jm}(\eta) = 0 \tag{D15}$$

where

$$\kappa^{nj} = \begin{pmatrix} 0 & -2\partial_\eta\theta_0 \\ 2\partial_\eta\theta_0 & 0 \end{pmatrix} \tag{D16}$$

$$(\mathcal{W}^2)^{nj} = \begin{pmatrix} k^2 + (-2M^2a^2 + 3\lambda Y_0^2) - (\partial_\eta\theta_0)^2 - \frac{\partial_\eta^2 a}{a} & 2\partial_\eta\theta_0\left(\frac{\partial_\eta Y_0}{Y_0}\right) \\ -2\partial_\eta\theta_0\left(\frac{\partial_\eta Y_0}{Y_0}\right) & k^2 + (-2M^2a^2 + \lambda Y_0^2) - (\partial_\eta\theta_0)^2 - \frac{\partial_\eta^2 a}{a} \end{pmatrix}. \tag{D17}$$

1. Normal modes

We will now solve the system of equations given in Eq. (D15) during the conformal regime. Hence, we propose the following ansatz

$$\begin{pmatrix} h_k^{1r}(\eta) \\ h_k^{2r}(\eta) \end{pmatrix} = \sum_j c_j \delta_j^r \begin{pmatrix} A_j^1 \\ A_j^2 \end{pmatrix} e^{-i\omega_j\eta} \tag{D18}$$

for time-independent mode vectors $\left(A_j^1, A_j^2\right)$. Substituting this ansatz into Eq. (D15) we obtain

$$\sum_r \left[\delta^{nj}\partial_\eta^2 + \kappa^{nj}\partial_\eta + (\mathcal{W}^2)^{nj}\right] \begin{pmatrix} A_r^1 \\ A_r^2 \end{pmatrix} e^{-i\omega_r\eta} = 0, \tag{D19}$$

which is rewritten as

$$\begin{pmatrix} b + 2\lambda Y_0^2 & \frac{2L}{Y_0^2}\left(i\omega_r + \frac{\partial_\eta Y_0}{Y_0}\right) \\ \frac{2L}{Y_0^2}\left(-i\omega_r - \frac{\partial_\eta Y_0}{Y_0}\right) & b \end{pmatrix} \begin{pmatrix} A_r^1 \\ A_r^2 \end{pmatrix} = 0 \tag{D20}$$

where we have replaced $\partial_\eta\theta_0$ with the conserved angular momentum L from Eq. (12) and $b = -\omega_r^2 + k^2 + (-2M^2a^2 + \lambda Y_0^2) - \left(\frac{L}{Y_0^2}\right)^2 - \frac{\partial_\eta^2 a}{a}$.

Since we solve Eq. (D15) at an early time $\eta_i \to -\infty$ and in the conformal limit $Y_0 \approx Y_c = \left(L^2/\lambda\right)^{1/6}$ and $\partial_\eta \theta_0 = L/Y_0^2$, we can neglect any small amplitude oscillations of the background radial field. In the conformal limit $\lambda Y_0^2 \gg M^2 a^2 \sim H^2 a^2 \sim \partial_\eta^2 a/a$, and hence we arrive at the reduced expression for Eq. (D20) given as

$$\begin{pmatrix} -\omega_r^2 + k^2 + 2\lambda Y_c^2 & i\frac{2L}{Y_c^2}\omega_r \\ -i\frac{2L}{Y_c^2}\omega_r & -\omega_r^2 + k^2 \end{pmatrix} \begin{pmatrix} A_r^1 \\ A_r^2 \end{pmatrix} = 0. \tag{D21}$$

We note that in the conformal limit, our system is defined by time-independent coefficients. The distinct "real" frequency solutions obtained by solving[17] Eq. (D21) are

$$\omega_r = \{\omega_{--}, \omega_{+-}, \omega_{-+}, \omega_{++}\} \tag{D22}$$

where

$$\omega_{s_1 s_2} \equiv s_1 \sqrt{k^2 + 3\lambda Y_c^2 + s_2 Y_c \sqrt{\lambda\left(4k^2 + 9\lambda Y_c^2\right)}}, \tag{D23}$$

and $s_{1,2} \in [+, -]$. In the IR limit

$$1 \ll k^2 \ll \lambda Y_c^2, \tag{D24}$$

the two distinct frequency squared

$$\omega_{\pm-}^2 \approx \frac{k^2}{3} + O\left(\frac{k^4}{\lambda Y_c^2}\right), \tag{D25}$$

and

$$\omega_{\pm+}^2 \approx 6\lambda Y_c^2 + \frac{5k^2}{3} + O\left(\frac{k^4}{\lambda Y_c^2}\right) \tag{D26}$$

correspond to low and high frequency solutions and are separated by the large $O\left(\lambda Y_c^2/k^2\right)$ hierarchy. In the UV limit,

$$\lim_{k \gg \lambda Y_c^2} \omega_{\pm\pm}^2 \to k^2 \tag{D27}$$

and the two frequency solutions become degenerate.

We write the full mode function h^{nr} as

$$\begin{pmatrix} h_k^{1r}(\eta) \\ h_k^{2r}(\eta) \end{pmatrix} = c_{++}\delta_{++}^r \begin{pmatrix} A_{++}^1 \\ A_{++}^2 \end{pmatrix} e^{-i\omega_{++}\eta} + c_{+-}\delta_{+-}^r \begin{pmatrix} A_{+-}^1 \\ A_{+-}^2 \end{pmatrix} e^{-i\omega_{+-}\eta}$$

$$+ c_{-+}\delta_{-+}^r \begin{pmatrix} A_{-+}^1 \\ A_{-+}^2 \end{pmatrix} e^{-i\omega_{-+}\eta} + c_{--}\delta_{--}^r \begin{pmatrix} A_{--}^1 \\ A_{--}^2 \end{pmatrix} e^{-i\omega_{--}\eta} \tag{D28}$$

---

[17] Obtained by equating the determinant of the coefficient matrix in Eq. (D21) to zero and solving for ω

where $r \in [++, +-, -+, --]$ counts distinct frequencies given by Eq. (D23). The normal vectors corresponding to each frequency are given by the ratios

$$\frac{A_{++}^2}{A_{++}^1} = -\frac{A_{-+}^2}{A_{-+}^1} = i \left(\frac{-2\left(\frac{L}{Y_c^2}\right)\omega_{++}}{\frac{1}{2}\left(\omega_{++}^2 - \omega_{+-}^2\right) + (\lambda Y_c^2) + 2\left(\frac{L}{Y_c^2}\right)^2} \right), \tag{D29}$$

$$\frac{A_{+-}^2}{A_{+-}^1} = -\frac{A_{--}^2}{A_{--}^1} = i \left(\frac{2\left(\frac{L}{Y_c^2}\right)\omega_{+-}}{\frac{1}{2}\left(\omega_{++}^2 - \omega_{+-}^2\right) - (\lambda Y_c^2) - 2\left(\frac{L}{Y_c^2}\right)^2} \right), \tag{D30}$$

which are purely "imaginary". Hence, we can rewrite the solution for the mode function as

$$\begin{pmatrix} h_k^{1r}(\eta) \\ h_k^{2r}(\eta) \end{pmatrix} = c_{++}\delta_{++}^r \begin{pmatrix} 1 \\ \frac{A_{++}^2}{A_{++}^1} \end{pmatrix} e^{-i\omega_{++}\eta} + c_{+-}\delta_{+-}^r \begin{pmatrix} 1 \\ \frac{A_{+-}^2}{A_{+-}^1} \end{pmatrix} e^{-i\omega_{+-}\eta} +$$

$$+ c_{-+}\delta_{-+}^r \begin{pmatrix} 1 \\ \frac{A_{++}^2}{A_{++}^1} \end{pmatrix}^* e^{i\omega_{++}\eta} + c_{--}\delta_{--}^r \begin{pmatrix} 1 \\ \frac{A_{+-}^2}{A_{+-}^1} \end{pmatrix}^* e^{i\omega_{+-}\eta} \tag{D31}$$

where the frequencies ω_{++} are constant, real and positive and the ratios A_r^2/A_r^1 are purely imaginary. In the decoupling limit where $L \to 0$ the kinetic terms mixing $\delta\Gamma$ and $\delta\chi$ vanish and the decoupled solution becomes :

$$\lim_{L\to 0} \begin{pmatrix} h_k^{1r}(\eta) \\ h_k^{2r}(\eta) \end{pmatrix} = c_{++}\delta_{++}^r \begin{pmatrix} 1 \\ 0 \end{pmatrix} e^{-i\omega_{++}\eta} + c_{-+}\delta_{-+}^r \begin{pmatrix} 1 \\ 0 \end{pmatrix} e^{-i\omega_{-+}\eta}$$

$$+ c_{+-}\delta_{+-}^r \begin{pmatrix} 0 \\ 1 \end{pmatrix} e^{-i\omega_{+-}\eta} + c_{--}\delta_{--}^r \begin{pmatrix} 0 \\ 1 \end{pmatrix} e^{-i\omega_{--}\eta},$$

$$h_k^{1r}(\eta) = c_{++}\delta_{++}^r e^{-i\omega_{++}\eta} + c_{-+}\delta_{-+}^r e^{-i\omega_{-+}\eta},$$

$$h_k^{2r}(\eta) = c_{+-}\delta_{+-}^r e^{-i\omega_{+-}\eta} + c_{--}\delta_{--}^r e^{-i\omega_{--}\eta}.$$

where the decoupled "instantaneous" frequencies[18] are

$$\lim_{L\to 0} \omega_{s_1 s_2} \equiv s_1 \sqrt{k^2 + 2\lambda Y_c^2 + s_2\left(\lambda Y_c^2\right)} \tag{D32}$$

for

$$\omega_{\pm+} = \pm\sqrt{k^2 + 3\lambda Y_c^2} \tag{D33}$$

$$\omega_{\pm-} = \pm\sqrt{k^2 + \lambda Y_c^2}. \tag{D34}$$

---

[18] In the decoupled limit, the background solution for the radial field is not conformal due to the quartic potential which will induce large amplitude oscillations. Hence, we cannot assume that $Y_0 \approx$ constant. Therefore, we give instantaneous frequencies.

Substituting our solution for h_k^{nr} from Eq. (D31) into the expression for $\delta\psi^n$ we obtain

$$\delta\psi^n = \int \frac{d^3p\, e^{i\vec{p}\cdot\vec{x}}}{(2\pi)^{3/2}} \left[a_{\vec{p}}^{++} c_{++} V_{++}^n e^{-i\omega_{++}\eta} + a_{\vec{p}}^{+-} c_{+-} V_{+-}^n e^{-i\omega_{+-}\eta} \right.$$
$$\left. + a_{-\vec{p}}^{++\dagger} c_{++}^* V_{++}^{n*} e^{i\omega_{++}\eta} + a_{-\vec{p}}^{+-\dagger} c_{+-}^* V_{+-}^{n*} e^{i\omega_{+-}\eta} \right] \tag{D35}$$

where

$$V_{++}^n = \begin{pmatrix} 1 \\ \mathcal{R}_{++} \end{pmatrix}, \quad V_{+-}^n = \begin{pmatrix} 1 \\ \mathcal{R}_{+-} \end{pmatrix}, \quad V_{-+}^n = V_{++}^* = \begin{pmatrix} 1 \\ -\mathcal{R}_{++} \end{pmatrix}, \quad V_{--}^n = V_{+-}^* = \begin{pmatrix} 1 \\ -\mathcal{R}_{+-} \end{pmatrix} \tag{D36}$$

and

$$\mathcal{R}_{++} = \frac{A_{++}^2}{A_{++}^1}, \quad \mathcal{R}_{+-} = \frac{A_{+-}^2}{A_{+-}^1}. \tag{D37}$$

2. Ladder algebra

To evaluate the ladder algebra, we first express the ladder operators: $a_{\vec{p}}^{++}$, $a_{\vec{p}}^{+-}$ and their conjugates in terms of the fields $\delta\psi^n$ and its conjugate momenta π^n. To this end, we define

$$L^n[w, \vec{q}] = \frac{1}{(2\pi)^{3/2}} \int d\eta\, e^{iw\eta} \int d^3x\, e^{-i\vec{q}\cdot\vec{x}} \delta\psi^n \tag{D38}$$

and

$$N^n[w, \vec{q}] \equiv \frac{1}{(2\pi)^{3/2}} \int d\eta\, e^{iw\eta} \int d^3x\, e^{-i\vec{q}\cdot\vec{x}} \partial_\eta \delta\psi^n. \tag{D39}$$

From the above definition and Eq. (D35), we conclude that

$$J^n = \int_{-\infty}^{\infty} \frac{dw}{2\pi} L^n[w, \vec{q}] = a_{\vec{q}}^{++} c_{++} V_{++}^n + a_{\vec{q}}^{+-} c_{+-} V_{+-}^n + a_{-\vec{q}}^{\dagger++} c_{++}^* V_{++}^{n*} + a_{-\vec{q}}^{\dagger+-} c_{+-}^* V_{+-}^{n*}, \tag{D40}$$

$$J^{n+2} = i \int_{-\infty}^{\infty} \frac{dw}{2\pi} N^n[w, \vec{q}] = a_{\vec{q}}^{++} \omega_{++} c_{++} V_{++}^n + a_{\vec{q}}^{+-} \omega_{+-} c_{+-} V_{+-}^n$$
$$- a_{-\vec{q}}^{\dagger++} \omega_{++} c_{++}^* V_{++}^{n*} - a_{-\vec{q}}^{\dagger+-} \omega_{+-} c_{+-}^* V_{+-}^{n*}, \tag{D41}$$

where n is the flavor index of our two-field coupled system and runs from 1 to 2. From Eqs. (D40) and (D41) we setup the following system of equations to solve for the ladder operators

$$\begin{pmatrix} c_{++}V_{++}^1 & c_{+-}V_{+-}^1 & c_{++}^*V_{++}^{1*} & c_{+-}^*V_{+-}^{1*} \\ c_{++}V_{++}^2 & c_{+-}V_{+-}^2 & c_{++}^*V_{++}^{2*} & c_{+-}^*V_{+-}^{2*} \\ \omega_{++}c_{++}V_{++}^1 & \omega_{+-}c_{+-}V_{+-}^1 & -\omega_{++}c_{++}^*V_{++}^{1*} & -\omega_{+-}c_{+-}^*V_{+-}^{1*} \\ \omega_{++}c_{++}V_{++}^2 & \omega_{+-}c_{+-}V_{+-}^2 & -\omega_{++}c_{++}^*V_{++}^{2*} & -\omega_{+-}c_{+-}^*V_{+-}^{2*} \end{pmatrix} \begin{pmatrix} a_{\vec{q}}^{++} \\ a_{\vec{q}}^{+-} \\ a_{-\vec{q}}^{++\dagger} \\ a_{-\vec{q}}^{+-\dagger} \end{pmatrix} = \begin{pmatrix} J^1 \\ J^2 \\ J^3 \\ J^4 \end{pmatrix}. \tag{D42}$$

Solving the above equation yields

$$
\begin{aligned}
a_{\vec{q}}^{++} = & -\frac{\mathcal{R}_{+-}\omega_{+-}J^1}{2c_{++}\left(\mathcal{R}_{++}\omega_{++} - \mathcal{R}_{+-}\omega_{+-}\right)} + \frac{\omega_{+-}J^2}{2c_{++}\left(\mathcal{R}_{++}\omega_{+-} - \mathcal{R}_{+-}\omega_{++}\right)} \\
& + \frac{J^4}{2c_{++}\left(\mathcal{R}_{++}\omega_{++} - \mathcal{R}_{+-}\omega_{+-}\right)} - \frac{\mathcal{R}_{+-}J^3}{2c_{++}\left(\mathcal{R}_{++}\omega_{+-} - \mathcal{R}_{+-}\omega_{++}\right)} \\
a_{-\vec{q}}^{++\dagger} = & -\frac{\mathcal{R}_{+-}\omega_{+-}J^1}{2c_{++}^*\left(\mathcal{R}_{++}\omega_{++} - \mathcal{R}_{+-}\omega_{+-}\right)} + \frac{\mathcal{R}_{+-}J^3}{2c_{++}^*\left(\mathcal{R}_{++}\omega_{+-} - \mathcal{R}_{+-}\omega_{++}\right)} \\
& + \frac{J^4}{2c_{++}^*\left(\mathcal{R}_{++}\omega_{++} - \mathcal{R}_{+-}\omega_{+-}\right)} - \frac{\omega_{+-}J^2}{2c_{++}^*\left(\mathcal{R}_{++}\omega_{+-} - \mathcal{R}_{+-}\omega_{++}\right)} \\
a_{\vec{q}}^{+-} = & -\frac{\mathcal{R}_{+-}\omega_{+-}J^1}{2c_{+-}\left(\mathcal{R}_{+-}\omega_{+-} - \mathcal{R}_{++}\omega_{++}\right)} + \frac{\mathcal{R}_{++}\omega_{+-}J^2}{2\mathcal{R}_{+-}c_{+-}\left(\mathcal{R}_{+-}\omega_{++} - \mathcal{R}_{++}\omega_{+-}\right)} \\
& + \frac{J^4}{2c_{+-}\left(\mathcal{R}_{+-}\omega_{+-} - \mathcal{R}_{++}\omega_{++}\right)} - \frac{\mathcal{R}_{++}J^3}{2c_{+-}\left(\mathcal{R}_{+-}\omega_{++} - \mathcal{R}_{++}\omega_{+-}\right)} + \frac{J^2}{2\mathcal{R}_{+-}c_{+-}} + \frac{J^1}{2c_{+-}} \\
a_{-\vec{q}}^{+-\dagger} = & -\frac{\mathcal{R}_{+-}\omega_{+-}J^1}{2c_{+-}^*\left(\mathcal{R}_{+-}\omega_{+-} - \mathcal{R}_{++}\omega_{++}\right)} + \frac{\mathcal{R}_{++}J^3}{2c_{+-}^*\left(\mathcal{R}_{+-}\omega_{++} - \mathcal{R}_{++}\omega_{+-}\right)} \\
& + \frac{J^4}{2c_{+-}^*\left(\mathcal{R}_{+-}\omega_{+-} - \mathcal{R}_{++}\omega_{++}\right)} - \frac{\mathcal{R}_{++}\omega_{+-}J^2}{2\mathcal{R}_{+-}c_{+-}^*\left(\mathcal{R}_{+-}\omega_{++} - \mathcal{R}_{++}\omega_{+-}\right)} - \frac{J^2}{2\mathcal{R}_{+-}c_{+-}^*} + \frac{J^1}{2c_{+-}^*}
\end{aligned}
$$

$$\tag{D43}$$

where we use Eq. (D36) to set

$$
V_{++}^1 = V_{+-}^1 = 1 \quad \text{and,} \quad V_{++}^2 = \mathcal{R}_{++}, \quad V_{+-}^2 = \mathcal{R}_{+-}. \tag{D44}
$$

We can summarize these results as

$$
a_{\vec{p}}^r = \sum_{n=1}^{4} U_n^r J^n, \tag{D45}
$$

$$
a_{-\vec{p}}^{r\dagger} = \sum_{n=1}^{4} W_n^r J^n, \tag{D46}
$$

where $r = (++, +-)$. The J^n and J^{n+2} operators appearing on the RHS of Eq. (D42) can be evaluated as

$$
J^n \equiv \int_{-\infty}^{\infty} \frac{dw}{2\pi}\left\{L^n[w, \vec{q}]\right\} \tag{D47}
$$

$$
= \int_{-\infty}^{\infty} \frac{dw}{2\pi}\left\{\frac{1}{(2\pi)^{3/2}}\int d\eta\, e^{iw\eta}\int d^3x\, e^{-i\vec{q}\cdot\vec{x}}\delta\psi^n\right\} \tag{D48}
$$

$$
= \frac{1}{(2\pi)^{3/2}}\int d^3x\, e^{-i\vec{q}\cdot\vec{x}}\delta\psi^n(0, \vec{x}) \tag{D49}
$$

and,

$$J^{n+2} \equiv i \int_{-\infty}^{\infty} \frac{dw}{2\pi} \left\{ N^n[w, \vec{q}] \right\} \tag{D50}$$

$$= i \int_{-\infty}^{\infty} \frac{dw}{2\pi} \left\{ \frac{1}{(2\pi)^{3/2}} \int d\eta e^{iw\eta} \int d^3 x e^{-i\vec{q}\cdot\vec{x}} \partial_\eta \delta\psi^n \right\} \tag{D51}$$

$$= i \frac{1}{(2\pi)^{3/2}} \int d^3 x e^{-i\vec{q}\cdot\vec{x}} \partial_\eta \delta\psi^n(0, \vec{x}) \tag{D52}$$

where we used $\int_{-\infty}^{\infty} \frac{dw}{2\pi} \int d\eta e^{iw\eta} f(\eta) = \int d\eta f(\eta) \int_{-\infty}^{\infty} \frac{dw}{2\pi} e^{iw\eta} = \int d\eta f(\eta)\delta(\eta) = f(0)$. It follows then that the commutators of J^n and J^{n+2} operators can be obtained from the commutator relations in Eq. (D11). Hence,

$$[J^1, J^2] = 0$$
$$[J^1, J^3] = -\delta^{(3)}(\vec{q} + \vec{q}')$$
$$[J^1, J^4] = 0. \tag{D53}$$
$$[J^2, J^3] = 0.$$
$$[J^2, J^4] = -\delta^{(3)}(\vec{q} + \vec{q}')$$
$$[J^3, J^4] = -i2\partial_\eta \theta_0 \delta^{(3)}(\vec{q} + \vec{q}')$$

3. Ladder commutators

Using the solution for the ladder operators $a_{\vec{p}}^{++}, a_{\vec{p}}^{+-}$ and their conjugates as given in Eq. (D43), and the commutator algebra of J operators given in Eq. (D53), we can evaluate the ladder commutators. There are 6 unique combinations of the commutators for $+\pm$ frequencies that we present below. We work out the first commutator in detail and leave the remaining for the readers as an exercise:

$$\left[a_{\vec{q}}^{++}, a_{-\vec{q}'}^{++\dagger} \right] = [U_1^{++} J^1, W_2^{++} J^2 + W_3^{++} J^3 + W_4^{++} J^4] + [U_2^{++} J^2, W_1^{++} J^1 + W_3^{++} J^3 + W_4^{++} J^4]$$
$$+ [U_3^{++} J^3, W_1^{++} J^1 + W_2^{++} J^2 + W_4^{++} J^4] + [U_4^{++} J^4, W_1^{++} J^1 + W_2^{++} J^2 + W_3^{++} J^3]$$
$$= \left(U_1^{++} W_3^{++} - U_3^{++} W_1^{++} \right)(-1)$$
$$+ \left(U_2^{++} W_4^{++} - U_4^{++} W_2^{++} \right)(-1) + \left(U_3^{++} W_4^{++} - U_4^{++} W_3^{++} \right)(-i2\partial_\eta \theta_0)$$
$$= \frac{\left((\mathcal{R}_{+-})^2 - 1 \right)\omega_{+-} + 2i\partial_\eta \theta_0 \mathcal{R}_{+-}}{2c_{++}c_{++}^* (\mathcal{R}_{+-}\omega_{+-} - \mathcal{R}_{++}\omega_{++})(\mathcal{R}_{+-}\omega_{++} - \mathcal{R}_{++}\omega_{+-})} \delta^{(3)}(\vec{q} + \vec{q}'). \tag{D54}$$

$$\left[a_{\vec{q}}^{+-}, a_{-\vec{q}'}^{+-\dagger}\right] = \frac{\left((\mathcal{R}_{++})^2 - 1\right)\omega_{++} + 2i\partial_\eta\theta_0\mathcal{R}_{++}}{2c_{+-}c_{+-}^*\left(\mathcal{R}_{+-}\omega_{+-} - \mathcal{R}_{++}\omega_{++}\right)\left(\mathcal{R}_{+-}\omega_{++} - \mathcal{R}_{++}\omega_{+-}\right)}\delta^{(3)}\left(\vec{q} + \vec{q}'\right)$$

$$\left[a_{\vec{q}}^{++}, a_{\vec{q}'}^{+-}\right] = \delta^{(3)}\left(\vec{q} + \vec{q}'\right)\frac{(\mathcal{R}_{++}\mathcal{R}_{+-} + 1)\omega_{+-} - (\mathcal{R}_{++}\mathcal{R}_{+-} + 1)\omega_{++} + 2i\partial_\eta\theta_0\left(\mathcal{R}_{++} - \mathcal{R}_{+-}\right)}{4c_{+-}c_{++}\left(\mathcal{R}_{+-}\omega_{+-} - \mathcal{R}_{++}\omega_{++}\right)\left(\mathcal{R}_{+-}\omega_{++} - \mathcal{R}_{++}\omega_{+-}\right)}$$

$$= 0$$

$$\left[a_{\vec{q}}^{1++}, a_{-\vec{q}}^{2++\dagger}\right] = \delta^{(3)}\left(\vec{q} + \vec{q}'\right)\frac{(1 - \mathcal{R}_{++}\mathcal{R}_{+-})\omega_{+-} + (1 - \mathcal{R}_{++}\mathcal{R}_{+-})\omega_{++} - 2i\partial_\eta\theta_0\left(\mathcal{R}_{++} + \mathcal{R}_{+-}\right)}{4c_{++}c_{+-}^*\left(\mathcal{R}_{+-}\omega_{+-} - \mathcal{R}_{++}\omega_{++}\right)\left(\mathcal{R}_{+-}\omega_{++} - \mathcal{R}_{++}\omega_{+-}\right)}$$

$$= 0$$

$$\left[a_{\vec{q}}^{+-}, a_{-\vec{q}'}^{++\dagger}\right] = 0$$

$$\left[a_{-\vec{q}}^{++\dagger}, a_{-\vec{q}'}^{+-\dagger}\right] = 0\,.$$

Hence for the operator set defined as

$$u_{\vec{q}}^n = \left(a_{\vec{q}}^{++}, a_{-\vec{q}}^{++\dagger}, a_{\vec{q}}^{+-}, a_{-\vec{q}}^{+-\dagger}\right)^n \tag{D55}$$

the commutators are

$$[u_{\vec{q}}^n, u_{\vec{q}'}^m] = \begin{bmatrix} 0 & 1 & 0 & 0 \\ -1 & 0 & 0 & 0 \\ 0 & 0 & 0 & 1 \\ 0 & 0 & -1 & 0 \end{bmatrix}^{nm} \delta^{(3)}\left(\vec{q} + \vec{q}'\right) \tag{D56}$$

where we set the coefficients $c_{+\pm}$ through the expressions

$$c_{++}c_{++}^* = -\frac{\left(1 - (\mathcal{R}_{+-})^2\right)\omega_{+-} - 2i\partial_\eta\theta_0\mathcal{R}_{+-}}{2\left(\mathcal{R}_{+-}\omega_{+-} - \mathcal{R}_{++}\omega_{++}\right)\left(\mathcal{R}_{+-}\omega_{++} - \mathcal{R}_{++}\omega_{+-}\right)}, \tag{D57}$$

$$c_{+-}c_{+-}^* = -\frac{\left(1 - (\mathcal{R}_{++})^2\right)\omega_{++} - 2i\partial_\eta\theta_0\mathcal{R}_{++}}{2\left(\mathcal{R}_{+-}\omega_{+-} - \mathcal{R}_{++}\omega_{++}\right)\left(\mathcal{R}_{+-}\omega_{++} - \mathcal{R}_{++}\omega_{+-}\right)}. \tag{D58}$$

Clearly, the ladder operators associated with distinct frequencies commute with each other. Hence, we can define a common vacuum state $|0\rangle$ which is annihilated simultaneously by both $a_{\vec{q}}^{++}$ and $a_{\vec{q}}^{+-}$ for all $\vec{q}$:

$$a_{\vec{q}}^{++}|0\rangle = 0, \tag{D59}$$

$$a_{\vec{q}}^{+-}|0\rangle = 0. \tag{D60}$$

Note that the normal mode vectors $V_{+\pm}^n$ associated with the corresponding ladder operators $a^{+\pm}$ are not orthogonal.

4. Hamiltonian

We conclude our discussion on the quantization of the coupled system by evaluating its Hamiltonian. We show that in the conformal limit, the normal mode solution given in Eq. (D31) diagonalizes the Hamiltonian such that the vacuum state $|0\rangle$ is the state of minimum energy.

Hence, let us consider the Hamiltonian density defined through the expression

$$\mathcal{H}_2 = \sum_n \pi^n \partial_\eta \psi^n - \mathcal{L}_2 \tag{D61}$$

and the Hamiltonian given by

$$H(\eta) = \int d^3x \mathcal{H}(\eta, \vec{x}). \tag{D62}$$

In the time-independent conformal regime when $Y_0 = Y_c$ and $\partial_\eta \theta_0$ are constants, the Hamiltonian simplifies to

$$\mathcal{H} = \frac{1}{2}(\partial_\eta \delta Y)^2 + \frac{1}{2}(\partial_\eta \delta X)^2 + \frac{1}{2}(\partial_i \delta \Gamma)^2 + \frac{1}{2}(\partial_i \delta \chi)^2$$
$$- \frac{1}{2}(\delta Y)^2 (\partial_\eta \theta_0)^2 + \left(\frac{3\lambda}{2} Y_c^2\right)(\delta Y)^2. \tag{D63}$$

We introduce Fourier notation

$$\delta \psi^n_{\vec{k}}(\eta) \equiv \int d^3x \, e^{-i\vec{k}\cdot\vec{x}} \delta \psi^n(\eta, \vec{x}), \tag{D64}$$

$$\delta \psi^n(\eta, \vec{x}) \equiv \int \frac{d^3k}{(2\pi)^3} e^{i\vec{k}\cdot\vec{x}} \delta \psi^n_{\vec{k}}(\eta), \tag{D65}$$

$$\partial_\eta \delta \psi^n(\eta, \vec{x}) \equiv \int \frac{d^3k}{(2\pi)^3} e^{i\vec{k}\cdot\vec{x}} \partial_\eta \delta \psi^n(\eta), \tag{D66}$$

$$\partial_i \psi^n(\eta, \vec{x}) \equiv \int \frac{d^3k}{(2\pi)^3} i\vec{k} e^{i\vec{k}\cdot\vec{x}} \delta \psi^n_{\vec{k}}(\eta). \tag{D67}$$

Taking the Fourier transform of the fields we write the Hamiltonian as

$$H = \int d^3x \mathcal{H}$$
$$= \int d^3x \int \frac{d^3k}{(2\pi)^3} e^{i\vec{k}\cdot\vec{x}} \int \frac{d^3q}{(2\pi)^3} e^{i\vec{q}\cdot\vec{x}} \left(A^{mn} \partial_\eta \delta \psi^n_{\vec{k}} \partial_\eta \delta \psi^m_{\vec{q}} - \left(\vec{k}\cdot\vec{q}\right) B^{mn} \delta \psi^n_{\vec{k}} \delta \psi^m_{\vec{q}} + C^{mn} \delta \psi^n_{\vec{k}} \delta \psi^m_{\vec{q}}\right)$$
$$= \int \frac{d^3k}{(2\pi)^3} \int \frac{d^3q}{(2\pi)^3} \int d^3x e^{i(\vec{k}+\vec{q})\cdot\vec{x}} \left(A^{mn} \partial_\eta \delta \psi^n_{\vec{k}} \partial_\eta \delta \psi^m_{\vec{q}} - \left(\vec{k}\cdot\vec{q}\right) B^{mn} \delta \psi^n_{\vec{k}} \delta \psi^m_{\vec{q}} + C^{mn} \delta \psi^n_{\vec{k}} \delta \psi^m_{\vec{q}}\right)$$
$$= \int \frac{d^3k}{(2\pi)^3} \left(A^{mn} \partial_\eta \delta \psi^n_{\vec{k}} \partial_\eta \delta \psi^m_{-\vec{k}} + B^{mn} \delta \psi^n_{\vec{k}} \delta \psi^m_{-\vec{k}}\right)$$

where

$$A^{mn} = \frac{1}{2} \begin{bmatrix} 1 & 0 \\ 0 & 1 \end{bmatrix}, \tag{D68}$$

$$B^{mn} = \frac{1}{2} \begin{bmatrix} \left(k^2 + 3\lambda Y_c^2 - (\partial_\eta \theta_0)^2\right) & 0 \\ 0 & k^2 \end{bmatrix}. \tag{D69}$$

Hence, in the conformal limit the Hamiltonian is diagonal in terms of the fields and its time-derivatives.

Using our general solution for the fields

$$\delta\psi^n = \int \frac{d^3k}{(2\pi)^{3/2}} \sum_r \left(a_{\vec{k}}^r h_k^{nr}(\eta) + a_{-\vec{k}}^{r\dagger} h_k^{nr*}\right) e^{i\vec{k}\cdot\vec{x}} \tag{D70}$$

it is possible to write

$$\left(A^{mn}\partial_\eta \delta\psi_{\vec{k}}^n \partial_\eta \delta\psi_{-\vec{k}}^m + B^{mn}\delta\psi_{\vec{k}}^n \delta\psi_{-\vec{k}}^m\right) = \sum_{r,s}\left[T_1^{rs} a_{\vec{k}}^r a_{-\vec{k}}^s + T_2^{rs} a_{-\vec{k}}^{r\dagger} a_{-\vec{k}}^s + T_3^{rs} a_{\vec{k}}^r a_{\vec{k}}^{s\dagger} + T_4^{rs} a_{-\vec{k}}^{r\dagger} a_{\vec{k}}^{s\dagger}\right] \tag{D71}$$

where the indices $r, s \in (++, +-)$. Below we evaluate T_1^{rs}:

$$\begin{aligned} T_1^{rs} &= A^{mn}\left(\partial_\eta h_k^{nr}\right)\left(\partial_\eta h_{-k}^{ms}\right) + a^{-2}B^{mn}h_k^{nr}h_{-k}^{ms} \\ &= \frac{1}{2}\partial_\eta h_k^{1r}\partial_\eta h_{-k}^{1s} + \frac{1}{2}\left(k^2 + 3\lambda Y_0^2 - (\partial_\eta \theta_0)^2\right) h_k^{1r}h_{-k}^{1s} + \frac{1}{2}\partial_\eta h_k^{2r}\partial_\eta h_{-k}^{2s} + \frac{1}{2}\left(k^2\right) h_k^{2r}h_{-k}^{2s}. \end{aligned} \tag{D72}$$

Using the mode solution

$$h_k^{nr} = c_r V_r^n e^{-i\omega_r \eta} \qquad \partial_\eta h_k^{nr} = -i\omega_r c_r V_r^n e^{-i\omega_r \eta}, \tag{D73}$$

it follows that

$$\begin{aligned} \frac{T_1^{rs}}{e^{-i(\omega_r + \omega_s)\eta}c_r c_s} &= \left[-\omega_r\omega_s + k^2 + 3\lambda Y_0^2 - (\partial_\eta \theta_0)^2\right] V_r^1 V_s^1 + \left[-\omega_r\omega_s + k^2\right] V_r^2 V_s^2 \\ &= (\omega_r - \omega_s)\left(\omega_r V_r^1 V_s^1 - \omega_s V_r^2 V_s^2 - i2\partial_\eta \theta_0 V_s^1 V_r^2\right). \end{aligned}$$

In the above equation, the expression in the second bracket goes to when $r \neq s$. Hence, we conclude that $T_1^{rs} = 0$ for all combinations of r, s. Similar calculations show that $T_4^{rs} = 0$.

Next, we evaluate T_2^{rs}:

$$T_2^{rs} = A^{mn} \left(\partial_\eta h_k^{nr*}\right)\left(\partial_\eta h_k^{ms}\right) + B^{mn} h_k^{nr*} h_k^{ms}$$

$$= \frac{1}{2}\left[\partial_\eta h_k^{1r*}\partial_\eta h_k^{1s} + \left(k^2 + 3\lambda Y_c^2 - (\partial_\eta \theta_0)^2\right) h_k^{1r*} h_k^{1s}\right]$$

$$+ \frac{1}{2}\left[\partial_\eta h_k^{2r*}\partial_\eta h_k^{2s} + \left(k^2\right) h_k^{2r*} h_k^{2s}\right]$$

$$\frac{T_2^{rs}}{e^{i(\omega_r-\omega_s)\eta}c_r^* c_s} = \left[\omega_r\omega_s + k^2 + 3\lambda Y_c^2 - (\partial_\eta\theta_0)^2\right] V_r^{1*} V_s^1 + \left[\omega_r\omega_s + k^2\right] V_r^{2*} V_s^2$$

$$= (\omega_r + \omega_s)\left(\omega_r V_r^1 V_s^1 + \omega_s V_r^{2*} V_s^2 + i2\partial_\eta\theta_0 V_s^1 V_r^{2*}\right)$$

which is non zero only when $r = s$. Similarly

$$\frac{T_3^{rs}}{e^{-i(\omega_r-\omega_s)\eta}c_r c_s^*} = \left[\omega_r\omega_s + k^2 + 3\lambda Y_c^2 - (\partial_\eta\theta_0)^2\right] V_r^1 V_s^{1*} + \left[\omega_r\omega_s + k^2\right] V_r^2 V_s^{2*}$$

$$= (\omega_r + \omega_s)\left(\omega_r V_r^1 V_s^{1*} + \omega_s V_r^2 V_s^{2*} - i2\partial_\eta\theta_0 V_s^{1*} V_r^2\right)$$

vanishes when $r \neq s$. Hence we find that for the amplitudes $V_r^n(k, \eta_i)$, the coefficients $T_{1,4}^{rs}$ vanish for all combinations of r, s. Meanwhile, we find that $T_{2,3}^{rs}$ are non-zero only when $r = s$. Thus, the normal frequency solutions corresponding to ω_{++} and ω_{+-} diagonalize our Hamiltonian, which we write as

$$H = \int \frac{d^3k}{(2\pi)^3}\left(A^{mn}\partial_\eta\delta\psi_{\vec{k}}^n \partial_\eta\delta\psi_{-\vec{k}}^m + B^{mn}\delta\psi_{\vec{k}}^n\delta\psi_{-\vec{k}}^m\right)$$

$$= \sum_{r=++,+-} \int \frac{d^3k}{(2\pi)^3}\left[T_2^{rs} a_{-\vec{k}}^{r\dagger}a_{-\vec{k}}^r + T_3^{rs} a_{\vec{k}}^r a_{\vec{k}}^{r\dagger}\right]$$

$$= \sum_{r=++,+-} \int \frac{d^3k}{(2\pi)^3} c_r^* c_r \omega_r \left(\omega_r(1 - \mathcal{R}_r\mathcal{R}_r) - i2\partial_\eta\theta_0\mathcal{R}_r\right)\left(2a_{-\vec{k}}^{r\dagger}a_{\vec{k}}^r + \left[a_{\vec{k}}^r, a_{-\vec{k}}^{r\dagger}\right]\right).$$

Using the expression derived for the coefficients c_{++} from Eq. (D57) we find that

$$c_r^* c_r \left(\omega_r(1 - \mathcal{R}_r\mathcal{R}_r) - i2\partial_\eta\theta_0\mathcal{R}_r\right) = \frac{1}{2}, \tag{D74}$$

which allows us to write the final form of the Hamiltonian as

$$\lim_{\eta\to\eta_i} H = \sum_{r=++,+-} \int \frac{d^3k}{(2\pi)^3}\frac{\omega_r}{2}\left(2a_{-\vec{k}}^{r\dagger}a_{\vec{k}}^r + \left[a_{\vec{k}}^r, a_{-\vec{k}}^{r\dagger}\right]\right)$$

$$= \sum_{r=++,+-} \int \frac{d^3k}{(2\pi)^3}\omega_r\left(a_{-\vec{k}}^{r\dagger}a_{\vec{k}}^r + \frac{1}{2}\delta^{(3)}(0)\right).$$

The vacuum state $|0\rangle$ when applied to the above Hamiltonian results in the lowest energy state with ground state energy $E_0 = \frac{1}{2}\hbar(\omega_{++} + \omega_{+-})$. Also, we see that the one particle state $|r\rangle = a_{\vec{k}}^{r\dagger}|0\rangle$

is an eigenstate of the Hamiltonian with the energy eigenvalue $E_0 + \hbar\omega_r$. We note that any other choice for the mode amplitudes $V_r^n(k, \eta_i)$ other than that given in Eqs. (D29) and (D30) will lead to a higher energy for the vacuum state $|0\rangle$ and as such it would not be the correct ground state of our theory.

Appendix E: Correlation function

Through the quantization presented in Appendix D, we showed that our coupled system of mode functions $h_k(\eta)$ has two sets of normal frequencies ω_{++} and ω_{+-} with which they can be excited. Each frequency $\omega_r(k)$ corresponds to an independent quantum oscillator solution. In this Appendix we will evaluate the non-zero variance of these zero-point quantum fluctuations. Hence we consider the following expression for the two-correlation $\xi_{nm} = \langle \delta\psi^n(0, \eta) \delta\psi^m(0, \eta) \rangle$ and evaluate it as

$$
\begin{aligned}
\xi_{nm} &= \langle 0 \,|\delta\psi^n(0, \eta)\, \delta\psi^m(0, \eta)|\, 0 \rangle \\
&= \int \frac{d^3 k}{(2\pi)^{3/2}} \int \frac{d^3 p}{(2\pi)^{3/2}} \left\langle 0 \left| \left(a_{\vec{k}}^{++} h_k^{n++} + a_{\vec{k}}^{+-} h_k^{n+-} + h.c. \right) \right. \right. \\
&\quad \times \left. \left. \left(a_{\vec{p}}^{++} h_p^{m++} + a_{\vec{p}}^{+-} h_p^{m+-} + h.c. \right) \right| 0 \right\rangle \\
&= \int \frac{d^3 k}{(2\pi)^{3/2}} \int \frac{d^3 p}{(2\pi)^{3/2}} \left\langle 0 \left| a_{\vec{k}}^{++} a_{-\vec{p}}^{++\dagger} h_k^{n++} h_p^{m++*} + a_{\vec{k}}^{+-} a_{-\vec{p}}^{+-\dagger} h_k^{n+-} h_p^{m+-*} \right| 0 \right\rangle \\
&= \int \frac{d^3 k}{(2\pi)^{3/2}} \int \frac{d^3 p}{(2\pi)^{3/2}} h_k^{n++} h_p^{m++*} \left\langle 0 \left| \left[a_{\vec{k}}^{++}, a_{-\vec{p}}^{++\dagger} \right] \right| 0 \right\rangle + h_k^{n+-} h_p^{m+-*} \left\langle 0 \left| \left[a_{\vec{k}}^{+-}, a_{-\vec{p}}^{+-\dagger} \right] \right| 0 \right\rangle \\
&= \int \frac{d^3 k}{(2\pi)^{3/2}} \int \frac{d^3 p}{(2\pi)^{3/2}} \left(h_k^{n++} h_p^{m++*} + h_k^{n+-} h_p^{m+-*} \right) \delta^{(3)}(\vec{k} - \vec{p}) \\
&= \int d\ln k \, \frac{k^3}{2\pi^2} \left(h_k^{n++}(\eta) h_k^{m++*}(\eta) + h_k^{n+-}(\eta) h_k^{m+-*}(\eta) \right) \\
&= \int d\ln k \, \Delta^2_{\delta\psi^n \delta\psi^m}(k, \eta)
\end{aligned}
$$

where we define

$$
\Delta^2_{\delta\psi^n \delta\psi^m}(k, \eta) = \frac{k^3}{2\pi^2} \left(h_k^{n++}(\eta) h_k^{m++*}(\eta) + h_k^{n+-}(\eta) h_k^{m+-*}(\eta) \right) \tag{E1}
$$

such that

$$
\Delta^2_{\delta\phi^n \delta\phi^m}(k, \eta) = \frac{1}{a^2(\eta)} \frac{k^3}{2\pi^2} \left(h_k^{n++}(\eta) h_k^{m++*}(\eta) + h_k^{n+-}(\eta) h_k^{m+-*}(\eta) \right). \tag{E2}
$$

During conformal regime $\eta < \eta_{\text{tr}}$, the power spectra of the individual fields are given as

$$\Delta^2_{\delta\Gamma\delta\Gamma}(\eta < \eta_{\text{tr}}) = \frac{1}{a^2(\eta)} \frac{k^3}{2\pi^2} \left(\left| h_k^{1++}(\eta) \right|^2 + \left| h_k^{1+-}(\eta) \right|^2 \right) \tag{E3}$$

$$= \frac{1}{a^2(\eta)} \frac{k^3}{2\pi^2} \left(|c_{++}|^2 + |c_{+-}|^2 \right) \tag{E4}$$

$$\lim_{k \ll \partial_\eta \theta_0} \Delta^2_{\delta\Gamma\delta\Gamma}(\eta < \eta_{\text{tr}}) \approx \frac{1}{a^2(\eta)} \frac{k^2}{2\pi^2} \left(\frac{k/\partial_\eta\theta_0}{3^{1/2}2^{3/2}} \right) \tag{E5}$$

and

$$\Delta^2_{\delta\chi\delta\chi}(\eta < \eta_{\text{tr}}) = \frac{1}{a^2(\eta)} \frac{k^3}{2\pi^2} \left(\left| h_k^{2++}(\eta) \right|^2 + \left| h_k^{2+-}(\eta) \right|^2 \right) \tag{E6}$$

$$= \frac{1}{a^2(\eta)} \frac{k^3}{2\pi^2} \left(|c_{++}\mathcal{R}_{++}(\eta)|^2 + |c_{+-}\mathcal{R}_{+-}(\eta)|^2 \right) \tag{E7}$$

$$\lim_{k \ll \partial_\eta \theta_0} \Delta^2_{\delta\chi\delta\chi}(\eta < \eta_{\text{tr}}) \approx \frac{1}{a^2(\eta)} \frac{k^2}{2\pi^2} \left(\frac{1}{3^{1/2}2} \right). \tag{E8}$$

Similarly one can show that the dimensionless cross-correlation (covariance) vanishes,

$$\Delta^2_{\delta\Gamma\delta\chi}(\eta < \eta_{\text{tr}}) = \frac{1}{a^2(\eta)} \frac{k^3}{2\pi^2} \left(|c_{++}|^2 \mathcal{R}^*_{++}(\eta) + |c_{+-}|^2 \mathcal{R}^*_{+-}(\eta) \right)$$

$$= 0. \tag{E9}$$

The correlation between the time-derivatives of the fields $\Xi = \langle \partial_\eta \delta\psi^n (0, \eta) \, \partial_\eta \delta\psi^m (0, \eta) \rangle$ can be derived as

$$\Xi = \langle 0 | \partial_\eta \delta\psi^n (0, \eta) \, \partial_\eta \delta\psi^m (0, \eta) | 0 \rangle$$

$$= \int \frac{d^3 k}{(2\pi)^{3/2}} \int \frac{d^3 p}{(2\pi)^{3/2}} \left\langle 0 \left| \partial_\eta \left(a_{\vec{k}}^{++} h_k^{n++} + a_{\vec{k}}^{+-} h_k^{n+-} + h.c. \right) \right. \right.$$

$$\times \left. \left. \partial_\eta \left(a_{\vec{p}}^{++} h_p^{m++} + a_{\vec{p}}^{+-} h_p^{m+-} + h.c. \right) \right| 0 \right\rangle$$

$$= \int \frac{d^3 k}{(2\pi)^{3/2}} \int \frac{d^3 p}{(2\pi)^{3/2}} \left\langle 0 \left| a_{\vec{k}}^{++} a_{-\vec{p}}^{++\dagger} \partial_\eta h_k^{n++} \partial_\eta h_p^{m++*} + a_{\vec{k}}^{+-} a_{-\vec{p}}^{+-\dagger} \partial_\eta h_k^{n+-} \partial_\eta h_p^{m+-*} \right| 0 \right\rangle$$

$$= \int \frac{d^3 k}{(2\pi)^{3/2}} \int \frac{d^3 p}{(2\pi)^{3/2}} \partial_\eta h_k^{n++} \partial_\eta h_p^{m++*} \left\langle 0 \left| \left[a_{\vec{k}}^{++}, a_{-\vec{p}}^{++\dagger} \right] \right| 0 \right\rangle + \partial_\eta h_k^{n+-} \partial_\eta h_p^{m+-*} \left\langle 0 \left| \left[a_{\vec{k}}^{+-}, a_{-\vec{p}}^{+-\dagger} \right] \right| 0 \right\rangle$$

$$= \int \frac{d^3 k}{(2\pi)^{3/2}} \int \frac{d^3 p}{(2\pi)^{3/2}} \left(\partial_\eta h_k^{n++} \partial_\eta h_p^{m++*} + \partial_\eta h_k^{n+-} \partial_\eta h_p^{m+-*} \right) \delta^{(3)}(\vec{k} - \vec{p})$$

$$= \int d\ln k \frac{k^3}{2\pi^2} \left(\partial_\eta h_k^{n++}(\eta) \partial_\eta h_k^{m++*}(\eta) + \partial_\eta h_k^{n+-}(\eta) \partial_\eta h_k^{m+-*}(\eta) \right).$$

Using the above expression we find the cross-correlation

$$\langle \partial_\eta \delta Y (0, \eta) \, \partial_\eta \delta X (0, \eta) \rangle_{\eta < \eta_{\text{tr}}} = \int d\ln k \frac{k^3}{2\pi^2} \left(\omega_{++}^2 |c_{++}|^2 \mathcal{R}^*_{++} + \omega_{+-}^2 |c_{+-}|^2 \mathcal{R}^*_{+-} \right) \tag{E10}$$

$$= \int d\ln k \frac{k^3}{2\pi^2} \left(i\partial_\eta\theta_0 \right). \tag{E11}$$

As expected, the two point correlation of the field velocities is a non-vanishing observable at early-time. Likewise,

$$\lim_{k \ll \partial_\eta \theta_0} \langle \partial_\eta \delta Y (0, \eta) \, \partial_\eta \delta Y (0, \eta) \rangle_{\eta < \eta_{\mathrm{tr}}} \approx \int d\ln k \sqrt{\frac{3}{2}} \left(\frac{k^3}{2\pi^2} \partial_\eta \theta_0 \right), \tag{E12}$$

$$\lim_{k \ll \partial_\eta \theta_0} \langle \partial_\eta \delta X (0, \eta) \, \partial_\eta \delta X (0, \eta) \rangle_{\eta < \eta_{\mathrm{tr}}} \approx \int d\ln k \sqrt{\frac{2}{3}} \left(\frac{k^3}{2\pi^2} \partial_\eta \theta_0 \right). \tag{E13}$$

Appendix F: Relationship between radial and angular modes

Suppose we parameterize a $U(1)$ sigma model with the symmetry $\Phi \to e^{i\alpha} \Phi$ as

$$\Phi = \frac{1}{\sqrt{2}} (\Gamma_0 + \delta\Gamma) e^{i \left(\theta_0 + \frac{\delta\chi}{\Gamma_0} \right)}. \tag{F1}$$

There is a shift symmetry

$$\delta\chi \to \delta\chi + \alpha\Gamma_0 \tag{F2}$$

where α is a constant. If $\delta\chi$ obeys a linear equation of motion

$$\mathcal{O}\delta\chi = \beta \tag{F3}$$

where $\mathcal{O}$ and β are independent of $\delta\chi$ but can depend on Γ_0, then Eq. (F2) implies

$$\mathcal{O}\delta\chi + \alpha\mathcal{O}\Gamma_0 = \beta. \tag{F4}$$

Using Eq. (F3), we conclude

$$\mathcal{O}\Gamma_0 = 0 \tag{F5}$$

which can be a nonlinear equation.

This means that if β is negligible, then $\delta\chi$ and Γ_0 obey the same equation. In our model, the equation of motion for $\delta\chi$ (see Eq. (D2)) makes

$$\mathcal{O} = \partial_\eta^2 - a^{-2}\partial_i^2 + 2\frac{\partial_\eta a}{a}\partial_\eta + \left(-2M^2 a^2 + \lambda\Gamma_0^2 a^2 - (\partial_\eta \theta_0)^2 \right) \tag{F6}$$

in Eq. (F5) which upon expansion gives

$$\partial_\eta^2 \Gamma_0 + 2\frac{\partial_\eta a}{a}\partial_\eta \Gamma_0 + \left(-2M^2 a^2 + \lambda\Gamma_0^2 a^2 - (\partial_\eta \theta_0)^2 \right) \Gamma_0 = 0 \tag{F7}$$

matching Eq. (77). The β in this system is

$$\beta = -2\partial_\eta \theta_0 \Gamma_0 \partial_\eta \frac{\delta\Gamma}{\Gamma_0}. \tag{F8}$$

Because of the mismatch of β between Γ_0 and $\delta\chi$, we cannot conclude that $\delta\chi/\Gamma_0$ is constant from this argument alone.

We will now show that the conservation equation from $U(1)$ symmetry together with a mild assumption about the lack of resonance allows one to conclude that $\delta\chi(\eta)/\Gamma_0(\eta)$ is approximately frozen during and after the transition. Start with the linear perturbation equation for the the $U(1)$ current conservation

$$\partial_\eta \delta q + \frac{\left|\vec{k}\right|^2 (a\Gamma_0)\, \delta\chi}{Q^{(0)}} = 0 \tag{F9}$$

where we have defined

$$\delta q \equiv \frac{1}{(\partial_0 \theta_0)} \frac{1}{a} \frac{\partial}{\partial \eta} \left(\frac{\delta\chi}{a\Gamma_0}\right) + 2\frac{\delta\Gamma}{a\Gamma_0} \tag{F10}$$

and gone to Fourier space. Let η_i be the first time in the time-independent conformal era when the k^2 term can be neglected in Eq. (F9). We can conclude that δq which is set during the time-independent conformal era to be

$$\delta q \approx \frac{3c_{+-}}{a(\eta_i)\Gamma_0(\eta_i)} \approx \frac{3\delta\Gamma(\eta_i, \vec{k})}{a(\eta_i)\Gamma_0(\eta_i)} \tag{F11}$$

is conserved while our quantity of interest $\delta\chi/\Gamma_0$ is related to this constant through

$$\frac{\partial}{\partial \eta}\left(\frac{\delta\chi}{a\Gamma_0}\right) + 2\frac{\delta\Gamma}{a\Gamma_0} a\, (\partial_0 \theta_0) = \delta q a\, (\partial_0 \theta_0) \tag{F12}$$

coming from Eq. (F10). Integrating, we find

$$\frac{\delta\chi(\eta_f)}{a(\eta_f)\Gamma_0(\eta_f)} - \frac{\delta\chi(\eta_{tr})}{a(\eta_i)\Gamma_0(\eta_{tr})} = \int^{\eta_f} d\eta' \left\{ \delta q \partial_{\eta'}\theta_0(\eta') - 2\frac{\delta\Gamma(\eta', \vec{k})}{\Gamma_0(\eta')} \frac{1}{a(\eta')}\partial_{\eta'}\theta_0 \right\} \tag{F13}$$

$$\approx \int_{\eta_{tr}}^{\eta_f} d\eta' \left\{ \frac{3\delta\Gamma(\eta_{tr}, \vec{k})}{a(\eta_{tr})\Gamma_0(\eta_{tr})}\partial_{\eta'}\theta_0(\eta') - 2\frac{\delta\Gamma(\eta', \vec{k})}{\Gamma_0(\eta')} \frac{1}{a(\eta')}\partial_{\eta'}\theta_0 \right\} \tag{F14}$$

where η_{tr} is the time at which $\Gamma_0(\eta)a(\eta)$ starts to change in time (i.e. deviate from the conformal behavior). Because the lighter energy mode $|\omega_{+-}\rangle$ becomes purely the $\delta\chi$ after the Γ_0 settles to the minimum of the potential, we know $\delta\Gamma(\eta', \vec{k}) \to 0$ asymptotically. Hence, for $t' > t_{tr}$ we shall assume

$$\delta\Gamma(\eta', \vec{k}) \lesssim \delta\Gamma(\eta_{tr}, \vec{k}). \tag{F15}$$

Additionally we consider a smooth non-resonant adiabatic transition of the background radial field such that

$$\Gamma_0(\eta')a(\eta') \gtrsim \Gamma_0(\eta_{tr})a(\eta_{tr}) \tag{F16}$$

because the equation of motion near the transition time can be solved to obtain

$$Y_0(\eta) \approx Y_c \left(1 + \frac{(2M^2/H^2 + 2)}{f^2\eta^2} - \frac{(2M^2/H^2 + 2)}{f^2\eta_i^2} \cos\left(f\left(\eta - \eta_i\right)\right) \right) \tag{F17}$$

which shows that the coefficient of $\cos(f(\eta - \eta_i))$ is suppressed. Hence, compared to the first term, the second term in the integral falls off rapidly for $t > t_{tr}$. Thus, we simplify the integral as

$$\frac{\delta\chi(\eta_f)}{a(\eta_f)\Gamma_0(\eta_f)} - \frac{\delta\chi(\eta_{tr})}{a(\eta_i)\Gamma_0(\eta_{tr})} \lesssim \left| \frac{3\delta\Gamma(\eta_{tr}, \vec{k})}{a(\eta_{tr})\Gamma_0(\eta_{tr})} \right| \int_{\eta_{tr}}^{\eta_f} d\eta' \partial_{\eta'}\theta_0(\eta'). \tag{F18}$$

Using the conservation equation, this becomes

$$\frac{\delta\chi(\eta_f)}{a(\eta_f)\Gamma_0(\eta_f)} - \frac{\delta\chi(\eta_{tr})}{a(\eta_i)\Gamma_0(\eta_{tr})} \lesssim \left| \frac{3\delta\Gamma(\eta_{tr}, \vec{k})}{a(\eta_{tr})\Gamma_0(\eta_{tr})} \right| \frac{Q^{(0)}H^2}{\Gamma_0^2(\eta_{tr})} \left(-\eta_{tr}^3\right) \tag{F19}$$

where we used Eq. (F16). Since we can solve during the time-independent conformal era

$$\left| \frac{\delta\Gamma(\eta_{tr}, \vec{k})}{a(\eta_{tr})\Gamma_0(\eta_{tr})} \right| \approx \left(\frac{k}{\partial_\eta\theta_0(\eta_{tr})} \right) \left| \frac{\delta\chi(\eta_{tr}, \vec{k})}{a(\eta_{tr})\Gamma_0(\eta_{tr})} \right| \tag{F20}$$

we obtain the relation

$$\frac{\delta\chi(\eta_f)}{a(\eta_f)\Gamma_0(\eta_f)} - \frac{\delta\chi(\eta_{tr})}{a(\eta_{tr})\Gamma_0(\eta_{tr})} \lesssim \left| \frac{\delta\chi(\eta_{tr}, \vec{k})}{a(\eta_{tr})\Gamma_0(\eta_{tr})} \right| \left(\frac{k}{a_{tr}H} \right). \tag{F21}$$

This indicates that in the long wavelength limit, the isocurvature perturbation is conserved for modes outside of the horizon at the transition time even in the presence of a large rotating background.

---

[1] J. Chluba and D. Grin, *CMB spectral distortions from small-scale isocurvature fluctuations*, *Mon.Not.Roy.Astron.Soc.* **434** (2013) 1619–1635, [1304.4596].

[2] Y. Takeuchi and S. Chongchitnan, *Constraining isocurvature perturbations with the 21 cm emission from minihaloes*, *MNRAS* **439** (2014) 1125–1135.

[3] J. B. Dent, D. A. Easson and H. Tashiro, *Cosmological constraints from CMB distortion*, *Phys.Rev.* **D86** (2012) 023514, [1202.6066].

[4] D. J. H. Chung and H. Yoo, *Elementary Theorems Regarding Blue Isocurvature Perturbations*, *Phys. Rev.* **D91** (2015) 083530, [1501.05618].

[5] D. J. H. Chung, *Large blue isocurvature spectral index signals time-dependent mass*, *Phys. Rev.* **D94** (2016) 043524, [1509.05850].

[6] J. Chluba, *Which spectral distortions does ΛCDM actually predict?*, *Mon. Not. Roy. Astron. Soc.* **460** (2016) 227–239, [1603.02496].

[7] D. J. H. Chung and A. Upadhye, *Search for strongly blue axion isocurvature*, *Phys. Rev. D* **98** (2018) 023525, [1711.06736].

[8] PLANCK collaboration, Y. Akrami et al., *Planck 2018 results. X. Constraints on inflation*, *Astron. Astrophys.* **641** (2020) A10, [1807.06211].

[9] S. Chabanier, M. Millea and N. Palanque-Delabrouille, *Matter power spectrum: from Lyα forest to CMB scales*, *Mon. Not. Roy. Astron. Soc.* **489** (2019) 2247–2253, [1905.08103].

[10] N. Lee and Y. Ali-Haïmoud, *Probing small-scale baryon and dark matter isocurvature perturbations with cosmic microwave background anisotropies*, *Phys. Rev. D* **104** (2021) 103509, [2108.07798].

[11] A. Kurmus, S. Bose, M. Lovell, F.-Y. Cyr-Racine, M. Vogelsberger, C. Pfrommer et al., *The feasibility of constraining DM interactions with high-redshift observations by JWST*, 2203.04985.

[12] S. Kasuya, M. Kawasaki and T. Yanagida, *Domain Wall Problem of Axion and Isocurvature Fluctuations in Chaotic Inflation Models*, *Physics Letters, Section B: Nuclear, Elementary Particle and High-Energy Physics* **415** (sep, 1997) 117–121, [9709202].

[13] M. Kawasaki, N. Sugiyama and T. Yanagida, *Isocurvature and Adiabatic Fluctuations of Axion in Chaotic Inflation Models and Large Scale Structure*, *Physical Review D - Particles, Fields, Gravitation and Cosmology* **54** (dec, 1995) 2442–2446, [9512368].

[14] K. Nakayama and M. Takimoto, *Higgs inflation and suppression of axion isocurvature perturbation*, *Physics Letters, Section B: Nuclear, Elementary Particle and High-Energy Physics* **748** (may, 2015) 108–112, [1505.02119].

[15] K. Harigaya, M. Ibe, M. Kawasaki and T. T. Yanagida, *Dynamics of Peccei-Quinn Breaking Field after Inflation and Axion Isocurvature Perturbations*, *Journal of Cosmology and Astroparticle Physics* **2015** (jul, 2015) , [1507.00119].

[16] K. Kadota, J.-O. Gong, K. Ichiki and T. Matsubara, *CMB probes on the correlated axion isocurvature perturbation*, *Journal of Cosmology and Astroparticle Physics* **2015** (nov, 2014) , [1411.3974].

[17] N. Kitajima and F. Takahashi, *Resonant conversions of QCD axions into hidden axions and suppressed isocurvature perturbations*, *Journal of Cosmology and Astroparticle Physics* **2015** (nov, 2014) , [1411.2011].

[18] M. Kawasaki, N. Kitajima and F. Takahashi, *Relaxing Isocurvature Bounds on String Axion Dark Matter*, *Physics Letters, Section B: Nuclear, Elementary Particle and High-Energy Physics* **737** (jun, 2014) 178–184, [1406.0660].

[19] T. Higaki, K. S. Jeong and F. Takahashi, *Solving the Tension between High-Scale Inflation and Axion Isocurvature Perturbations*, *Physics Letters, Section B: Nuclear, Elementary Particle and High-Energy Physics* **734** (mar, 2014) 21–26, [1403.4186].

[20] K. S. Jeong and F. Takahashi, *Suppressing Isocurvature Perturbations of QCD Axion Dark Matter*, *Physics Letters, Section B: Nuclear, Elementary Particle and High-Energy Physics* **727** (apr, 2013) 448–451, [1304.8131].

[21] T. Kobayashi, R. Kurematsu and F. Takahashi, *Isocurvature Constraints and Anharmonic Effects on QCD Axion Dark Matter*, Journal of Cosmology and Astroparticle Physics **2013** (apr, 2013) , [1304.0922].

[22] J. Hamann, S. Hannestad, G. G. Raffelt and Y. Y. Y. Wong, *Isocurvature forecast in the anthropic axion window*, Journal of Cosmology and Astroparticle Physics **2009** (apr, 2009) , [0904.0647].

[23] M. P. Hertzberg, M. Tegmark and F. Wilczek, *Axion Cosmology and the Energy Scale of Inflation*, Physical Review D - Particles, Fields, Gravitation and Cosmology **78** (jul, 2008) , [0807.1726].

[24] M. Beltran, J. Garcia-Bellido and J. Lesgourgues, *Isocurvature bounds on axions revisited*, Physical Review D - Particles, Fields, Gravitation and Cosmology **75** (jun, 2006) , [0606107].

[25] P. Fox, A. Pierce and S. Thomas, *Probing a QCD String Axion with Precision Cosmological Measurements*, 0409059.

[26] M. Estevez and O. Santillán, *About the isocurvature tension between axion and high scale inflationary models*, European Physical Journal C **76** (jun, 2016) , [1606.02389].

[27] J. Kearney, N. Orlofsky and A. Pierce, *High-Scale Axions without Isocurvature from Inflationary Dynamics*, Physical Review D **93** (jan, 2016) , [1601.03049].

[28] Y. Nomura, S. Rajendran and F. Sanches, *Axion Isocurvature and Magnetic Monopoles*, Physical Review Letters **116** (nov, 2015) , [1511.06347].

[29] K. Kadota, T. Kobayashi and H. Otsuka, *Axion inflation with cross-correlated axion isocurvature perturbations*, Journal of Cosmology and Astroparticle Physics **2016** (sep, 2015) , [1509.04523].

[30] C. Hikage, M. Kawasaki, T. Sekiguchi and T. Takahashi, *CMB constraint on non-Gaussianity in isocurvature perturbations*, 1211.1095.

[31] D. Langlois, *Isocurvature cosmological perturbations and the CMB*, 2003. 10.1016/j.crhy.2003.09.004.

[32] S. Mollerach, *On the primordial origin of isocurvature perturbations*, Physics Letters B **242** (jun, 1990) 158–162.

[33] M. Axenides, R. Brandenberger and M. Turner, *Development of axion perturbations in an axion dominated universe*, Physics Letters B **126** (jun, 1983) 178–182.

[34] B. Jo, H. Kim, H. D. Kim and C. S. Shin, *Exploring the Universe with Dark Light Scalars*, Physical Review D **103** (oct, 2020) , [2010.10880].

[35] S. Iso, K. Kawana and K. Shimada, *Axion-CMB Scenario in Supercooled Universe*, 2105.06803.

[36] K. J. Bae, J. Kost and C. S. Shin, *Deformation of Axion Potentials: Implications for Spontaneous Baryogenesis, Dark Matter, and Isocurvature Perturbations*, Physical Review D **99** (nov, 2018) , [1811.10655].

[37] L. Visinelli, *Light axion-like dark matter must be present during inflation*, Physical Review D **96** (mar, 2017) , [1703.08798].

[38] Y. Takeuchi and S. Chongchitnan, *Constraining isocurvature perturbations with the 21cm emission from minihaloes*, 1311.2585.

[39] M. Bucher, K. Moodley and N. Turok, *Constraining isocurvature perturbations with CMB polarization, Phys. Rev. Lett.* **87** (2001) 191301, [`astro-ph/0012141`].

[40] S. Lu, *Axion isocurvature collider, JHEP* **04** (2022) 157, [`2103.05958`].

[41] A. S. Sakharov, Y. N. Eroshenko and S. G. Rubin, *Looking at the NANOGrav signal through the anthropic window of axionlike particles, Phys. Rev. D* **104** (2021) 043005, [`2104.08750`].

[42] J. a. G. Rosa and L. B. Ventura, *Spontaneous breaking of the Peccei-Quinn symmetry during warm inflation*, `2105.05771`.

[43] L. Jukko and A. Rajantie, *Stochastic isocurvature constraints for axion dark matter with high-scale inflation*, `2107.07948`.

[44] Z. Chen, A. Kobakhidze, C. A. J. O'Hare, Z. S. C. Picker and G. Pierobon, *Cosmology of the companion-axion model: dark matter, gravitational waves, and primordial black holes*, `2110.11014`.

[45] K. S. Jeong, K. Matsukawa, S. Nakagawa and F. Takahashi, *Cosmological effects of Peccei-Quinn symmetry breaking on QCD axion dark matter, JCAP* **03** (2022) 026, [`2201.00681`].

[46] M. Cicoli, A. Hebecker, J. Jaeckel and M. Wittner, *Axions in string theory — slaying the Hydra of dark radiation, JHEP* **09** (2022) 198, [`2203.08833`].

[47] E. Koutsangelas, *Removing the cosmological bound on the axion scale in the Kim-Shifman-Vainshtein-Zakharov and Dine-Fischler-Srednicki-Zhitnitsky models, Phys. Rev. D* **107** (2023) 095009, [`2212.07822`].

[48] M. Kawasaki and T. T. Yanagida, *Hill-top inflation from Dai-Freed anomaly in the standard model – A solution to the isocurvature problem of the axion dark matter*, `2306.14579`.

[49] S. Kasuya and M. Kawasaki, *Axion isocurvature fluctuations with extremely blue spectrum, Phys.Rev.* **D80** (2009) 023516, [`0904.3800`].

[50] H. K. Dreiner, F. Staub and L. Ubaldi, *From the unification scale to the weak scale: A self consistent supersymmetric Dine-Fischler-Srednicki-Zhitnitsky axion model, Phys. Rev. D* **90** (2014) 055016, [`1402.5977`].

[51] J. E. Kim and G. Carosi, *Axions and the Strong CP Problem, Rev. Mod. Phys.* **82** (2010) 557–602, [`0807.3125`].

[52] L. Di Luzio, M. Giannotti, E. Nardi and L. Visinelli, *The landscape of QCD axion models, Phys. Rept.* **870** (2020) 1–117, [`2003.01100`].

[53] R. Ebadi, S. Kumar, A. McCune, H. Tai and L.-T. Wang, *Gravitational Waves from Stochastic Scalar Fluctuations*, `2307.01248`.

[54] R. T. Co and K. Harigaya, *Axiogenesis, Phys. Rev. Lett.* **124** (2020) 111602, [`1910.02080`].

[55] R. T. Co, D. Dunsky, N. Fernandez, A. Ghalsasi, L. J. Hall, K. Harigaya et al., *Gravitational Wave and CMB Probes of Axion Kination*, `2108.09299`.

[56] P. Creminelli, M. Delladio, O. Janssen, A. Longo and L. Senatore, *Non-analyticity of the S-matrix with spontaneously broken Lorentz invariance*, `2312.08441`.

[57] L. Hui, I. Kourkoulou, A. Nicolis, A. Podo and S. Zhou, *S-matrix positivity without Lorentz invariance: a case study*, *JHEP* **04** (2024) 145, [`2312.08440`].

[58] A. J. Leggett, *Superfluidity*, *Rev. Mod. Phys.* **71** (1999) S318–S323.

[59] P. B. Greene, L. Kofman, A. D. Linde and A. A. Starobinsky, *Structure of resonance in preheating after inflation*, *Phys. Rev. D* **56** (1997) 6175–6192, [`hep-ph/9705347`].

[60] M. Kawasaki, T. T. Yanagida and K. Yoshino, *Domain wall and isocurvature perturbation problems in axion models*, *JCAP* **11** (2013) 030, [`1305.5338`].

[61] R. T. Co, L. J. Hall, K. Harigaya, K. A. Olive and S. Verner, *Axion Kinetic Misalignment and Parametric Resonance from Inflation*, *JCAP* **08** (2020) 036, [`2004.00629`].

[62] D. J. H. Chung and S. C. Tadepalli, *Analytic treatment of underdamped axionic blue isocurvature perturbations*, *Phys. Rev. D* **105** (2022) 123511, [`2110.02272`].

[63] D. J. H. Chung and A. Upadhye, *Bump in the blue axion isocurvature spectrum*, *Phys. Rev. D* **95** (2017) 023503, [`1610.04284`].

[64] Y. K. Semertzidis and S. Youn, *Axion dark matter: How to see it?*, *Sci. Adv.* **8** (2022) abm9928, [`2104.14831`].

[65] L. Visinelli and P. Gondolo, *Dark Matter Axions Revisited*, *Phys. Rev. D* **80** (2009) 035024, [`0903.4377`].

[66] J. Kearney, N. Orlofsky and A. Pierce, *High-Scale Axions without Isocurvature from Inflationary Dynamics*, *Phys. Rev. D* **93** (2016) 095026, [`1601.03049`].

[67] D. J. H. Chung, M. Münchmeyer and S. C. Tadepalli, *Search for isocurvature with large-scale structure: A forecast for Euclid and MegaMapper using EFTofLSS*, *Phys. Rev. D* **108** (2023) 103542, [`2306.09456`].

[68] P. H. Ginsparg, *APPLIED CONFORMAL FIELD THEORY*, in *Les Houches Summer School in Theoretical Physics: Fields, Strings, Critical Phenomena*, 9, 1988, `hep-th/9108028`.